https://ntrs.nasa.gov/search.jsp?R=19800002268 2020-03-21T20:21:34+00:00Z

43

NASA Technical Paper 1477

Light Airplane Crash Tests at Three Roll Angles

Claude B. Castle and Emilio Alfaro-Bou

OCTOBER 1979

NASA

NASA Technical Paper 1477

Light Airplane Crash Tests at Three Roll Angles

Claude B. Castle and Emilio Alfaro-Bou
Langley Research Center
Hampton, Virginia

National Aeronautics
and Space Administration

**Scientific and Technical
Information Branch**

1979

CONTENTS

SUMMARY

Three low-wing general-aviation airplanes, each with a mass of 2700 kg, were crash tested at 27 m/sec along a flight-path angle of -15° with roll angles of 0°, -15°, and -30° at the Langley impact dynamics research facility. These tests are part of a program being conducted under controlled impact conditions to determine the effects of selected impact parameters on crash response. In the present investigation, roll angle was the only impact parameter varied. Although other factors such as flight path, yaw, pitch, velocity, angular rates, impact surfaces, and fire can affect airplane crash behavior, such factors are not considered in this report.

The crash tests, irrespective of roll attitude, exhibited two distinct sequential impacts: an initial impact when the fuselage nose first contacted the ground, and a second impact when the cabin area in the vicinity of the wing spar contacted the ground. The second impact produced the highest accelerations in the cabin area. Changing the roll attitude from 0° to -15° or -30° resulted in a lower peak-to-peak normal acceleration trend in the cabin area. The peak-to-peak normal accelerations forward of the main spar increased slightly or remained at the level of the 0° test when roll was introduced. Forward of the main spar, the longitudinal accelerations were essentially the same for the -15° test and the 0° test, but were reduced by 50 percent in the -30° test. Longitudinal accelerations in the cabin area were approximately the same for all tests. There was a general reduction in peak-to-peak normal and longitudinal accelerations in the seat pan and dummy pelvis regions due to the introduction of roll.

INTRODUCTION

With the rapid growth of private and commercial air traffic since World War II, causes of passenger injuries and deaths in severe but potentially survivable crashes have been increasingly emphasized. The National Advisory Committee for Aeronautics (NACA), predecessor of the National Aeronautics and Space Administration (NASA), conducted a series of full-scale airplane crash tests with instrumented dummies in the early 1950's (refs. 1 and 2). These tests were performed by accelerating an airplane along a horizontal guide rail into an earthen mound. Later NACA studies shed some light on the dynamic response of seat structures to impact loads (ref. 3) and resulted in a Civil Aeronautics Administration (CAA) update in static seat strength requirements. The airplanes previously tested by NACA, however, were not structurally representative of current general-aviation airplanes. Therefore, in 1973, a joint general-aviation crash-test program was initiated by the Federal Aviation Administration (FAA) and NASA.

As part of this program, the NASA Langley Research Center (LaRC) is conducting a series of crash tests at the Langley impact dynamics research facility to obtain information on single- and twin-engine airplanes under controlled

free-flight conditions. The variations in desired impact parameters for the two-engine airplanes are shown in table I. Objectives of the test program are to derive an understanding of what happens to the structure of an airplane subjected to crash loads and to learn how various impact parameters affect the magnitude and pattern of the structural damage. This information is essential for predicting structural collapse and designing new concepts for seats, occupant restraint systems, and cabin interiors. Crash-test data can also be used to assess the validity of elasto-plastic, large-deflection analyses, as described in reference 4.

There are certain lethal crashes in which the airplane structure is so severely damaged that no hope of survival exists for the occupants. The crash studies at LaRC, however, are focused on those crashes in which the impacted structure retains sufficient "livable volume" for potential occupant survival. A "livable volume" is a volume sufficient to maintain space between the occupant and the structure.

In the present investigation, three airplanes were crash tested at an impact flight-path velocity of 27 m/sec, which is approximately 70 percent of the flight stall speed for this type of airplane, along a flight-path angle of -15°, with roll attitudes of 0°, -15°, and -30°. Effects of changing the roll angle at impact (with angle of attack, pitch, and flight-path velocity held constant) are discussed in terms of acceleration and structural damage. Other test parameters, particularly yaw angle and vertical velocity, varied from the nominal values in these tests. The effects of these variations were not considered in the analysis of the data. It should be emphasized that these tests were not conducted for the purpose of evaluating the safety of a particular airplane, but rather to gather data on crash phenomena which should be helpful in designing future airplanes.

The purpose of this report is to discuss structural damage and acceleration time histories for airplanes tested at three roll angles. A motion-picture film supplement on these tests at the three roll angles is available on loan. A request card form and a description of the film are found at the back of this paper.

TEST FACILITY

The full-scale crash tests were performed at the Langley impact dynamics research facility shown in figure 1. The facility is described more completely in reference 5. The basic structure of the facility is the gantry, which is 73 m high and 122 m long. A movable bridge spans the gantry at the 66-m level and can traverse the length of the gantry. A control room and an observation room are located in the building at the base of the gantry. Along the center line of the gantry at ground level is a strip of reinforced concrete 122 m long, 11 m wide, and 0.2 m thick which is used as the impact surface. The impact surface and a movable backboard have a painted 1-m grid system for photographic background.

The systems necessary to perform the full-scale crash tests are shown in figure 2. Swing-cable pivot-point platforms located at the west end of the

gantry support the winches, sheaves, and pulley systems for controlling the length of the swing cables. A pullback platform, attached to the underside of the movable bridge, supports a winch, sheave, and pulley system for controlling the length of the pullback cable. The swing and pullback cables attached to the lifting harness, which make up the test-specimen suspension system, are shown in figure 3.

The airplane, suspended by two swing cables from the gantry, is pulled to the desired height by the pullback cable. The test sequence begins when the airplane is released from the pullback cable and swings pendulum style into the impact surface, as shown in figure 4. The swing cables are pyrotechnically separated prior to ground contact when the specimen is approximately 2 m from the impact surface along the flight path. The airplane, therefore, is free from restraint during the crash sequence. The umbilical (fig. 3) remains attached during the impact for data acquisition and is pyrotechnically separated at approximately 0.75 sec after swing-cable separation.

The flight-path and attitude angles of the airplane are identified, together with the axes and force directions, in figure 5. The flight-path angle was set for -15° (fig. 4) by adjusting the length of the swing cables for each test (ref. 6), and the roll angle was obtained by individual relative adjustments of the swing cables. The pullback height of the airplane was calculated to give a flight-path velocity of 27 m/sec. This velocity is the maximum obtainable at the facility for a smooth gravity-induced swing and is approximately 70 percent of the flight stall speed for this type of airplane.

DESCRIPTION OF TEST AIRPLANES

The test airplanes were twin-engine general-aviation types with a nominal mass of 2700 kg and a capacity of six to eight passengers. The three airplanes and their test parameters are shown in figure 6. The airplanes consist of a fuselage structural shell, wings with nacelle fairings, and landing gear (retracted). The mass and center of gravity of the empennage were simulated by two concentrated masses which represent the fin-rudder and stabilizer-elevator combinations. The ailerons and flaps were also simulated by concentrated masses. Masses were added at the appropriate locations to simulate the mass and center of gravity of the engines, propellers, and spinners. The fuel bladders were filled with colored water to simulate the fuel mass and to help locate bladder leakage, if any, during the testing. Spoilers were attached to the wings to minimize the aerodynamic lift.

The selected arrangements of seats, anthropomorphic dummies, and restraint systems are shown in figure 7. For the -15° and -30° roll tests, Hybrid II anthropomorphic dummies were used (see ref. 7), and their respective masses are given beside each dummy in figure 7. For the 0° roll test, which was performed before the Hybrid II dummies had been acquired, dummies normally used for seat ejection studies were used. These earlier dummies have free hip joints in contrast to the restricted joints used on the Hybrid II dummies. The masses of these earlier dummies are also given in figure 7. The airplane used in the 0° roll test had no floor boards, instrument panel, or furnishings (except seats); whereas the airplanes used in -15° and -30° roll tests had floor

boards. All test airplanes contained batteries, instrumentation junction boxes, a pyrotechnic programmer, and various electrical junction boxes and circuits needed to perform the crash test. Concentrated masses were also used to simulate some items which are integral to a complete airplane and were arranged to provide the proper balance and center-of-gravity location.

INSTRUMENTATION

Onboard instrumentation consisted of accelerometers, load cells, and high-speed motion-picture cameras to provide data pertaining to the dynamic behavior of the airplane structure, cabin seats, and anthropomorphic dummies. External photographic coverage (see fig. 2) of the crash sequence was provided by tracking cameras and fixed motion-picture cameras located on the side of, in front of, and above the test specimen at impact position.

Accelerometers were calibrated in a centrifuge prior to each test and were linear in amplitude to ±1 percent throughout the frequency range of 4 to 5000 Hz. The accelerometer locations are shown in figure 8. The accelerometers were oriented in normal, longitudinal, and transverse directions with respect to the airplane axes. Each location - for example, 2B9N - is designated by its coordinates as follows: the first number "2" indicates the longitudinal coordinate; the first letter "B" indicates the vertical coordinate (floor to roof); the second number "9" indicates the transverse coordinate; and the second letter "N" indicates the accelerometer orientation with respect to the airplane body-axes system. (That is, the accelerometer location on the floor beam nearest the nose is designated "2B9," and the accelerometer at that location oriented in the normal direction is designated "2B9N.") The longitudinal and transverse orientations are designated "L" and "T," respectively.

Data signals were transmitted through an umbilical cable to a junction box on top of the gantry and from there, through hard wire, to the control room, where the data signals were recorded by FM tape recorders. To correlate data signals on the FM recorders and the external motion-picture film, a time code was recorded simultaneously on the magnetic tape and on the film. There was also a time-code generator onboard the airplane for use with the onboard cameras. To obtain the horizontal velocity of the airplane at impact, a Doppler radar unit was placed on the impact surface approximately 60 m aft of the impact point and the signal was recorded on the FM tapes.

The accelerometer data and data-reduction techniques are described briefly in the appendix and more completely in reference 8. Piezoelectric accelerometers were used on the airframe and the dummies in the 0° roll test. Strain-gage accelerometers were used in the anthropomorphic dummies for the -15° and -30° roll tests. The output of the piezoelectric accelerometers, however, exhibited various degrees of zero shift with increasing time. This problem was compounded by the multiplicity of pulses to which each accelerometer was subjected during the tests. As a result there is some unknown error in the absolute value of accelerations recorded from the piezoelectric accelerometers after the first pulse.

A casual inspection of the acceleration traces does not reveal the zero shift nor an error in the absolute value of the accelerations recorded. Only after the acceleration traces are integrated and the results are compared with known velocity values does the effect of zero shift become evident. All peak-to-peak acceleration values are believed to be accurate. Hence, data are analyzed in terms of peak-to-peak values for comparative purposes.

RESULTS AND DISCUSSION

Assessment of Structural Damage

Roll test at 0°.- The photographic sequence of the 0° roll test is presented in figure 9. the airplane on the glide path prior to impact is shown in figure 9(a). Figure 9(b) shows the airplane at 0.02 sec after impact with the swing cables separated to permit free flight at impact. Crushing of the nose (0.07 sec) is shown in figure 9(c), and figure 9(d) shows the wings flat on the impact surface and the initial movement of the dummies (0.12 sec). Figure 9(e) shows the slapdown of the aft fuselage section and the resulting wrinkles in the skin surface, separation of the fuselage along the lower window ledge, and the door opening (0.17 sec). The continuing deformation of the test specimen during slide out (0.22 sec) is shown in figure 9(f). Inspection of these figures indicates that the livable volume of the cabin was maintained throughout the crash sequence.

The exterior damage to the airplane for the 0° roll test is shown in figure 10. As seen in the overall view of the right side (fig. 10(a)), buckling occurred in the nose section, at the fire wall, and along the bottom of the fuselage. Rivet shear failure is evident aft from the escape hatch along the window ledge and downward at the rear of the third window. (See figs. 10(a) and 10(b).) Also, rivet failure is shown under the first-passenger window (fig. 10(c)) and across the top of the fuselage aft of the pilot and copilot seats (fig. 10(d)). The breakage of the pilot's windshield and side window occurred because of deformation of the forward cabin section (fig. 10(d)).

Damage to the cabin interior is shown in the four photographs of figure 11. The first photograph (fig. 11(a)) is a view looking aft from the cockpit, where buckling can be seen in the stiffeners which tie together the two main floor beams. Also shown is the five-point restraint worn by the first-passenger dummy. Figure 11(b) is a view looking forward from the tail section and again shows the main floor beams and the buckled stiffeners. The apparent upward movement of the floor section is shown by the outward rotation of the seats. The four photographs of figure 11 also show the layout of seats, dummies, additional masses, instrumentation equipment, and moderate interior damage.

Roll test at -15°.- Sequence photographs of the airplane during a -15° roll impact test are shown in figure 12. The photograph (fig. 12(a)) shows the cable separation and free-flight attitude prior to impact. Figure 12(b) (0.03 sec) shows the test airplane as the nose section contacts the impact surface and the left wing has impacted and begun to deform. In figure 12(c) (0.08 sec) the

fuselage in the vicinity of the fire wall has made contact, and the initial reaction of the dummy pilot and first-passenger dummy to the crash is evident. As the main fuselage contacts the impact surface (0.13 sec) and right wing, slapdown (0.18 sec, figs. 12(d) and 12(e)) has occurred, the pilot dummy impacts the instrument panel, and the fuselage has begun to separate along the window ledge on the left side of the test specimen; also, the door has started to open. In figures 12(e) and 12(f), as tail slapdown occurs (0.18 sec and 0.23 sec, respectively), the tensile loading in the top portion of the fuselage causes separation of the left and center windshield supports. This failure of the windshield supports then causes separation of the windshield and a rearward movement of the top portion of the cabin. These effects are shown by the misalignment of the painted black lines on the fuselage side representing the underlying structure. The top portion of the cabin in the vicinity of the first- and second-passenger dummies has begun to "neck down" and the first-passenger dummy has impacted the pilot seat. The engine cowling on the left side has sheared its rivets and separation has begun. Also shown is the window breakage along the left side.

The exterior damage resulting from the impact is shown in figure 13. The rear view of the left side in figure 13(a) shows structural damage to the top surface of the wing at about one-third of the wing semispan from the tip. The rear view of the right side in figure 13(b) shows the tail-section separation and loose emergency escape hatch with rivet shear and sheet metal separation under the window frame in the vicinity of the second-passenger seat. A full view of the left side of the test airplane in figure 13(c) shows the damaged wing, cabin and tail separation, broken windows, and the misalignment of the top portion of the cabin. A close-up view (fig. 13(d)) of the right side of the cabin and cockpit areas shows the loosened escape hatch, buckling of the skin, broken copilot side window, and separation and deformation of the windshield corner post. Figures 13(e) and 13(f) show more clearly the damage at the base of the windshield and left side. The deformation across the top of the cabin (fig. 13(e)) and the subfloor crushing did not significantly reduce the livable volume inside the cabin area.

The damage done to the airplane interior in the -15° roll test is shown in figure 14. A view looking forward in the cabin area (fig. 14(a)) shows only a slight apparently upward movement of the center floor area, as can be determined by the outward rotation of the accelerometer blocks. Figure 14(b) shows the forward cabin and cockpit area with fixtures removed. Also evident are slight apparently upward movement of the cabin floor center section and the separation of the cabin along the window ledge. The buckled left main spar near the main spar splice can be seen in figure 14(c), which is a top view of the main spar inside the cabin. A view of the floor support with small amounts of buckling of the cross-support structures is shown in figure 14(d). The torn and separated tail section shown in figure 14(e), in a view aft of the door, shows the effects of tail slapdown during impact.

Roll test at -30°.- The photographic sequence of the -30° roll test is shown in figure 15. Wing deformation after initial impact is shown in figure 15(a). Figures 15(b) to 15(f) graphically illustrate how the left wing of the airplane bends during impact and attenuates some of the impact energy.

Movement of the pilot dummy has started and may be noted in figure 15(c). The airplane pivots about its left wing after initial impact for approximately 0.30 sec before right wing slapdown occurs. The resulting cabin deformation and slide out are shown in figures 15(d) to 15(f). It can be seen that the livable volume was maintained throughout the impact sequence.

The exterior damage to this airplane is shown in figure 16. An overall front view of the airplane in figure 16(a) shows the upward deformation of the left wing and the left and center windshield posts separated at their lower fuselage attachments. The separation of the posts was caused by the tensile load on the top portion of the cabin during tail slapdown. Evidence of the tensile load can be seen in figure 16(b) by the misalignment of the black vertical skin lines (reference lines) between the pilot and first-passenger dummies. In the right side views (figs. 16(c) and 16(d)) skin buckling is shown in the aft portion of the fuselage. A rear view of the left side of the airplane (fig. 16(e)) shows separation of the cabin along the window ledge and misalignment of the painted lines of the underlying airframe sections.

The interior cabin damage in the -30° roll test is shown in figure 17. A view looking forward in the cabin section (fig. 17(a)) shows only a slight apparent rise in the center portion of the floor manifested by the outward rotation of the seats. A view of the rear section of the airplane (fig. 17(b)) shows only minor fuselage separation along the lower portion of the fuselage. The windshield post, pilot side window, and copilot windshield were broken and are shown in figure 17(c); also shown is a slight buckling of the main spar. Damage to the cross members between the floor beams is shown in figure 17(d). Damage to the main spar is shown in a top view in figure 17(e).

The left wing in the -30° roll test is shown in figure 18 with skin damage evident on the top surface (fig. 18(a)) and with skin tears and rivet shear shown in the close-up (fig. 18(b)). A section of the damaged wing with the upper skin removed is shown in figures 18(c) and 18(d). Rib and rear spar fracture is evident in the close-up view (fig. 18(d)) in the vicinity of the outboard fuel bladder. The broken rib sections punctured the fuel bladder in several places.

Comparison of Damage

External damage to the nose section of the three airplanes was most severe in the -30° roll test. Buckling was more pronounced both in a wider area of the nose section and in the fire wall for the 0° roll test than for the -15° roll test. All three tests experienced some windshield post separation, but damage was most severe in the -15° roll test, where all three posts separated.

On the left side of the fuselage, damage was most severe for the -15° roll test and least severe for the 0° roll test. There was more rivet shear and wider separation of the lower edge of the first- and third-passenger window frames for the -15° roll test than for the -30° roll test.

Damage on the right side of the fuselage was most severe in the -15° roll test and least severe in the -30° test. Separation of the lower portion of the

escape hatch frame from the fuselage occurred in the -15° roll test; rivet shear under the fourth-passenger window frame occurred in the 0° roll test. Only minor wrinkling of the skin occurred in the right side of the fuselage for the -30° roll test.

The tail sections of the airplanes received almost equal damage for the 0° and -30° roll tests; this damage was most severe for the -15° roll test, where damage to the skin (wrinkling) was more pronounced. There was a slight separation of the tail section at the lower right corner of the door frame in the -30° roll test, while in the -15° roll test, almost the entire tail section separated from the fuselage at the aft edge of the door. The tail section was held to the fuselage only along the right lower side.

In the 0° roll test, severe rivet shear failure occurred on the roof between the pilot and first-passenger location, leaving a gap from aft of the pilot window to aft of the copilot window. A slight rivet shear failure occurred in the -30° roll test; least damage was observed in the -15° roll test. Also, buckling along the length of the roof about 15 cm to the left of center occurred in the 0° roll test, while none was observed in the other two tests.

Interior damage was most severe in the 0° roll test in the pilot and copilot floor and fire wall area and least severe in the same areas in the -30° roll test. Damage to the main spar inside the cabin was about the same for the 0° and -15° roll tests; it was less severe for the -30° roll test. Damage in the cross members between the floor beams was also most severe for the 0° roll test and least severe for the -30° roll test. Cross members between the window side and floor beams experienced most damage in the -15° roll test and least damage in the -30° roll test. In the interior of the tail section, however, damage was most severe in the -15° roll test and least severe in the 0° roll test.

Overall comparisons indicate that the -30° roll test resulted in the least damage in and around the passenger compartment.

Floor-Beam Normal Accelerations

For completeness, all acceleration data for each crash test are included in the appendix in plots according to their location and orientation. Data for selected portions of normal, longitudinal, and transverse acceleration along the floor beam on the floor under the first-passenger seat (fig. 7) and in the pelvis of the first-passenger dummy are presented in the following sections.

Roll test at 0°.- In figure 19(a), eight normal acceleration traces from the 0° roll test are presented, and the times of significant events are noted. The eight accelerometers were spaced along the left floor beam of the airplane (see insert, fig. 19(a) and fig. 8(a)) from the first nose frame (2B9N) to the door of the cabin (19B9N). Accelerations in the cabin compartment reached a maximum in the vicinity of the main spar and diminished progressively from that point rearward. At 0.091 sec (fig. 19(a)) the wing made ground contact and

peak-to-peak accelerations of 130g and 50g occurred on the floor next to the first-passenger aisle seat legs (15B9N and 17B9N).

Roll test at -15°.- Nine normal acceleration traces along the floor structure are shown in figure 19(b) for the -15° roll test. Only those five along the left floor beam are compared with the 0° roll test. Four additional accelerometers were added along the right floor beam for the -15° and -30° tests.

The initial impact of the left wing prior to zero time of this plot caused only slight fuselage accelerations before initial nose contact was made at 0.025 sec. For the -15° roll test, the right wing slapdown (second impact) occurred at 0.155 sec; 5 milliseconds later the cabin separated at the door. This separation produced tail section slapdown and induced low accelerations in the cabin section (small positive peaks of 16B9N) at 0.161 sec.

Roll test at -30°.- The accelerometers along the floor structure in the -30° roll test (fig. 19(c)) were in the same locations as those in the -15° roll test (fig. 8(b)). Again, only the four accelerations along the left floor beam are compared with the 0° roll test.

Accelerations were highest at the nose of the airplane and diminished toward the pilot-copilot compartment and then increased slightly in the cabin area. The right wing slapdown (second impact) occurred at 0.280 sec, but only small acceleration peaks occurred in the floor beam.

Comparisons of normal floor-beam accelerations.- In the 0° roll test the nose section was first to make contact with the impact surface, whereas in the -15° and -30° roll tests the airplane skidded on the left wing for 0.095 and 0.290 sec, respectively, before nose contact was made.

For each test, a comparison of floor acceleration traces indicates, in general, higher accelerations forward of the main spar compared with accelerations aft of the main spar. Higher amplitude accelerations with longer duration were experienced at the front of the nose section (2B9N) in the 0° roll test than in the -15° roll test; lower values were experienced for the -30° roll test. At the fire wall (8B9N), accelerations were highest for the 0° roll test and lowest for the -15° roll test. At the first-passenger location (15B9N and 16B9N) accelerations were highest for the 0° roll test and lowest for the -30° roll test. At the third-passenger location, accelerations were highest for the -15° roll test and lowest for the 0° roll test.

Floor-Beam Longitudinal Accelerations

In figure 20, fuselage floor-beam longitudinal accelerations are presented for the 0°, -15°, and -30° roll tests, with times of significant events noted.

Roll test at 0°.- Seven accelerometers (fig. 20(a)) were spaced along the left floor beam of the airplane from the first nose frame (2B9L) to the rear of the third-passenger seat (19B9L). The response to ground contact is felt initially at the first nose frame (2B9L). As contact progresses rearward to the

instrument panel (9B9L), the longitudinal acceleration magnitudes diminish to about 50 percent of the normal acceleration magnitudes. Wing ground contact (second impact) is shown at 0.091 sec. The positive acceleration peak in 17B9L and 19B9L at 0.164 sec coincides with the time of fuselage separation across the cabin roof in the vicinity of the main spar, as determined from motion pictures.

Roll test at -15°.- Nine longitudinal accelerometer traces along the floor structure in the -15° roll impact test are shown in figure 20(b). Again, for comparison purposes, only those four along the left floor beam are discussed. As for the normal accelerations, the fuselage floor structure does not exhibit significant longitudinal accelerations during initial wing ground contact. Accelerations occur in the cabin (aft of the main spar) when the fuselage in the vicinity of the main spar contacts the impact surface. It can be seen in figure 20(b) that all acceleration traces exhibit rather low accelerations with less rearward progression of the impulse than occurred in the 0° test.

Roll test at -30°.- In figure 20(c), nine acceleration traces along the floor structure are presented for the -30° roll test. Only the four along the left floor beam are compared with the 0° roll test. As in the -15° roll test, the floor structure does not experience longitudinal acceleration pulses during the initial impact of the left wing and only exhibits an acceleration pulse forward of the main spar during nose impact. The cabin (aft of the main spar) does not respond to the nose impact, but to the fuselage contact with the impact surface in the vicinity of the main spar.

The accelerations in the -30° roll test forward of the main spar were less than half of those obtained for the 0° and -15° roll tests. In the cabin section aft of the main spar, the -30° roll test shows acceleration magnitudes approximately the same as those for the 0° roll test, but higher than those for the -15° roll test. The cabin longitudinal accelerations at fuselage main spar contact are about one-half the magnitude of the normal accelerations for the -30° test.

The right wing slapdown in the -15° and -30° roll tests causes very little disturbance of the fuselage longitudinal accelerations. Longitudinal accelerations at the nose (2B9N) and fire wall (8B9N) were highest in the 0° roll test and lowest in the -30° roll test. In the cabin area the accelerations were low for all three tests, approximately 50g but were highest for the -30° roll test and lowest for the -15° roll test.

Floor-Beam Transverse Accelerations

Roll test at -15°.- The fuselage floor-beam transverse accelerations are presented in figure 21. For the -15° roll test (fig. 21(a)), only minimal excitation of these accelerometers occurred before nose contact was made. Nose contact produced high accelerations in the first two nose frames while the cockpit area experienced low accelerations. The cabin (aft of the main spar) did not respond until the fuselage at the main spar made contact with the impact

surface; then the two accelerometers mounted nearest the main spar (16B9T and 16B10T) showed low acceleration pulses of approximately 10g, but higher magnitudes were measured for the two aft (19B9T and 19B10T) accelerometers. These higher accelerations in the third-passenger area are caused by the rolling of the fuselage upon impact and by the lateral momentum of the tail. At the time of right wing slapdown (0.156 sec), an acceleration pulse of about 20g was produced in these four locations.

Roll test at -30°.- In figure 21(b), nine transverse acceleration traces are shown for the -30° roll test and, in general, they show acceleration magnitudes similar to the -15° roll test.

Floor-Beam Maximum Peak-to-Peak Normal and Longitudinal Accelerations

Figure 22 shows a profile of the maximum normal and longitudinal peak-to-peak accelerations along the left floor beam for the 0°, -15°, and -30° roll tests. The highest peak-to-peak levels measured at any time during the tests at each accelerometer location along the floor beam are shown.

The average value of the highest peak-to-peak accelerations along the floor beam in the normal direction (fig. 22(a)) for the 0°, -15°, and -30° roll tests is shown (fig. 22(a)) to be 106g, 80g, and 91g, respectively. In the longitudinal direction (fig. 22(b)), the average of the peak-to-peak acceleration values for the 0°, -15°, and -30° roll tests was 47g, 43g, and 34g, respectively.

The profile of normal peak-to-peak accelerations in figure 22(a) indicates the effect of airplane roll on the floor structure accelerations during impact. The 0° roll test had the highest peak-to-peak acceleration pulses in the nose and in the vicinity of the main spar. The -15° and -30° roll tests had the highest normal peak-to-peak accelerations in the nose of the airplane. As opposed to the 0° roll test, however, the accelerations decreased from the nose to the vicinity of the cockpit; then they increased toward the aft portion of the airplane cabin.

As shown in figure 22(b), the 0° and -15° roll tests had nearly constant longitudinal peak-to-peak acceleration profiles for the entire length of the floor beam.

Accelerations on Cabin Seats and Occupants

The normal accelerations on the floor under the seat and on the pelvis of the first passenger are presented in figure 23. Accelerometers were mounted on the floor adjacent to each of the four seat legs in the specimen for the 0° roll test. In the specimens used for the -15° and -30° roll tests, one accelerometer each was mounted in the dummy pelvis, on the seat pan, and on the floor midway

between the two seat legs on the aisle side and midway between the two seat legs on the window side.

Normal accelerations at 0° roll.- Figure 23(a) shows the normal accelerations for the 0° roll test specimen. Peak-to-peak accelerations of 130g and 81g were recorded on the floor under the two front seat legs at the first-passenger location, and accelerations of 76g were recorded in the pelvis approximately 0.024 sec later. The peak-to-peak accelerations on the floor under the rear seat legs were 60g and 80g. A 36g pulse on the pelvis occurred approximately 0.017 sec later.

Normal accelerations at -15° roll.- The accelerations for the first-passenger seat, seat pan, and dummy pelvis are shown in figure 23(b). The accelerations on the seat pan and dummy pelvis show the reaction of the dummy to the impact of the nose section. Following wing impact, the dummy at the first-passenger position was forced toward the left window and then back into an upright position. This uprighting was associated with a 10g pulse on both the pelvis and seat pan (0.04 sec). During fuselage main spar contact, a positive 10g pulse caused the dummy to rebound and lift up on the seat. The primary input to the seat occurred at fuselage main spar contact (0.12 sec).

Normal accelerations at -30° roll.- Accelerations for the floor under the first-passenger seat, seat pan, and dummy pelvis for the -30° roll test specimen are shown in figure 23(c). The accelerometer on the window side of the first-passenger seat shows the same oscillatory motion as in the -15° roll test resulting from the loading of the wing aft attachment to the fuselage. Accelerations on the aisle side are low during the wing skid time as a result of the deformation and failure of the wing structure (see fig. 18), which resulted in discontinuities and less transmission of forces to the fuselage. As the fuselage at the main spar location contacts the impact surface, accelerations of about -40g and -50g on the floor under the aisle and window side seats are reflected as a pulse of approximately 20g on the seat pan at about the same time. The dummy pelvis acceleration also was approximately 20g. As in the -15° roll test specimen, the small reversing of the acceleration traces on the seat pan and dummy pelvis prior to nose contact is associated with the uprighting of the dummy in its seat. Normal accelerations on the floor at the first-passenger location and at the dummy's pelvis were highest for the 0° roll test and lowest for the -15° roll test. It should be noted that piezoelectric accelerometers were used in the dummy pelvis for the 0° roll test, whereas strain-gage accelerometers were used for the -15° and -30° roll tests.

Longitudinal accelerations at 0°, -15°, and -30° roll.- The longitudinal accelerations for the first-passenger seat and dummy pelvis are shown in figure 24. Accelerometer locations were the same as for the normal accelerometers except for the seat pan accelerations, which are not shown. Instead, lap-belt time history forces (loads) are shown for the -15° and -30° roll tests.

Floor longitudinal accelerations for the three tests were not higher than 60g at the first-passenger location. Response to the impact at the dummy's pelvis was an acceleration pulse of 115g for the 0° roll test and 10g for the -15° and -30° tests. Lap-belt loads were approximately 600 N for both -15° and -30° tests. Belt loads were not measured in the 0° roll test.

Transverse accelerations at -15° and -30° roll.- The transverse acceleration time histories are presented in figure 25 for the -15° and -30° roll test specimens. The accelerometers were mounted in the dummy pelvis and on the floor beam midway between the aisle-seat legs and on the frame midway between the two window-seat legs. There were no transverse accelerometers for the 0° roll test specimen for the first-passenger location.

Transverse accelerations for the -15° and -30° roll tests (figs. 25(a) and 25(b)) were generally below 50g at both floor locations when the right wing of the airplane slammed onto the impact surface. Response to the impact at the dummy's pelvis was an acceleration pulse of about 5g for both tests.

SUMMARY OF RESULTS

Three full-scale twin-engine airplanes were crash tested at roll angles of 0°, -15°, and -30° with a flight-path angle of -15° and a velocity of 27 m/sec. These tests were part of a program to investigate airplane response to controlled crash conditions. The results are summarized in the following observations:

1. Structural damage to the fuselages in the 0°, -15°, and -30° tests consisted of skin buckling, rivet shear failure, and separation of the cabin along the window ledge. The rivet shear and deformation across the top of the cabin in all three tests did not significantly reduce the livable volume inside the cabin.

2. In the 0°, -15°, and -30° tests, moderate buckling of the floor beams and supporting frames and buckling of the left main spar near the spar splice were observed. The airplane used in the -15° roll test experienced a near total separation of the tail section, in the vicinity of the door.

3. Of the three airplanes tested, the airplane in the -30° roll test experienced the least structural damage, except for the left wing, which was severely damaged.

4. For each of the three tests, a trend in normal acceleration levels was observed along the left floor beam: accelerations were high in the nose, lower in the pilot-copilot compartment, and high in the cabin aft of the main spar. The longitudinal accelerations on the left floor beam showed average values of less than 50g for all three tests.

5. In the cabin area at the first-passenger location, normal accelerations on the floor (130g) and at the dummy's pelvis (76g) were highest for the 0° roll test and recorded 20g or less in the -15° and -30° roll tests. Floor longitudinal accelerations were not higher than 60g for all three tests. Longitudinal accelerations at the dummy's pelvis were 115g for the 0° test and 10g for the -15° and -30° tests. Lap belt loads were approximately 600 N for both the -15° and the -30° tests. Belt loads were not measured for the 0° test. Transverse accelerations on the floor were below 50g; in the dummy's pelvis transverse accelerations were about 5g for both the -15° and the -30° tests. Transverse accelerations were not measured at these locations in the 0° test.

6. For these particular tests on low-wing airplanes impacting a concrete surface, the introduction of roll angle reduced the loads transmitted to the occupant dummies.

Langley Research Center
National Aeronautics and Space Administration
Hampton, VA 23665
September 10, 1979

REFERENCES

1. Preston, G. Merritt; and Moser, Jacob C.: Crash Loads. NACA Conference on Airplane Crash-Impact Loads, Crash Injuries and Principles of Seat Design for Crash Worthiness (Cleveland, Ohio), Apr. 1956, pp. 2-1 - 2-47.

2. Eiband, A. Martin; Simpkinson, Scott H.; and Black, Dugald O.: Accelerations and Passenger Harness Loads Measured in Full-Scale Light-Airplane Crashes. NACA TN 2991, 1953.

3. Pinkel, I. Irving; and Rosenberg, Edmund G.: Seat Design for Crash Worthiness. NACA Rep. 1332, 1957. (Supersedes NACA TN 3777.)

4. Alfaro-Bou, E.; Hayduk, R. J.; Thomson, R. G.; and Vaughan, V. L., Jr.: Simulation of Aircraft Crash and Its Validation. Aircraft Crashworthiness, Kenneth Saczalski, George T. Singley III, Walter D. Pilkey, and Ronald L. Huston, eds., Univ. Press of Virginia, c.1975, pp. 485-497.

5. Vaughan, Victor L., Jr.; and Alfaro-Bou, Emilio: Impact Dynamics Research Facility for Full-Scale Aircraft Crash Testing. NASA TN D-8179, 1976.

6. Castle, Claude B.; and Alfaro-Bou, Emilio: Light Airplane Crash Tests at Three Flight-Path Angles. NASA TP-1210, 1978.

7. Humanoid Systems. Report on Part 572 (GM HYBRID-II) Anthropomorphic Test Dummy. Alderson Biotechnology Corp., Jan. 31, 1974.

8. Alfaro-Bou, Emilio; and Vaughan, Victor L., Jr.: Light Airplane Crash Test at Impact Velocities of 13 and 27 m/sec. NASA TP-1042, 1977.

TABLE I.- NOMINAL IMPACT PARAMETERS FOR TWIN-ENGINE AIRPLANE CRASH TEST PROGRAM

Flight path, deg	Pitch angle, deg	Roll angle, deg	Yaw angle, deg	Angle of attack, deg	Velocity, m/sec	Data source
-15	-15	0	0	0	13	Reference 8
[a]-15	-15	0	0	0	[b]27	Reference 8 and present paper
-30	-30	0	0	0	27	Reference 6
-45	-45	0	0	0	27	Reference 6
-15	0	0	0	15	27	Unpublished
-15	15	0	0	30	27	Unpublished
[a]-15	-15	-15	0	0	27	Present paper
[a]-15	-15	-30	0	0	27	Present paper

[a]Specifically discussed in present paper.
[b]Maximum velocity for free fall due to height limitation.

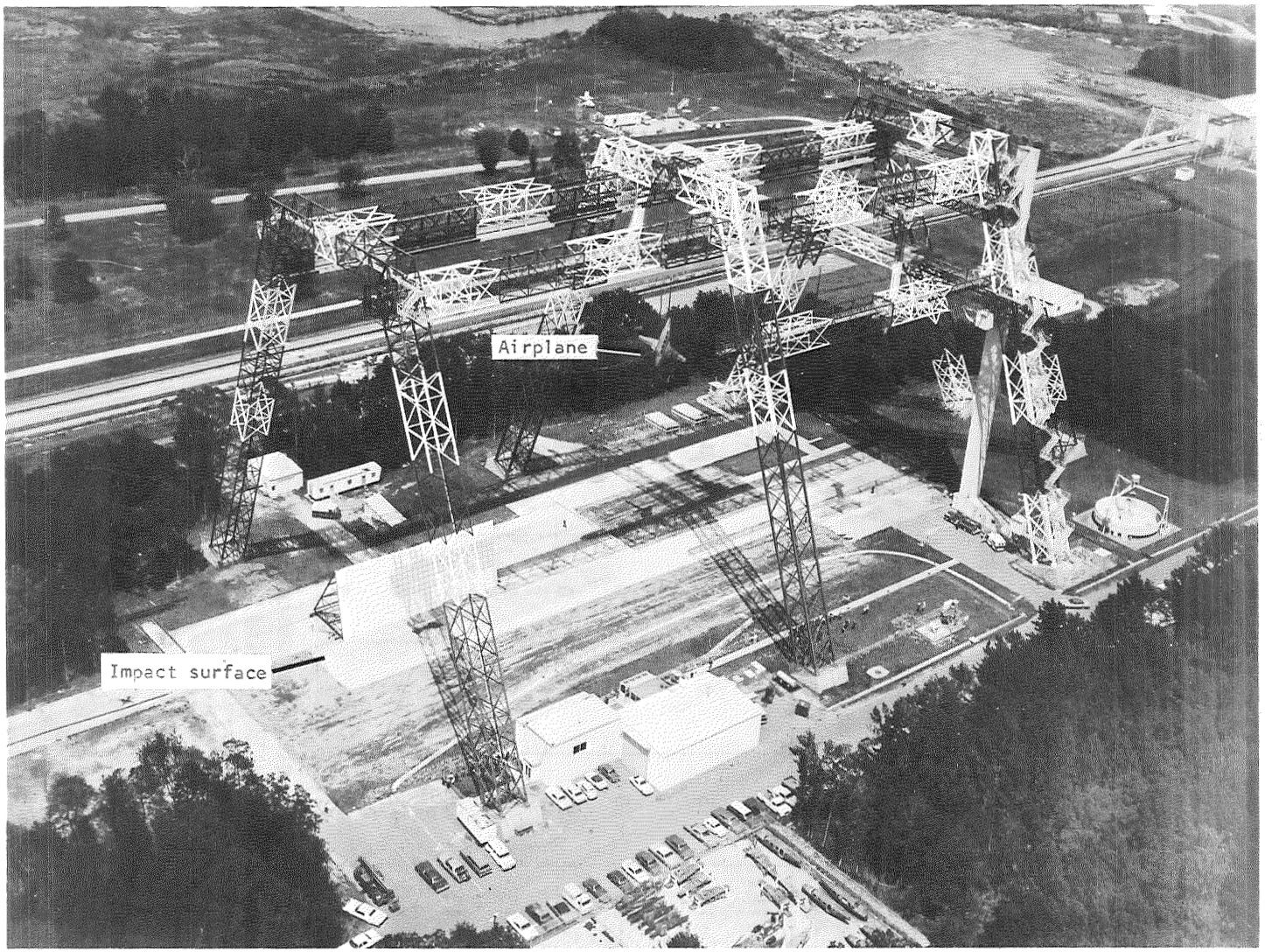

L-74-2505.5

Figure 1.- Langley impact dynamics research facility.

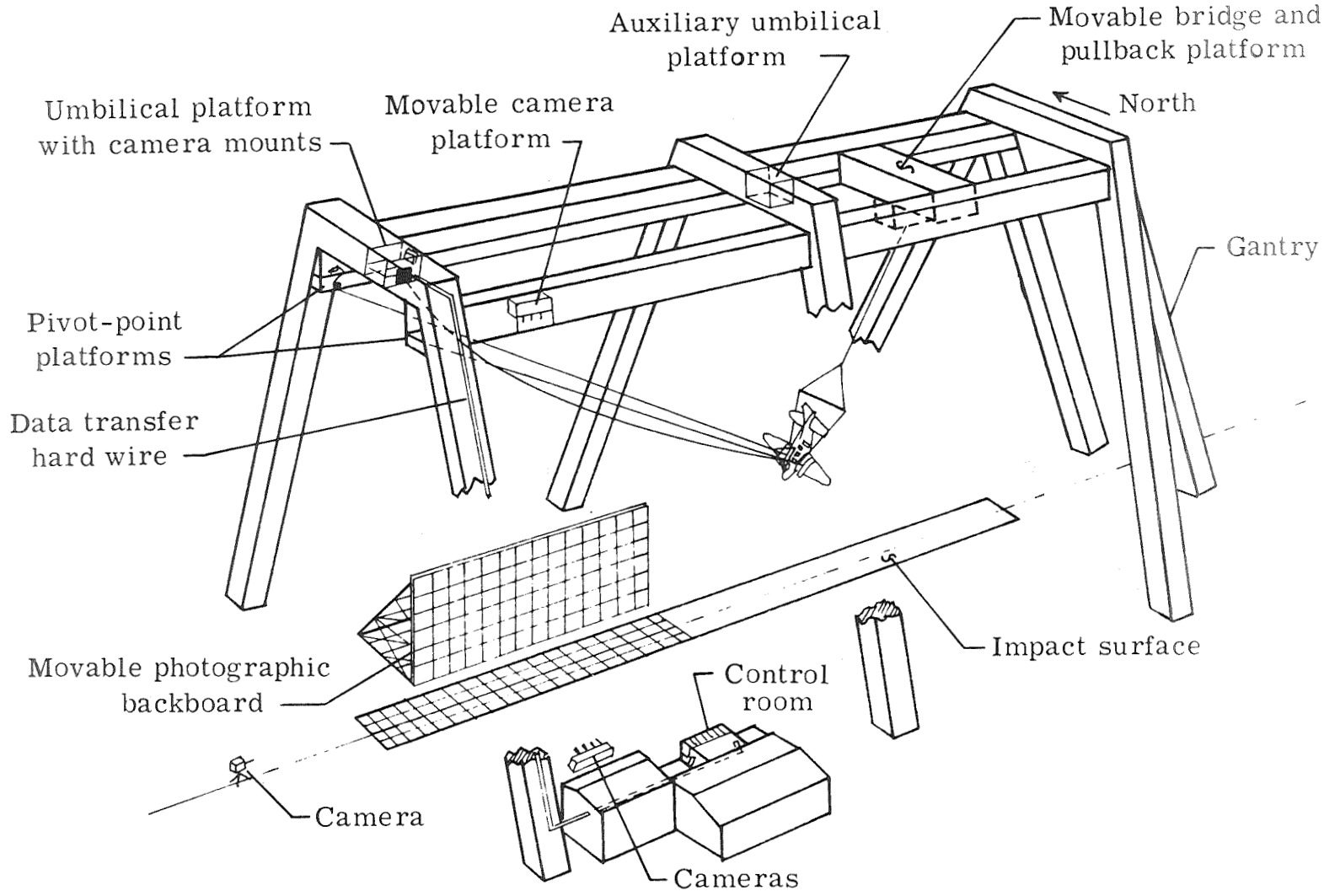

Figure 2.- Diagram of Langley impact dynamics research facility.

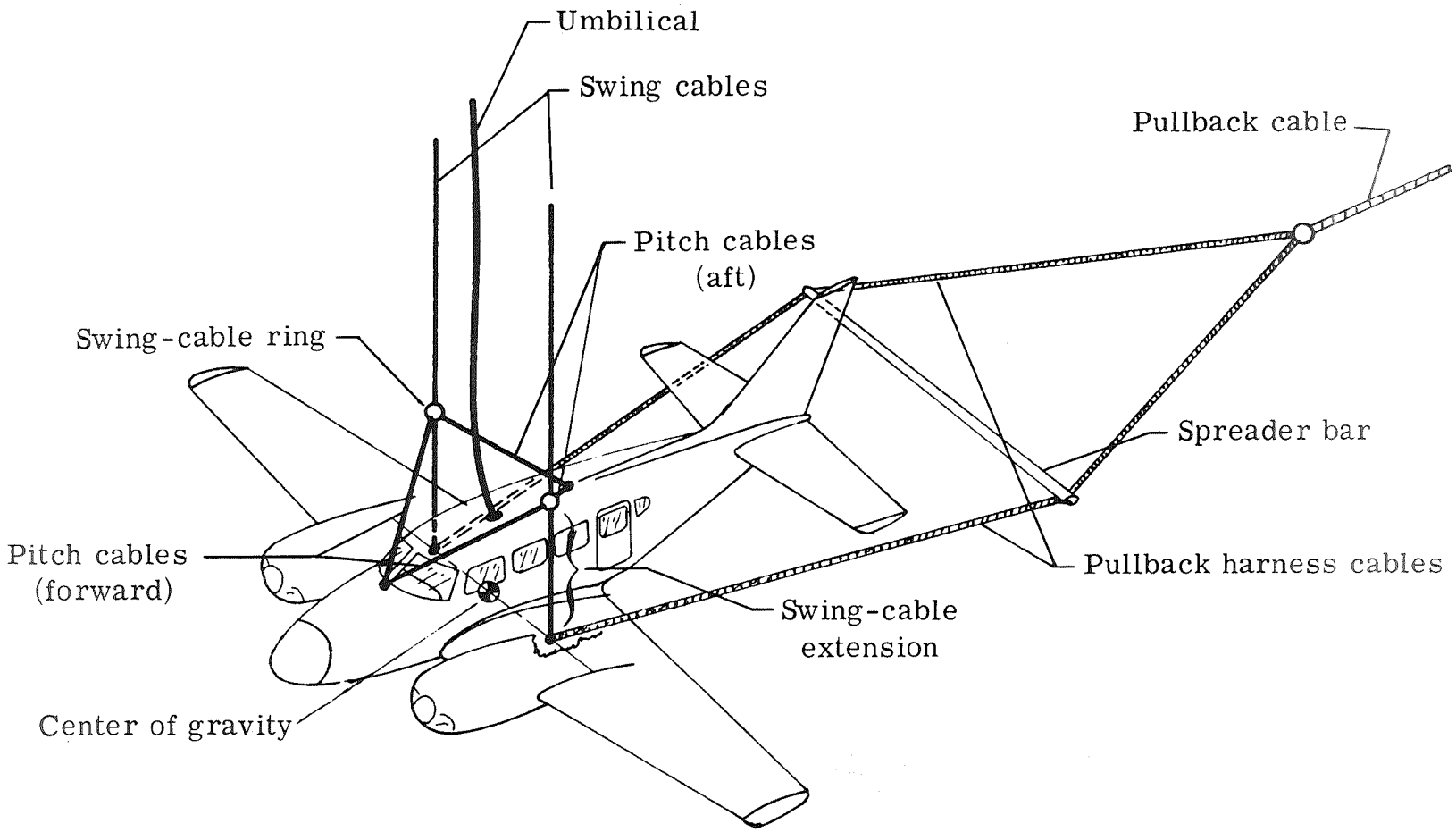

Figure 3.- Airplane suspension system.

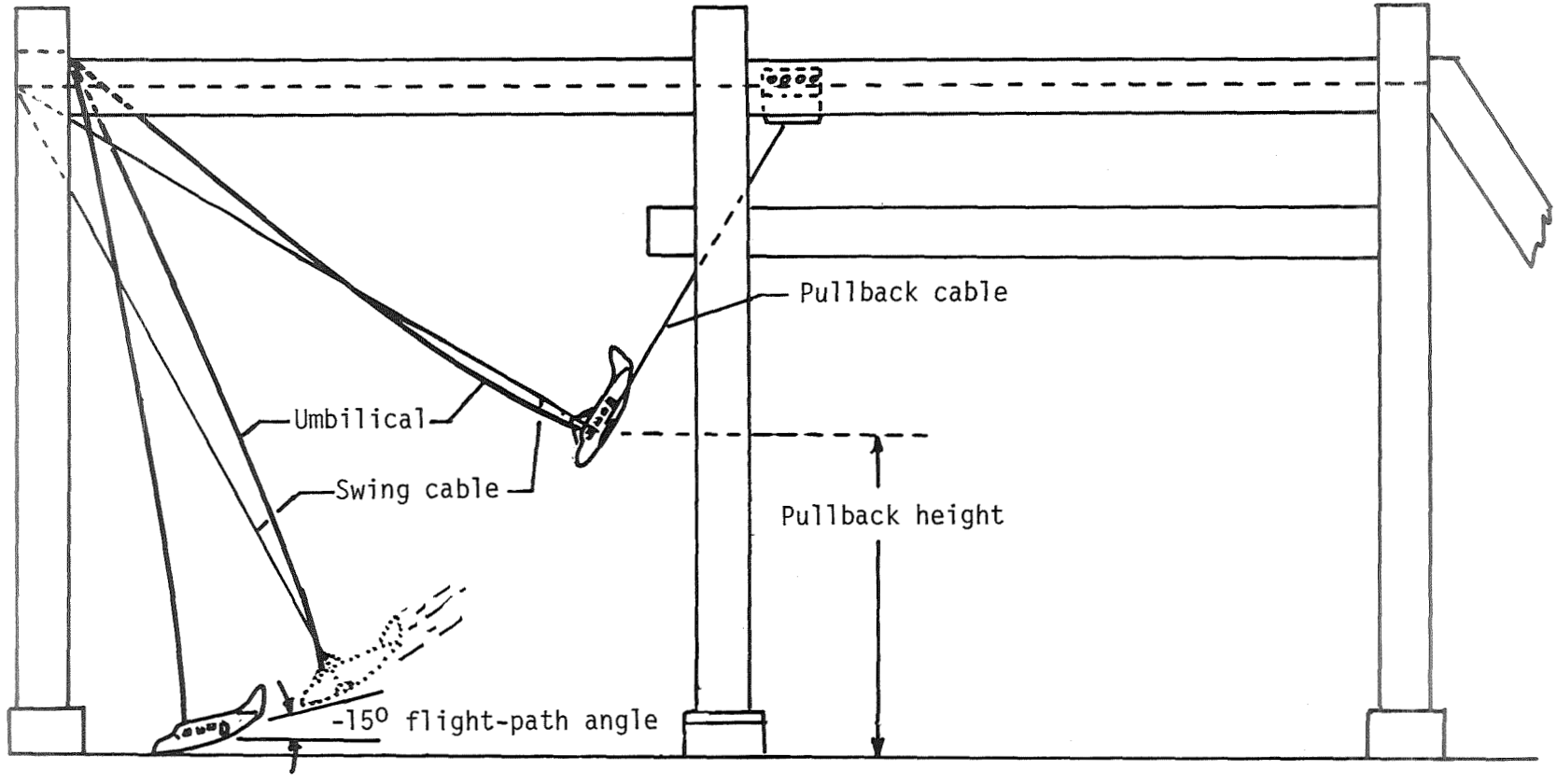

Figure 4.- Crash sequence of test airplane.

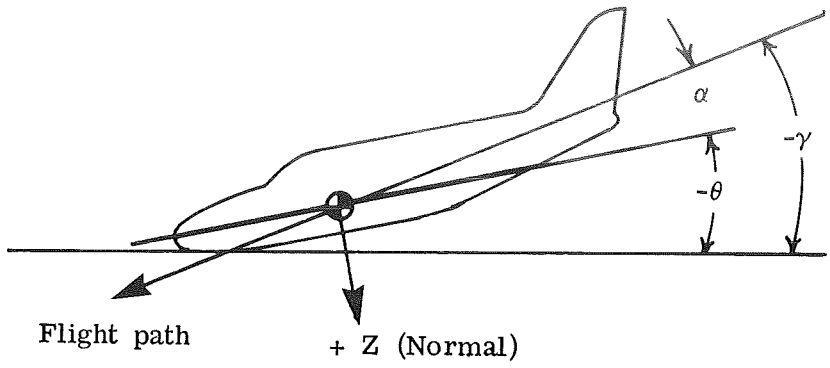

γ Flight-path angle
α Angle of attack
θ Pitch angle

$$\theta = \gamma + \alpha$$

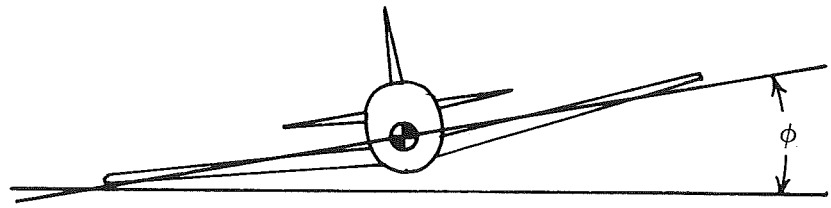

ϕ Roll angle

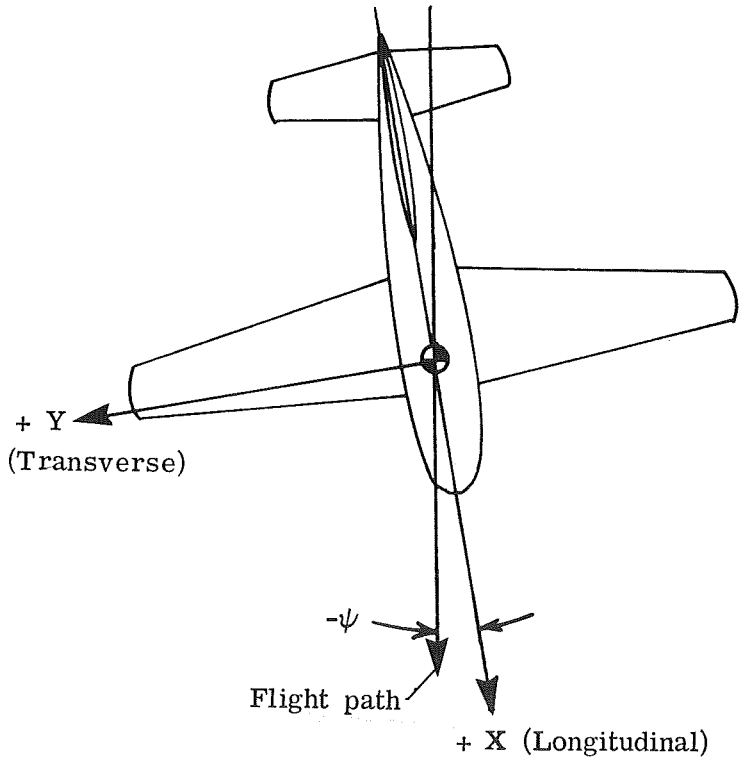

ψ Yaw angle

Figure 5.- Flight path, crash attitude, axes, and force directions.

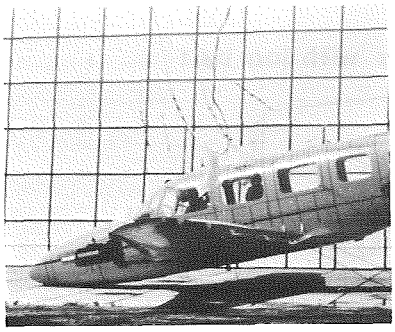

Test parameter	Planned	Actual
Flight path, deg	-15.0	-16.0
Free-flight time, sec	0.07	0.07
Angle of attack, deg	0.0	4.0
Pitch angle, deg	-15.0	-12.0
Yaw angle, deg	0.0	1.5
Roll angle, deg	0.0	0.0
Flight-path velocity, m/sec	26.8	26.6
Vertical velocity, m/sec	6.9	7.3
Horizontal velocity, m/sec	25.9	25.6

(a) 0° test.

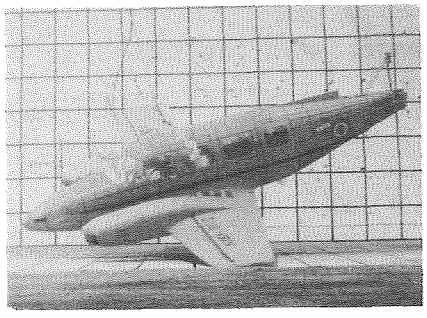

Test parameter	Planned	Actual
Flight path, deg	-15.0	-18
Free-flight time, sec	0.07	0.07
Angle of attack, deg	0.0	4
Pitch angle, deg	-15.0	-14
Yaw angle, deg	0.0	-8
Roll angle, deg	-15.0	-15
Flight-path velocity, m/sec	26.8	27.8
Vertical velocity, m/sec	6.9	8.6
Horizontal velocity, m/sec	25.9	26.4

(b) -15° test.

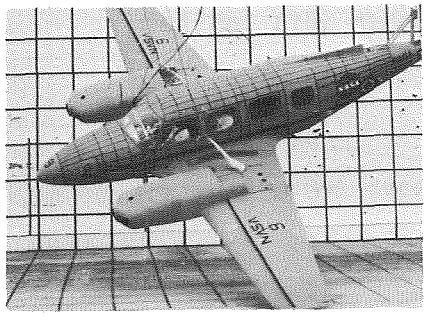

Test parameter	Planned	Actual
Flight path, deg	-15.0	-16
Free-flight time, sec	0.07	0.07
Angle of attack, deg	0.0	3
Pitch angle, deg	-15.0	-13
Yaw angle, deg	0.0	-14
Roll angle, deg	-30.0	-30
Flight-path velocity, m/sec	26.8	26.3
Vertical velocity, m/sec	6.9	7.3
Horizontal velocity, m/sec	25.9	25.3

(c) -30° test.

L-79-293

Figure 6.- Test airplanes and test parameters.

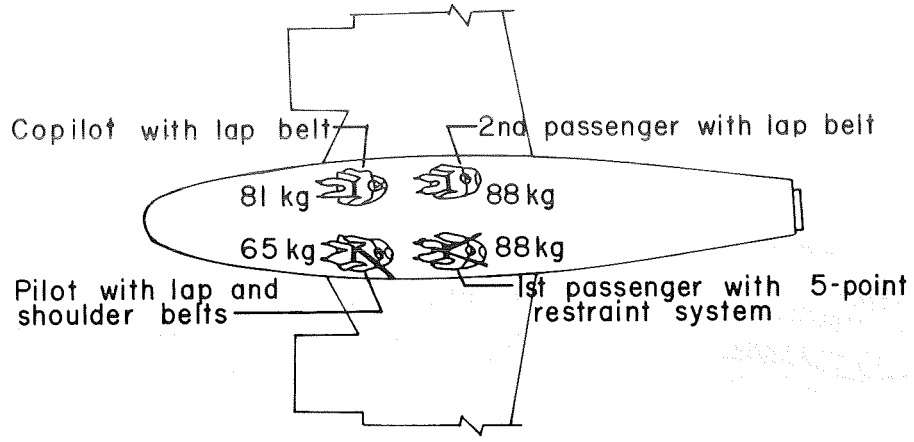

(a) 0° test specimen.

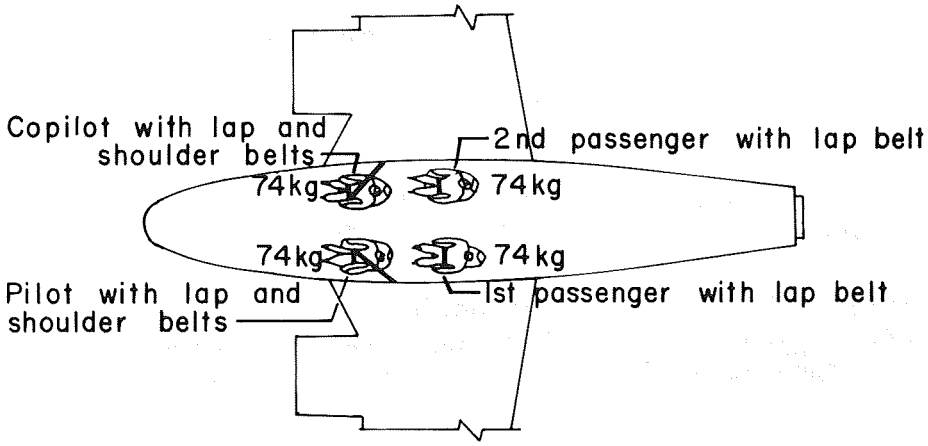

(b) -15° test specimen.

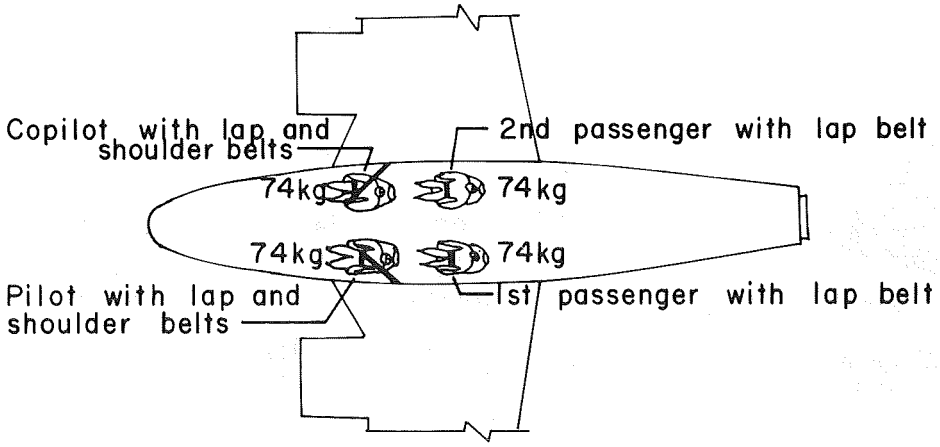

(c) -30° test specimen.

Figure 7.- Arrangement of seats, dummies, and restraint systems for various roll angles.

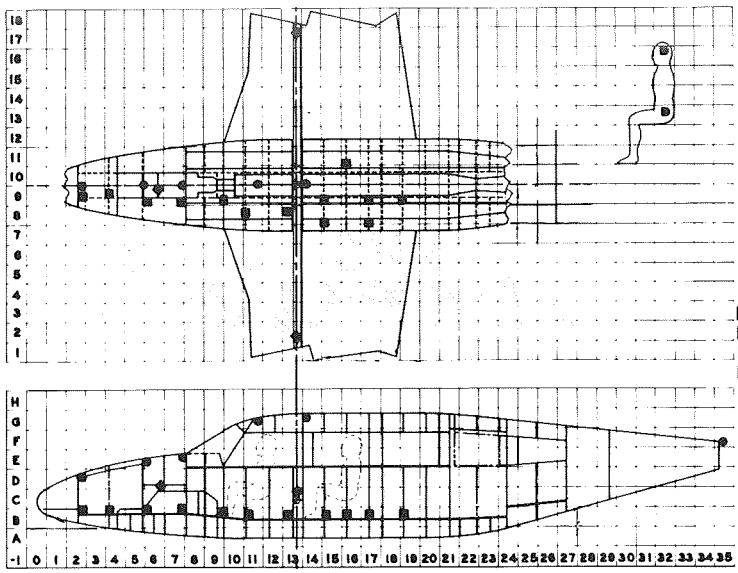

Accelerometer identification

- Floor
- Roof and tail
- Wheel well and wings
- Dummies

Accelerometers in dummies	
Pilot, pelvic, normal	11 C 8
Pilot, pelvic, longitudinal	11 C 8
Pilot, head, normal	12 F 8
Pilot, head, longitudinal	12 F 8
1st passenger, pelvic, normal	16 C 8
1st passenger, pelvic, longitudinal	16 C 8
1st passenger, head, normal	16 F 8
1st passenger, head, longitudinal	16 F 8

(a) 0° test.

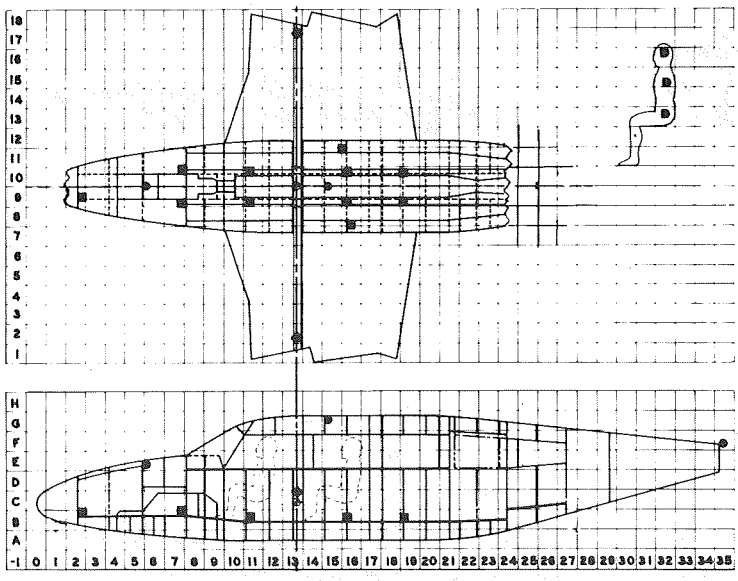

Accelerometers in dummies	
1st passenger, seat pan, normal	16 C 8
1st passenger, pelvic, normal	16 C 8
1st passenger, pelvic, longitudinal	16 C 8
1st passenger, pelvic, transverse	16 C 8
1st passenger, chest, normal	16 E 8
1st passenger, chest, longitudinal	16 E 8
1st passenger, chest, transverse	16 E 8
1st passenger, head, normal	16 F 8
1st passenger, head, longitudinal	16 F 8
1st passenger, head, transverse	16 F 8
2nd passenger, seat pan, normal	16 C 11
2nd passenger, pelvic, normal	16 C 11
2nd passenger, pelvic, longitudinal	16 C 11
2nd passenger, pelvic, transverse	16 C 11
2nd passenger, chest, normal	16 E 11
2nd passenger, chest, longitudinal	16 E 11
2nd passenger, chest, transverse	16 E 11
2nd passenger, head, normal	16 F 11
2nd passenger, head, longitudinal	16 F 11
2nd passenger, head, transverse	16 F 11
Load cells – restraint belts	
1st passenger, lap belt	16 D 8
2nd passenger, lap belt	16 D 11

(b) -15° and -30° test.

Figure 8.- Accelerometer locations.

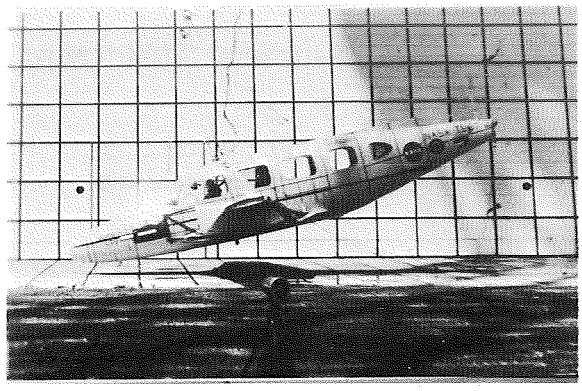

(a) Prior to impact.

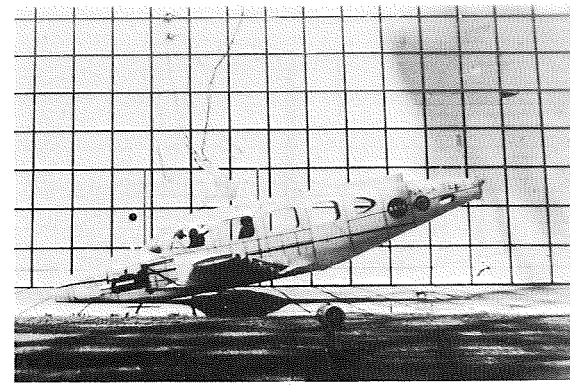

(b) Time = 0.02 sec.

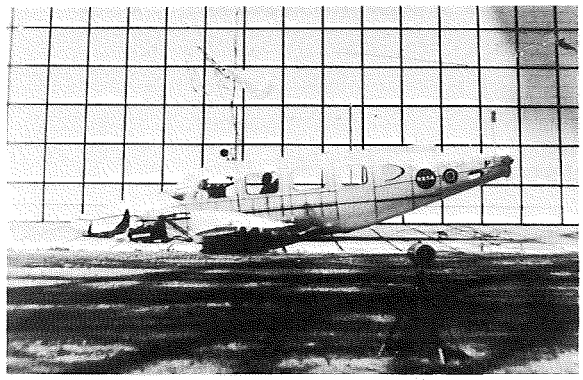

(c) Time = 0.07 sec.

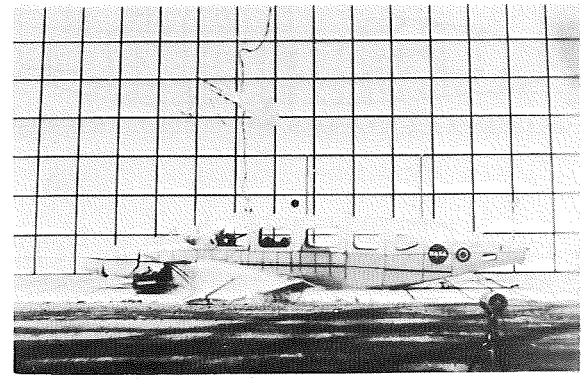

(d) Time = 0.12 sec.

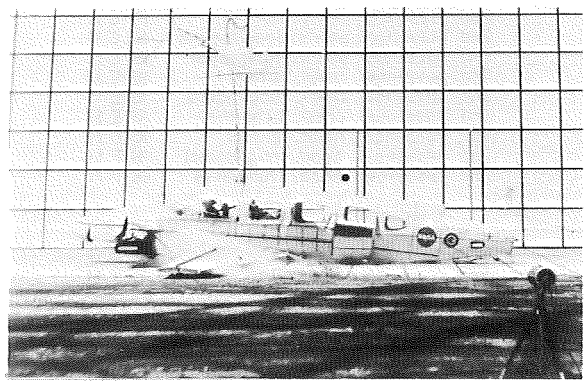

(e) Time = 0.17 sec.

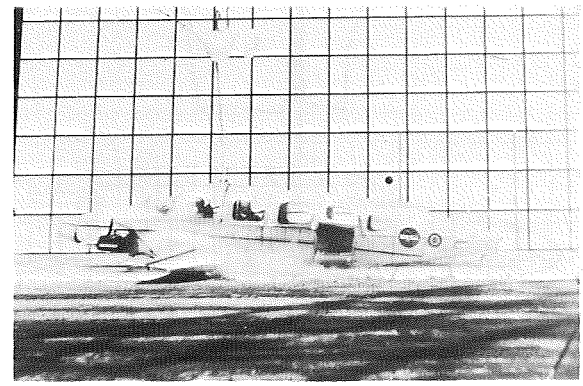

(f) Time = 0.22 sec.

L-79-294

Figure 9.- Photographic sequence of 0^{o} roll test.

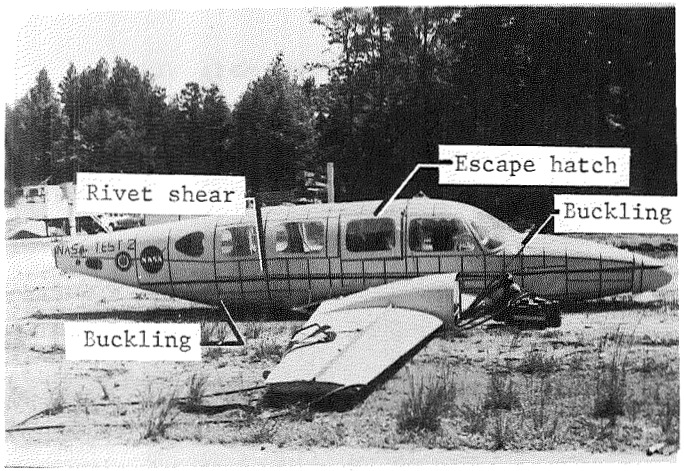

(a) Overall view of right side.

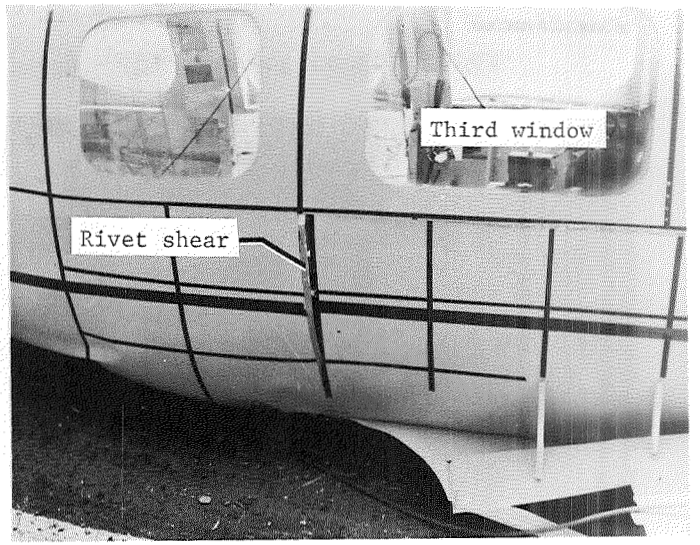

(b) Close-up view of right side.

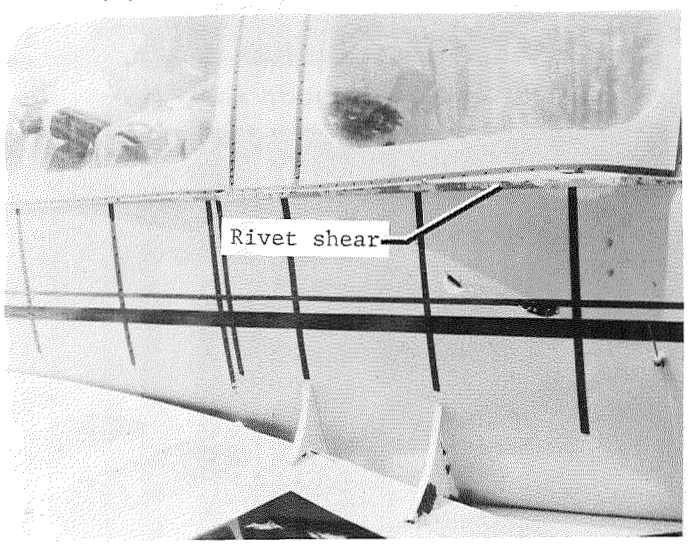

(c) Close-up view of left side.

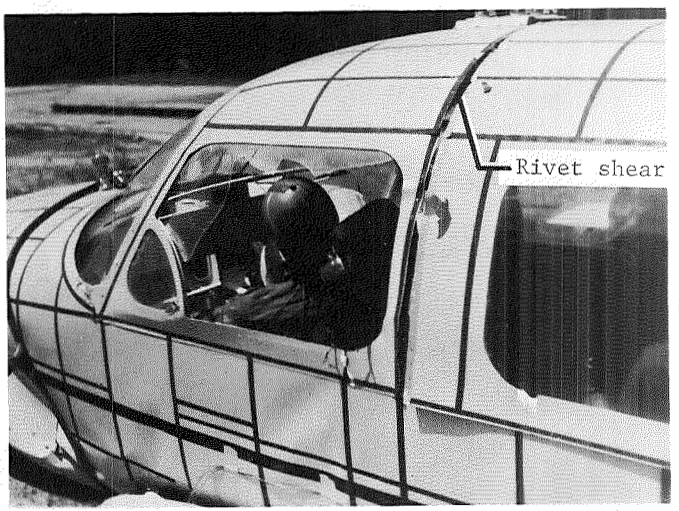

(d) Close-up view of left side and top of fuselage.

Figure 10.- Exterior damage to 0° test.

L-78-95.2

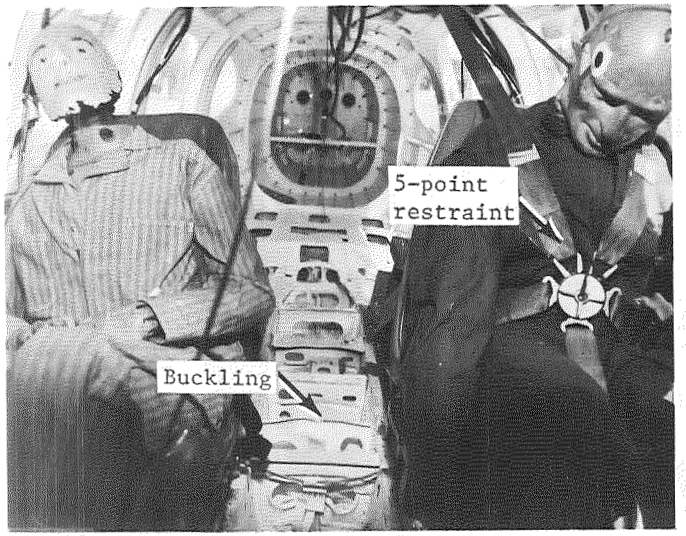

(a) View looking rearward.

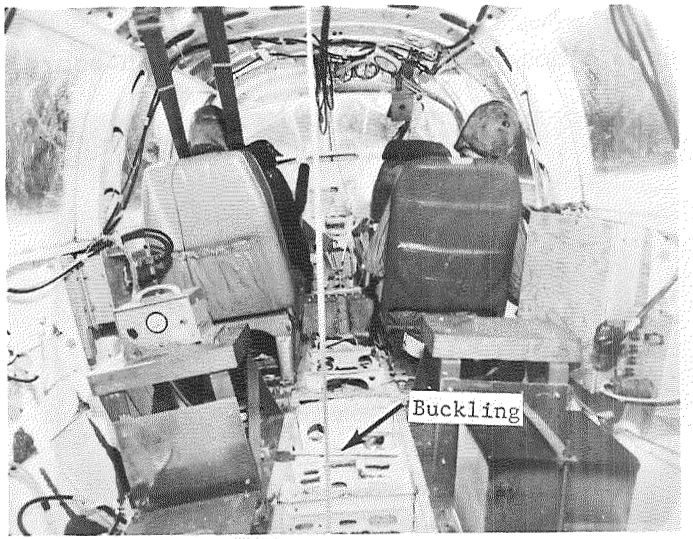

(b) View looking forward.

(c) View through doorway.

(d) View of cockpit area.

L-78-96

Figure 11.- Interior damage to 0° test.

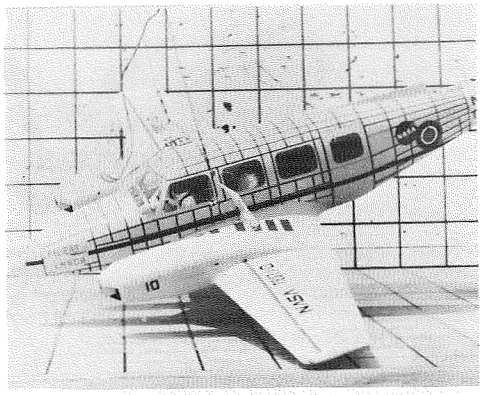

(a) Prior to impact.

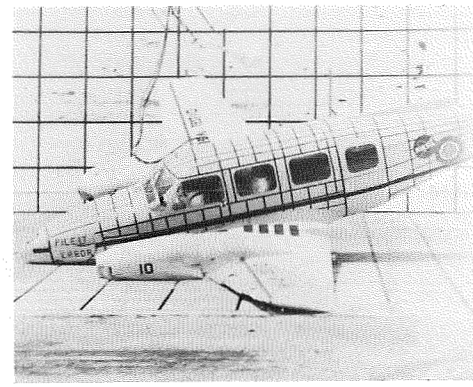

(b) Time = 0.03 sec.

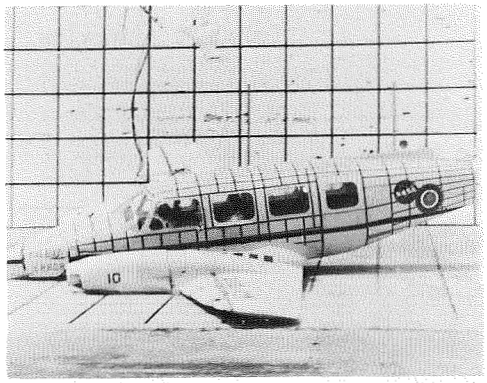

(c) Time = 0.08 sec.

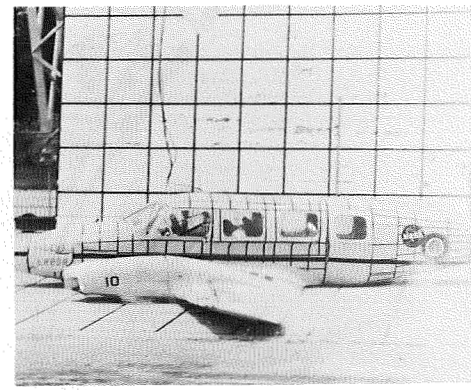

(d) Time = 0.13 sec.

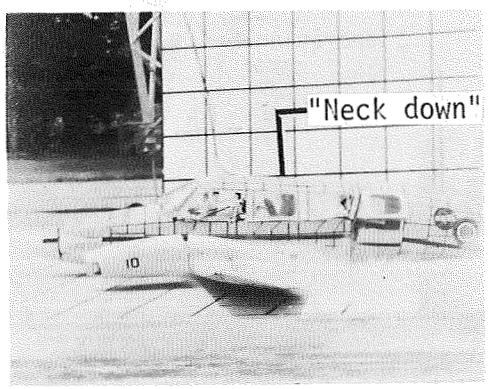

(e) Time = 0.18 sec.

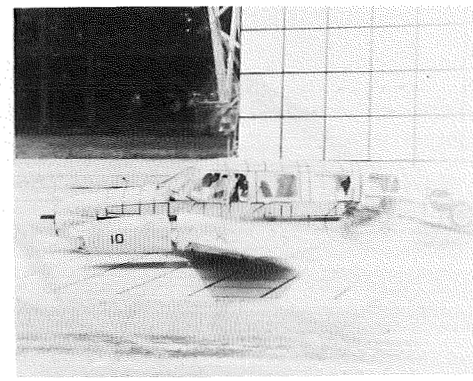

(f) Time = 0.23 sec.

L-79-295

Figure 12.- Photographic sequence of -15° roll test.

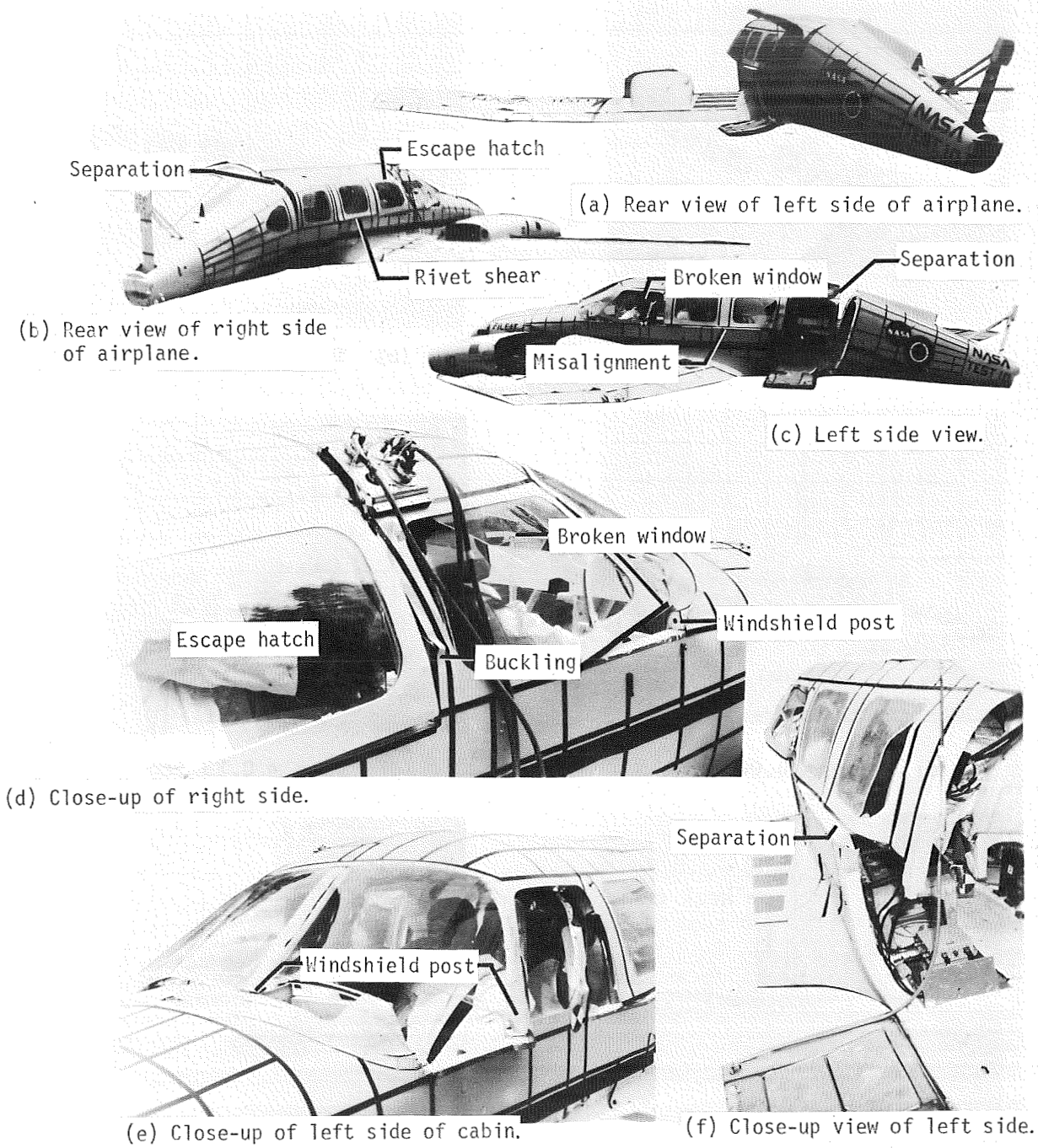

(a) Rear view of left side of airplane.

(b) Rear view of right side of airplane.

(c) Left side view.

(d) Close-up of right side.

(e) Close-up of left side of cabin.

(f) Close-up view of left side.

L-79-296

Figure 13.- Exterior damage to -15° test.

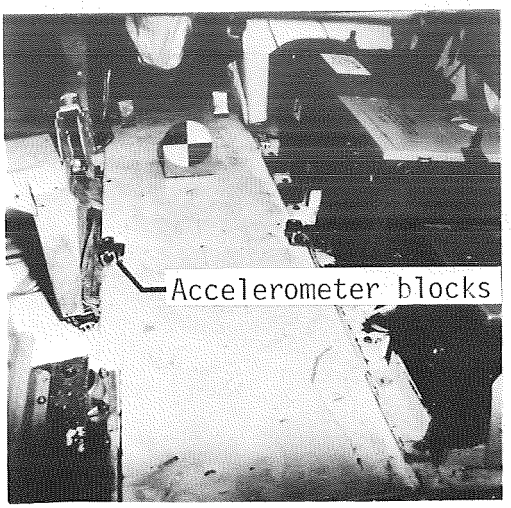

(a) View looking forward in cabin area with floor.

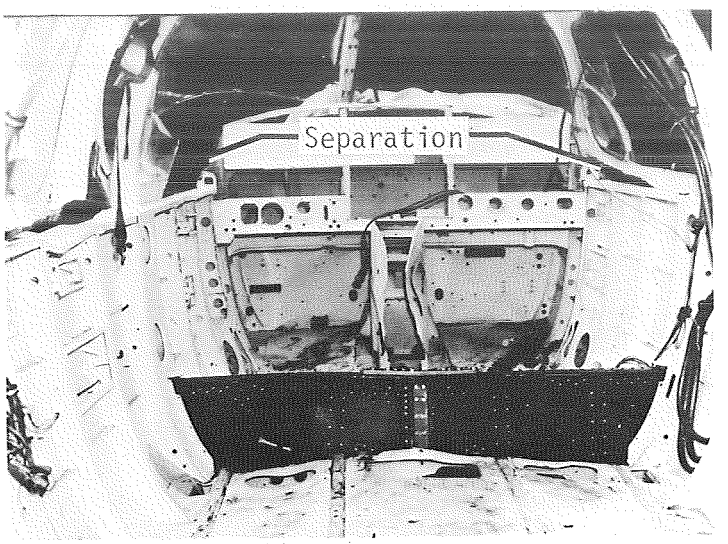

(b) View of cockpit area.

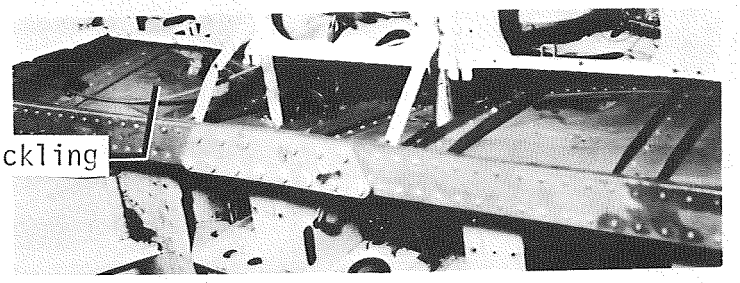

(c) Top view of main spar.

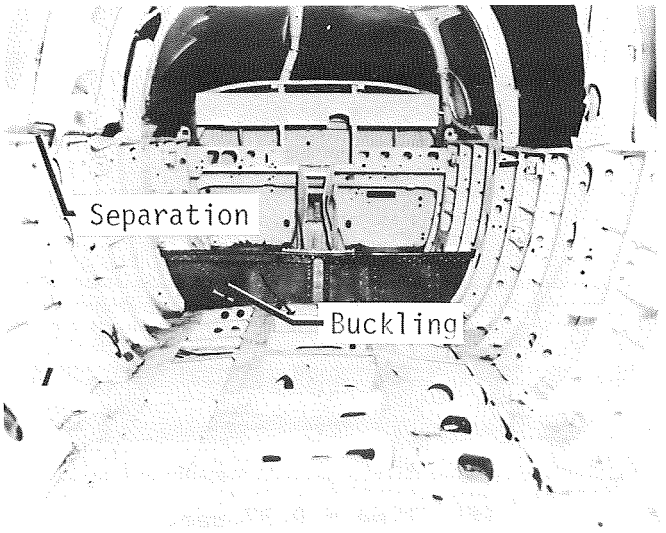

(d) View looking forward in cabin area with floor removed.

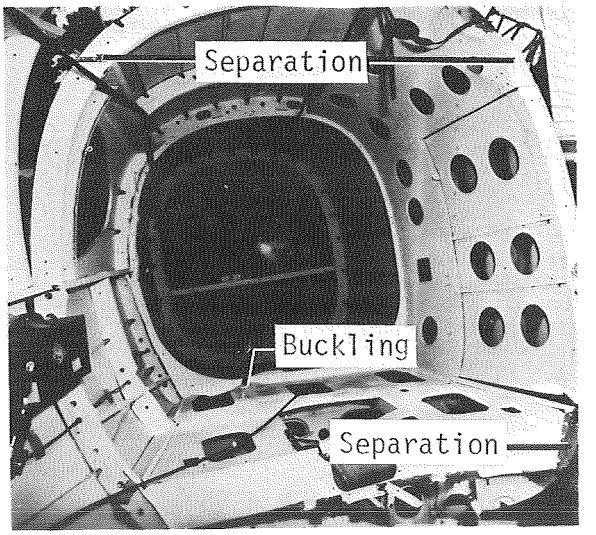

(e) View looking rearward.

L-79-297

Figure 14.- Interior damage to -15° test.

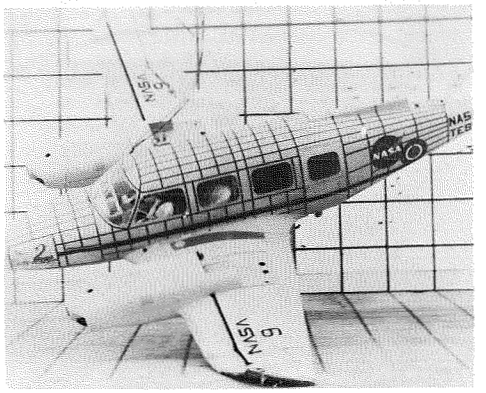

(a) Time = 0.02 sec.

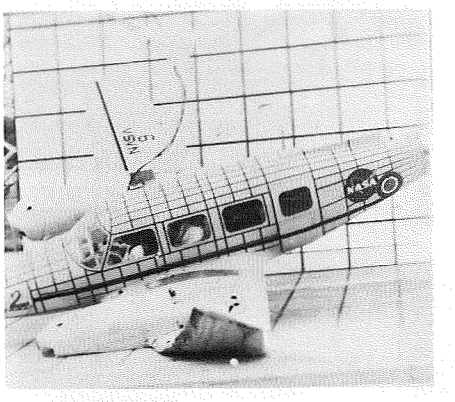

(b) Time = 0.12 sec.

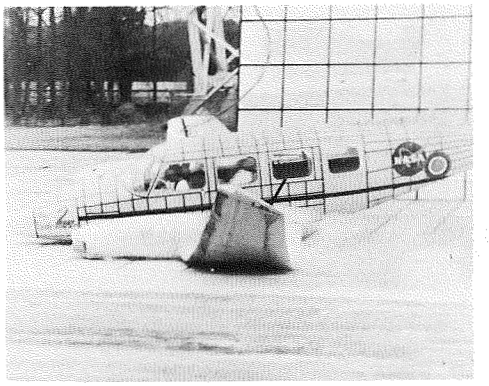

(c) Time = 0.22 sec.

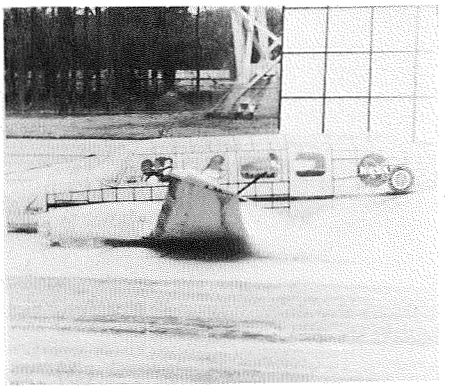

(d) Time = 0.27 sec.

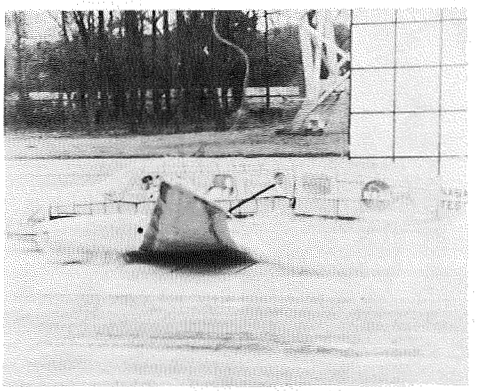

(e) Time = 0.32 sec.

(f) Time = 0.37 sec.

L-79-298

Figure 15.- Photographic sequence of -30° roll test.

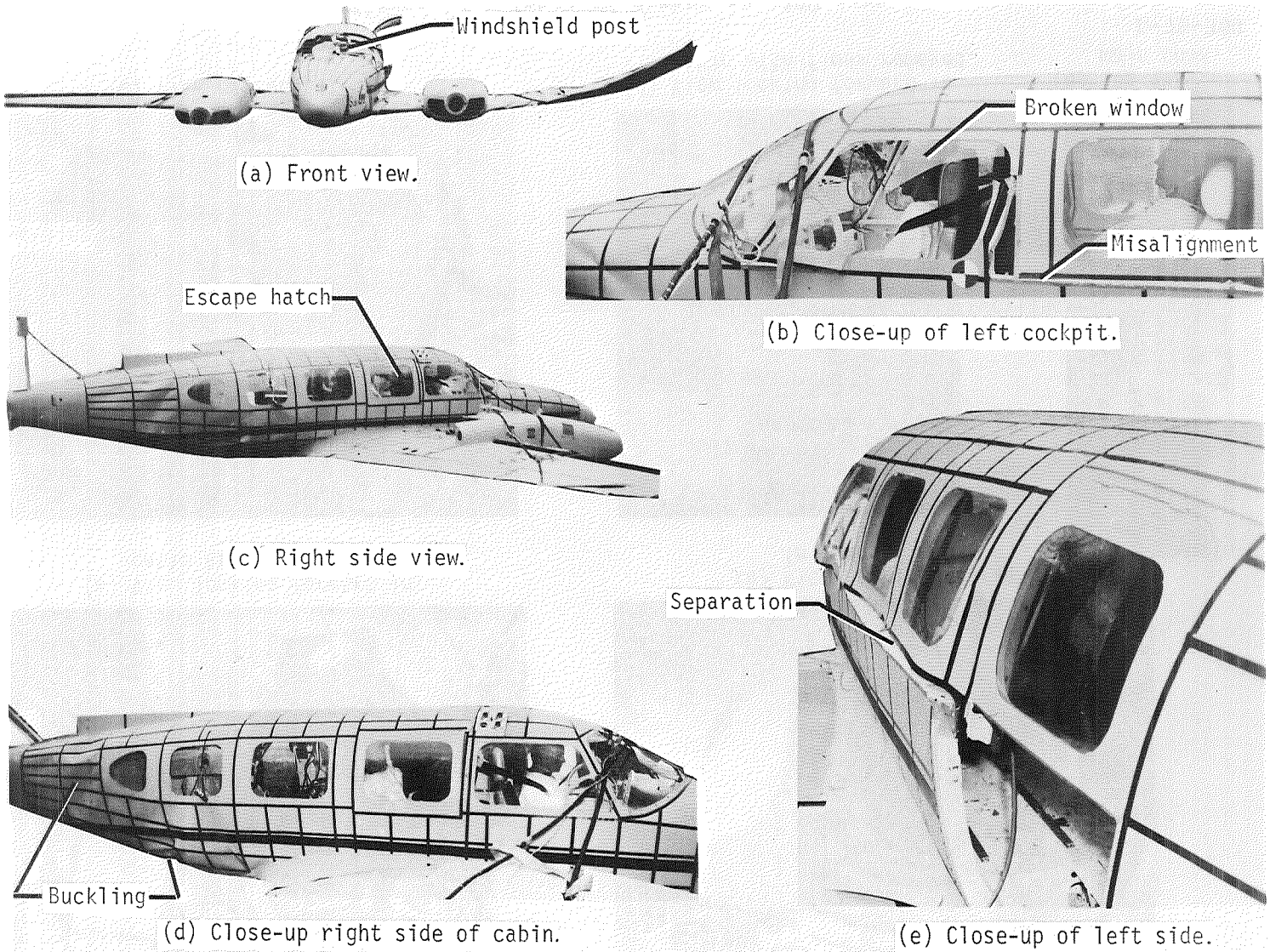

L-79-299

Figure 16.- Exterior damage to -30° test.

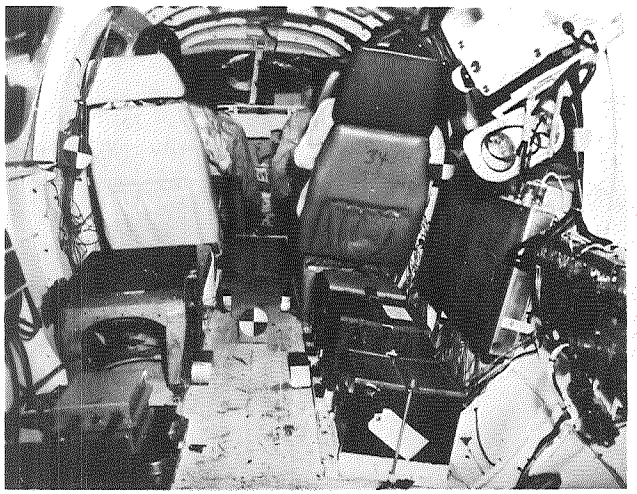

(a) View looking forward in cabin area with floor.

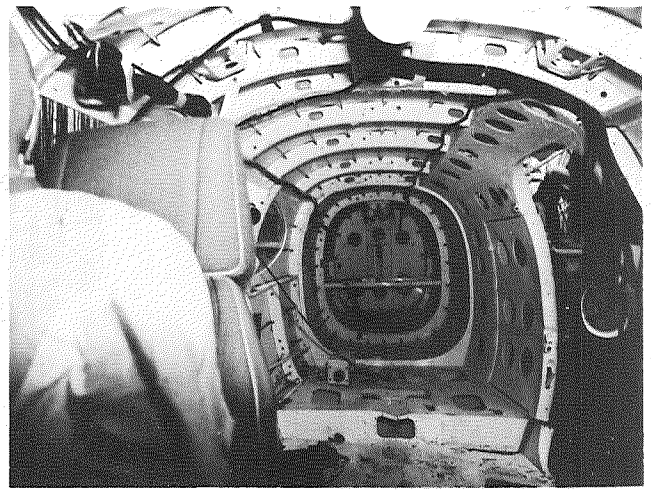

(b) View looking rearward in cabin.

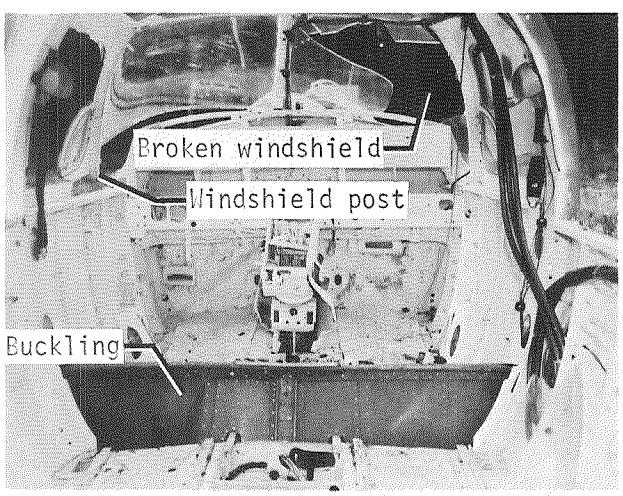

(c) View of cockpit.

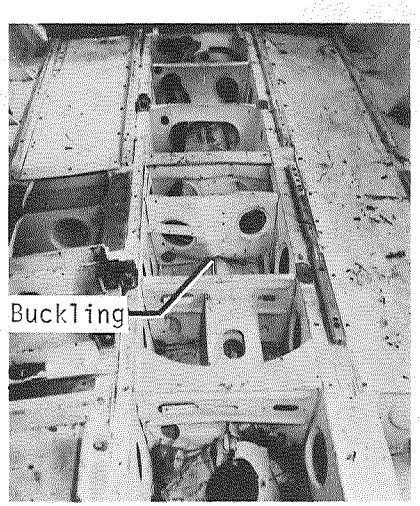

(d) View looking forward in cabin with floor removed.

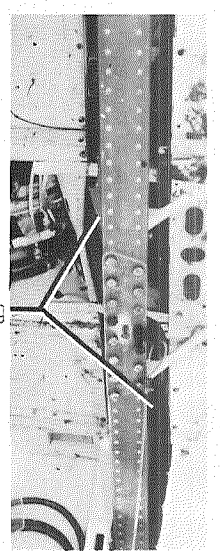

(e) Top view of main spar.

L-79-300

Figure 17.- Interior damage to -30° test.

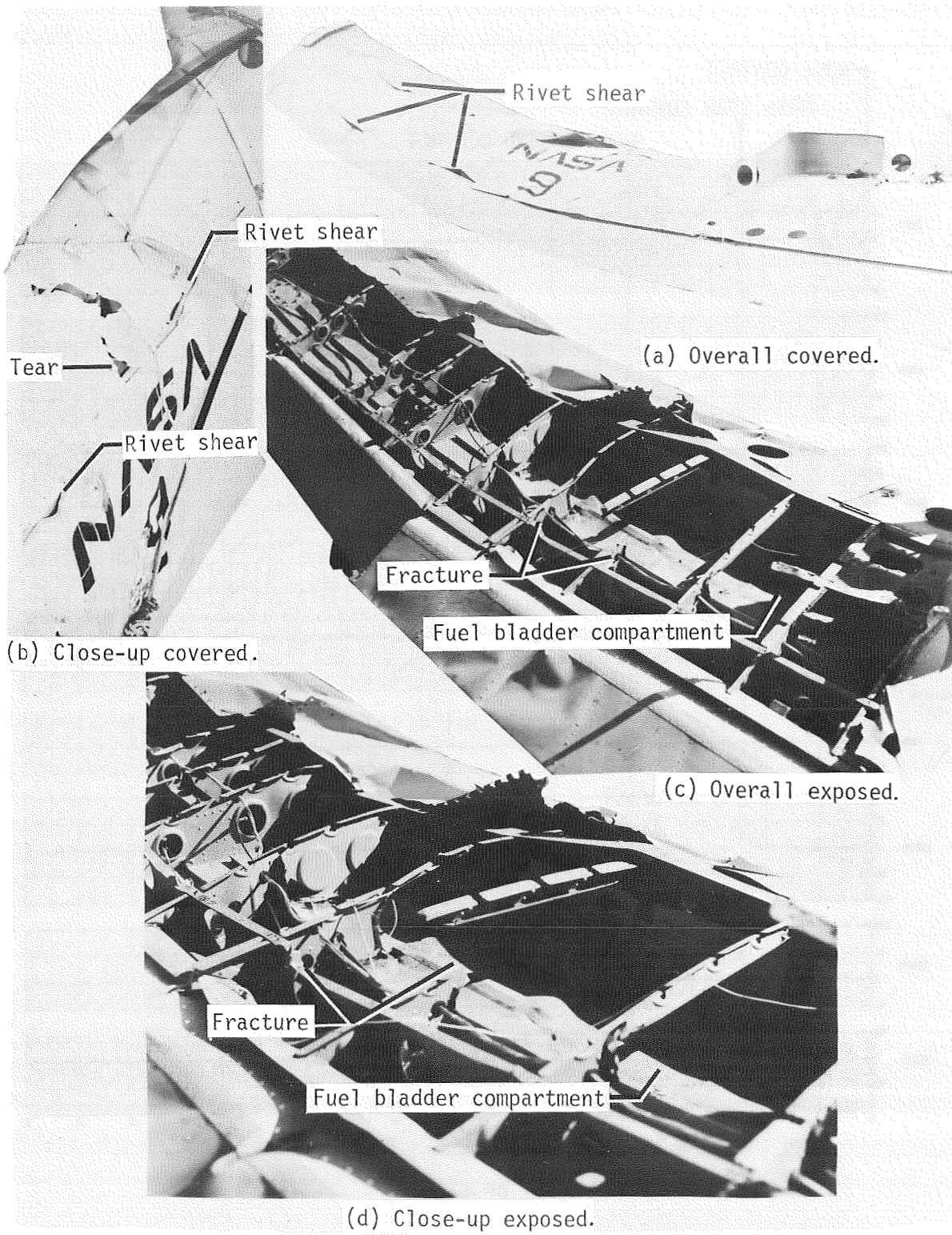

L-79-301

Figure 18.- Damage to left wing in -30° test.

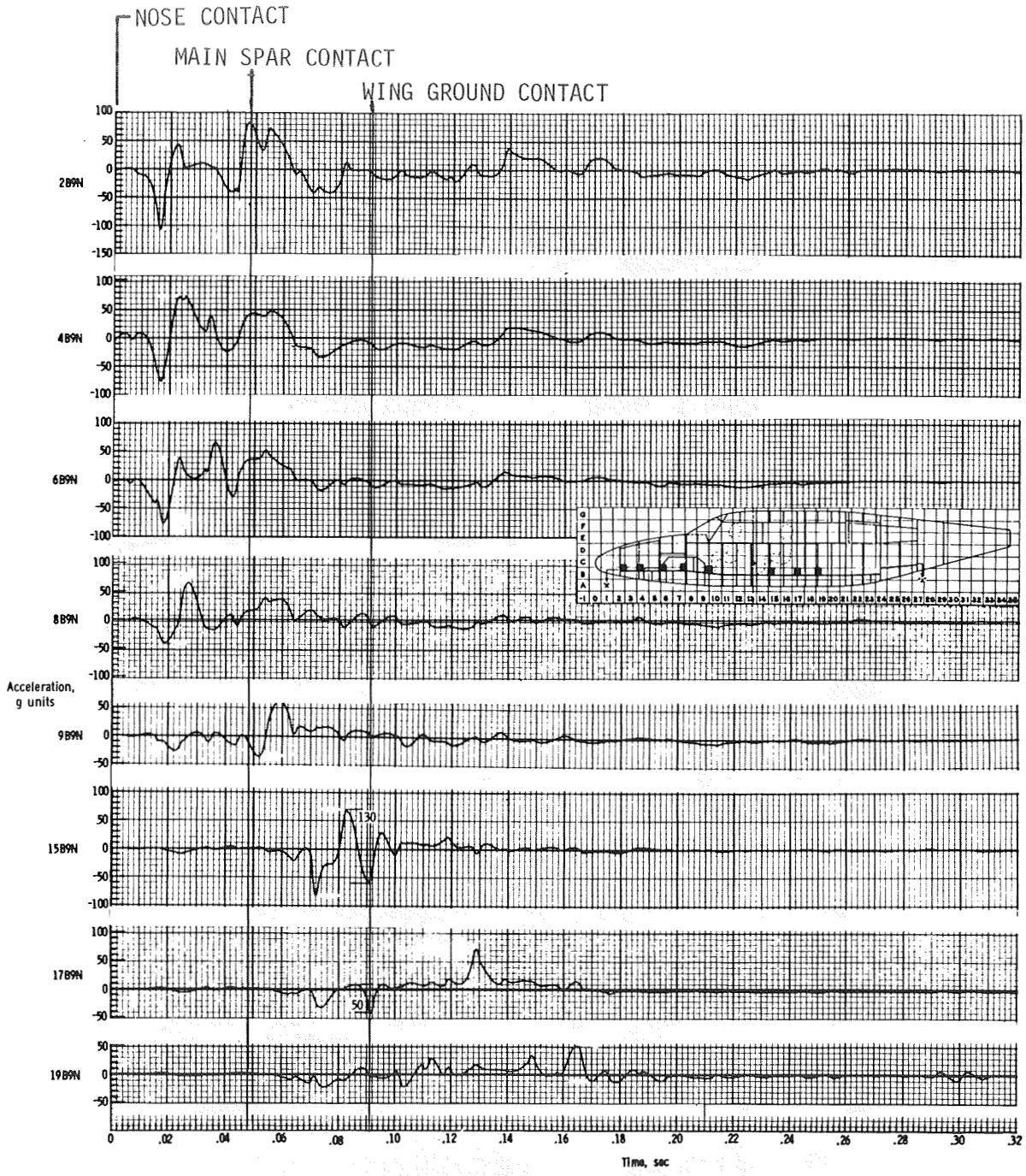

(a) 0° test.

Figure 19.- Time histories of normal accelerations.

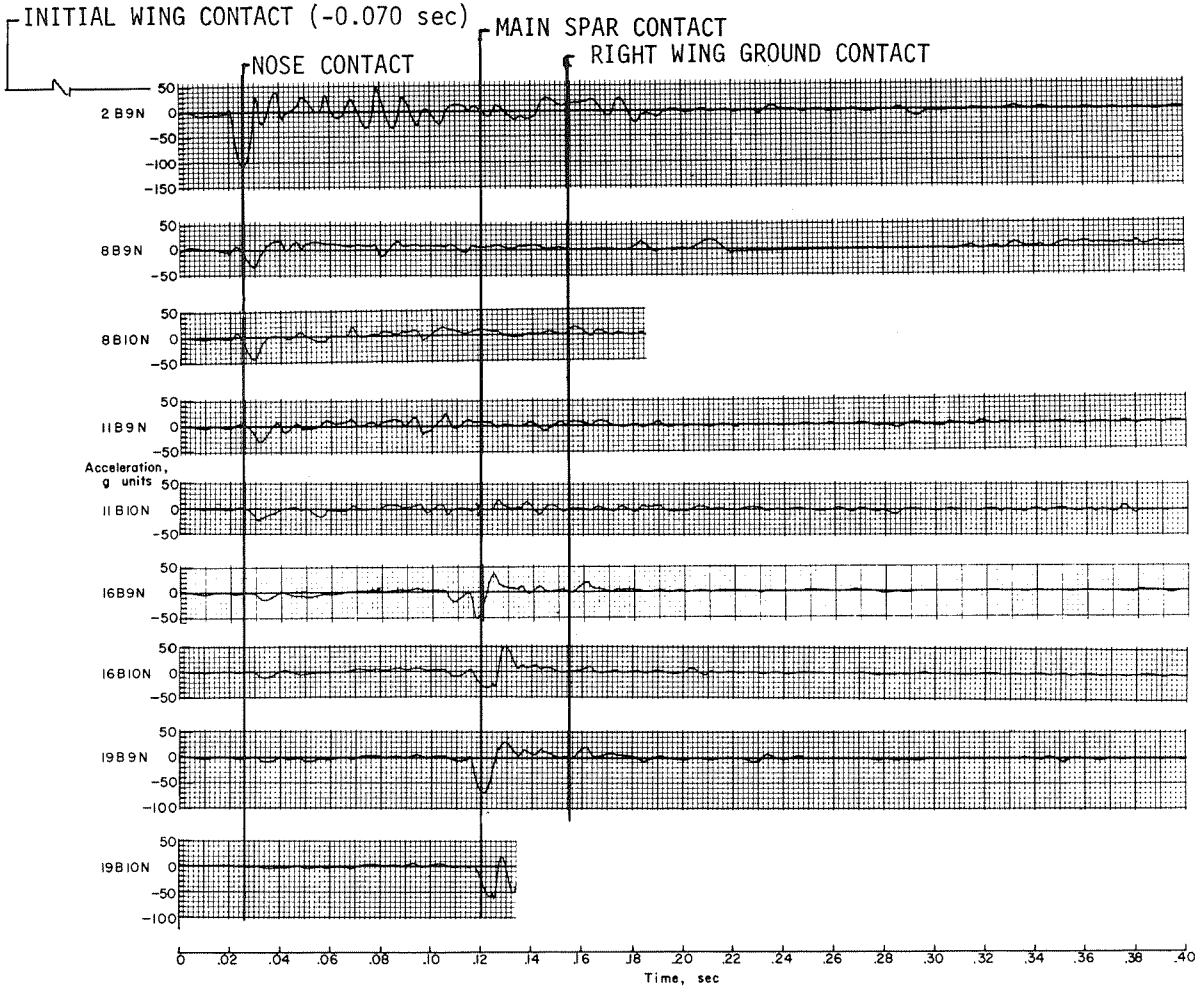

(b) -15^{o} test.

Figure 19.- Continued.

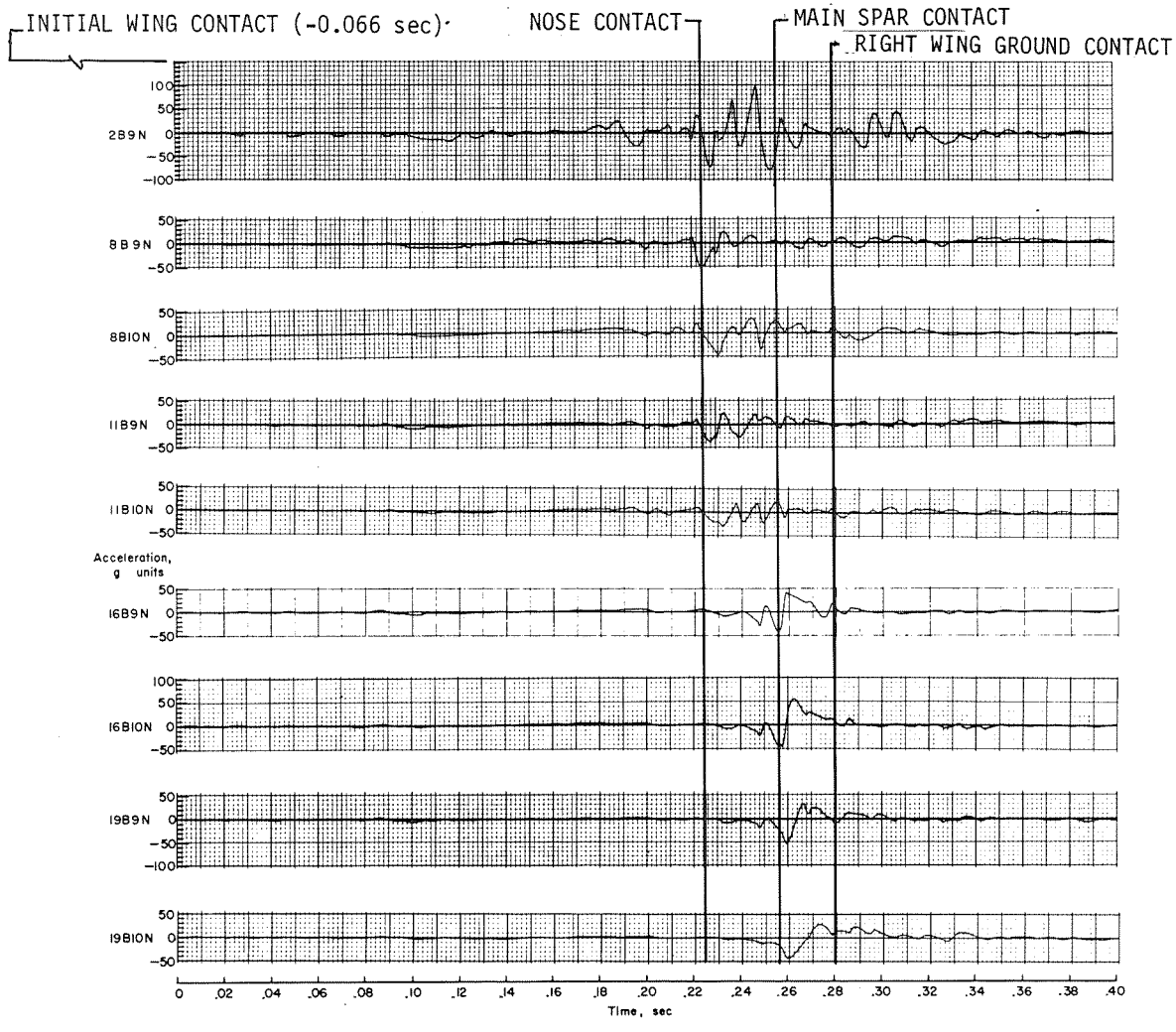

(c) -30^{o} test.

Figure 19.- Concluded.

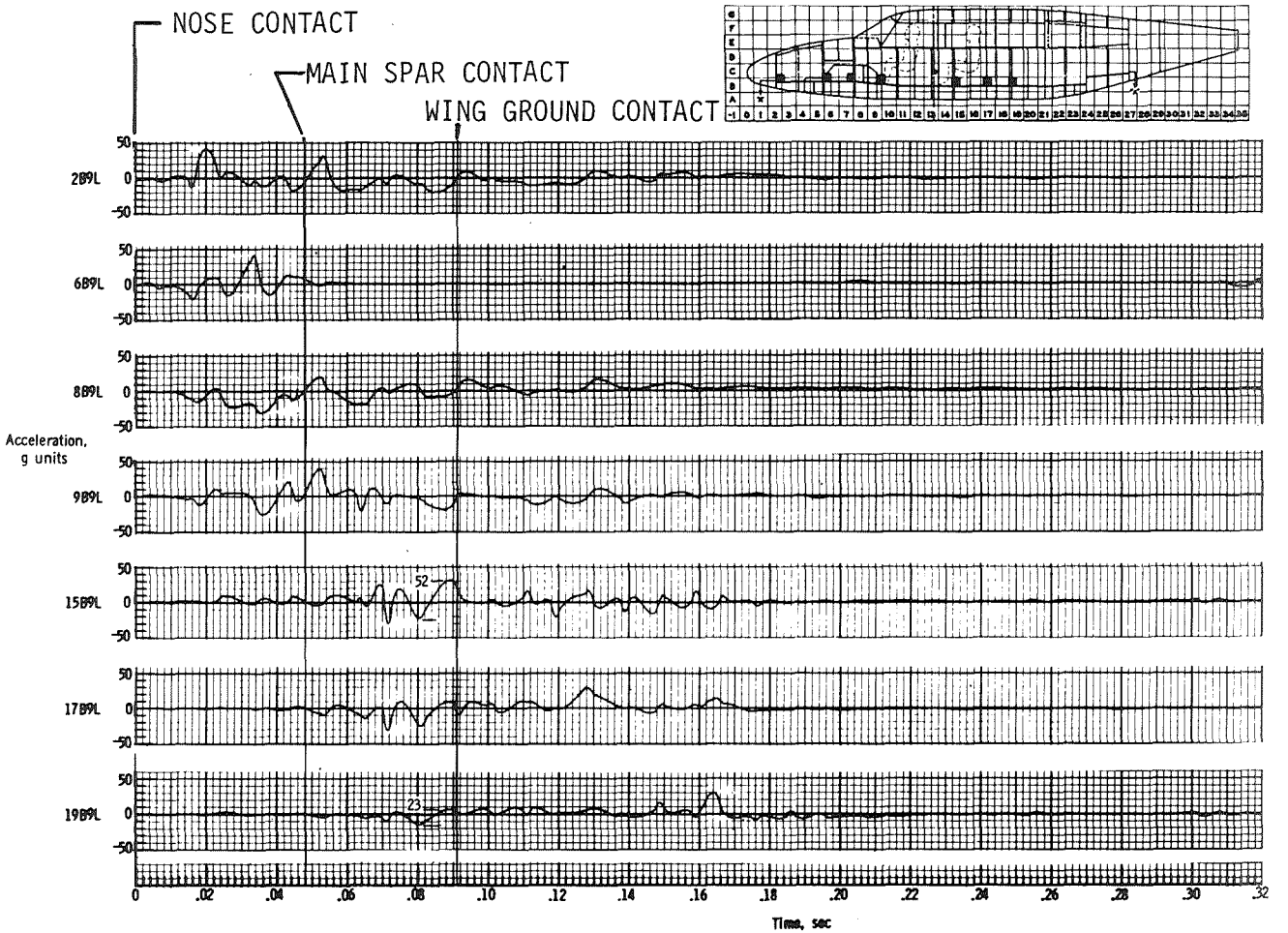

(a) 0^{o} test.

Figure 20.- Time histories of floor-beam longitudinal accelerations.

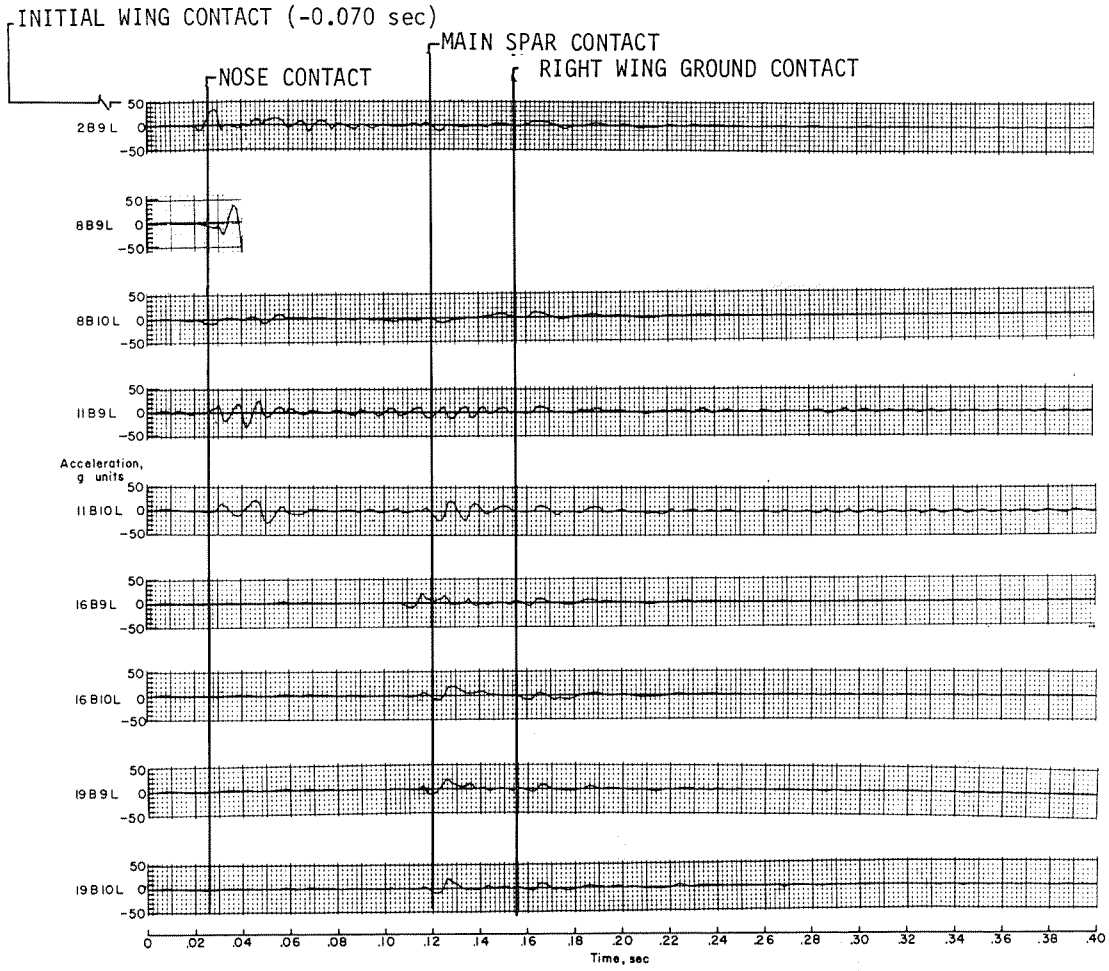

(b) -15° test.

Figure 20.- Continued.

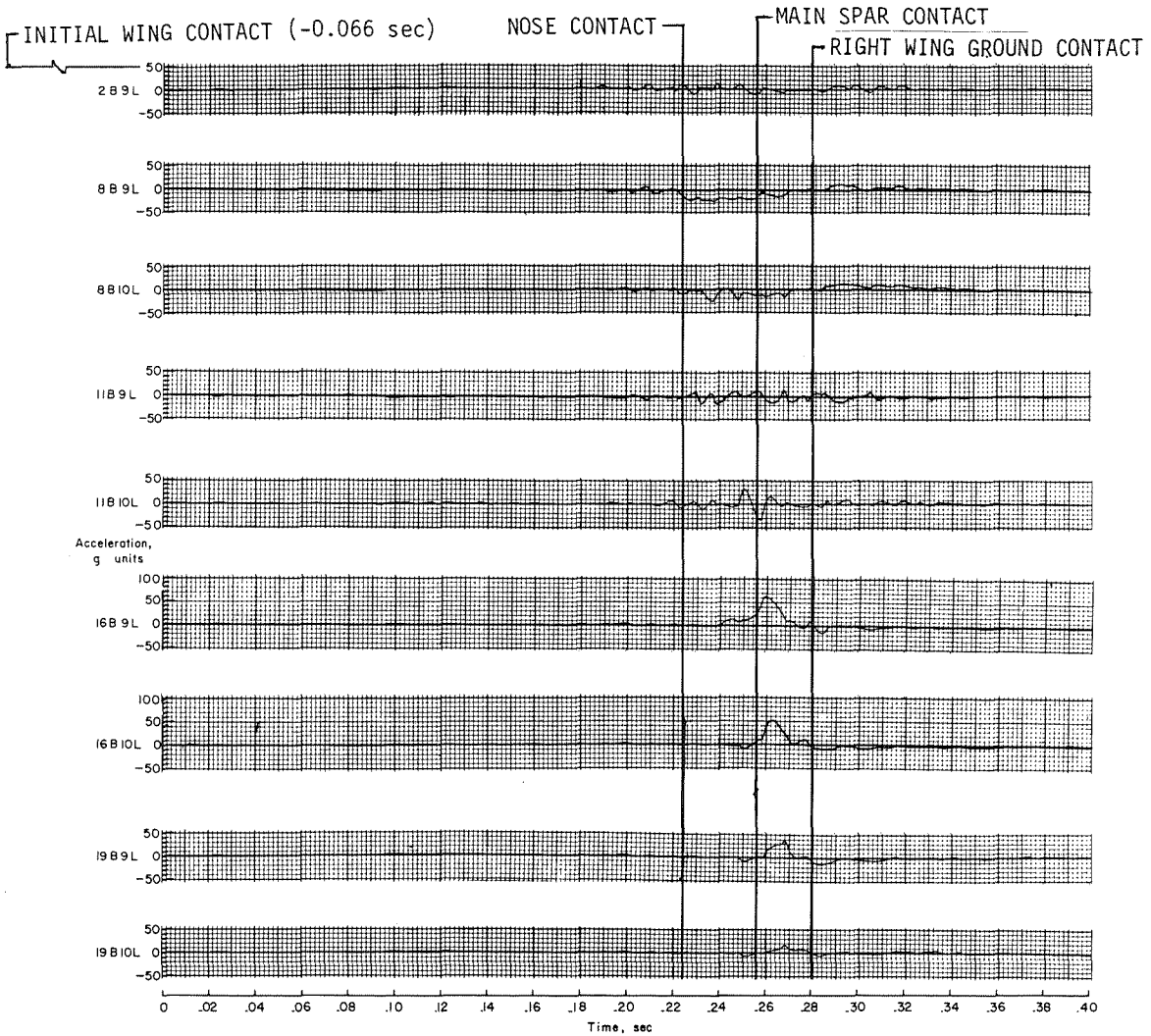

(c) -30^{o} test.

Figure 20.- Concluded.

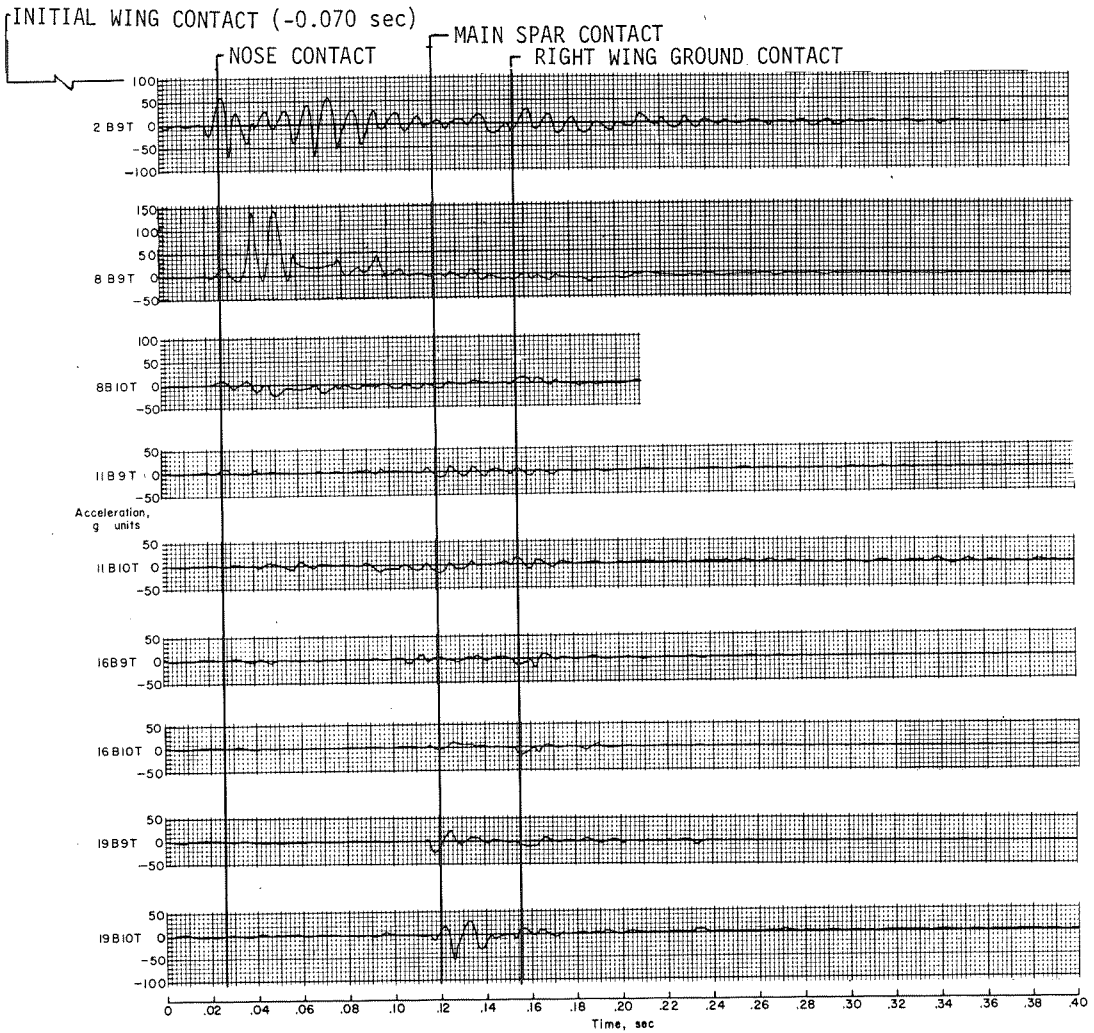

(a) -15° test.

Figure 21.- Time histories of floor-beam transverse accelerations.

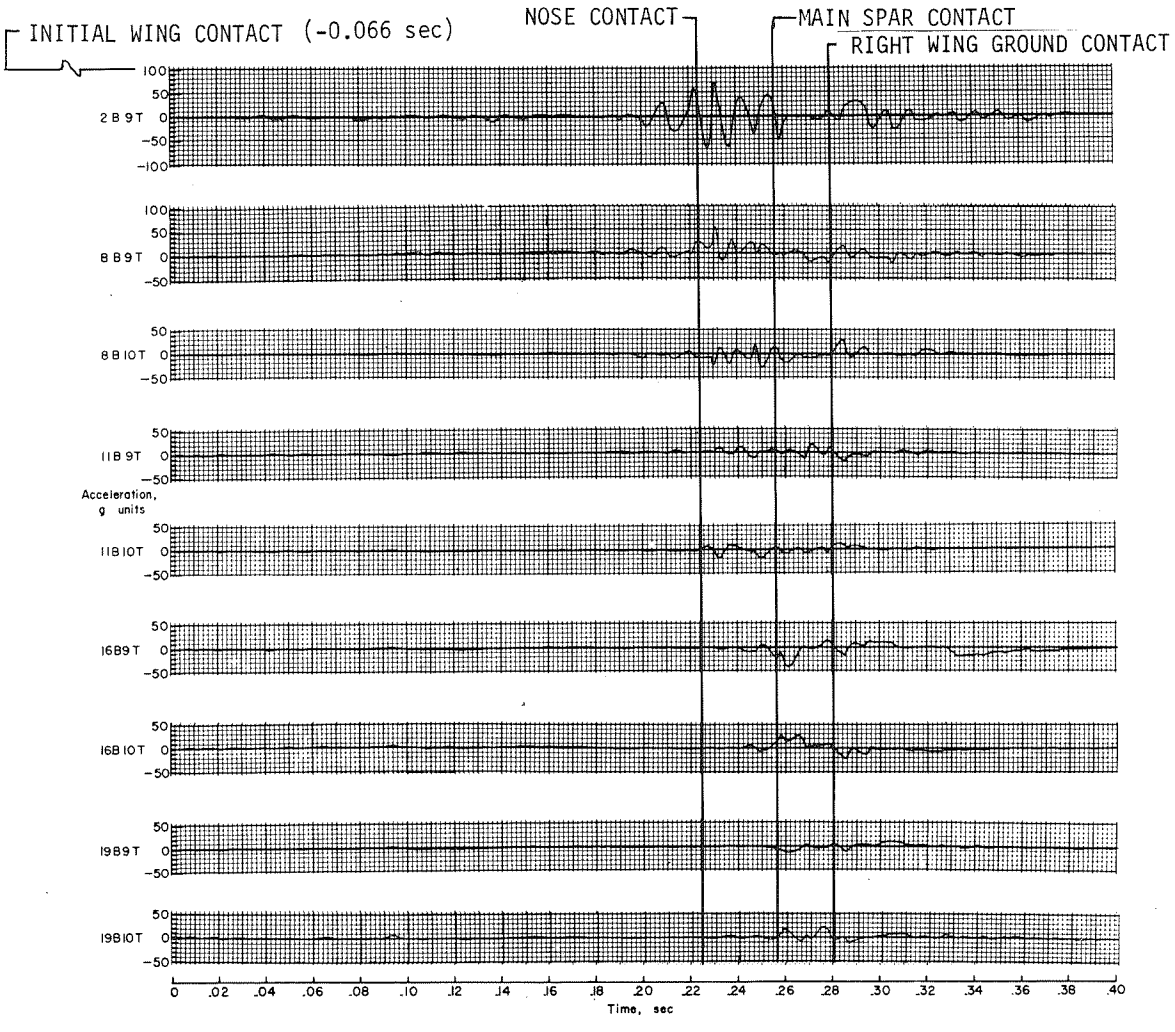

(b) -30^{o} test.

Figure 21.- Concluded.

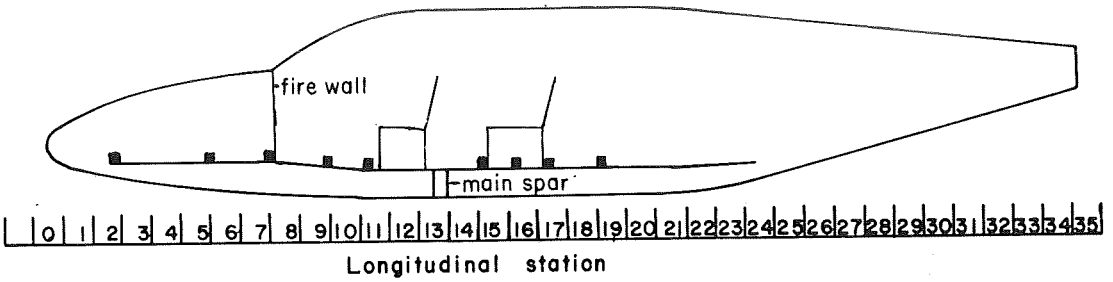

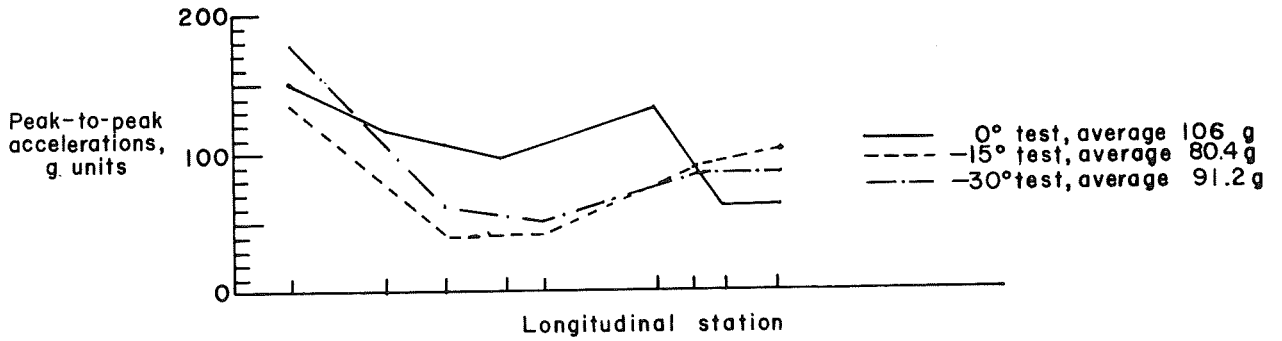

(a) Normal accelerations.

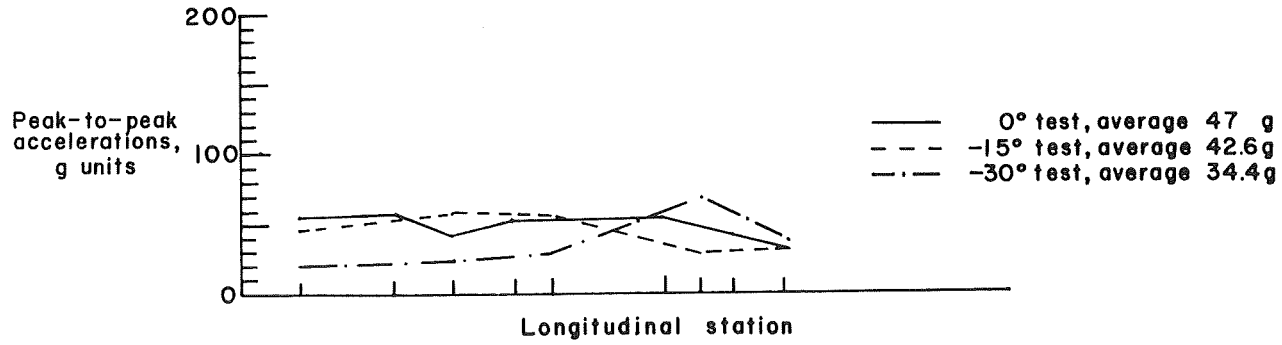

(b) Longitudinal accelerations.

Figure 22.- Peak-to-peak accelerations along the left floor beam.

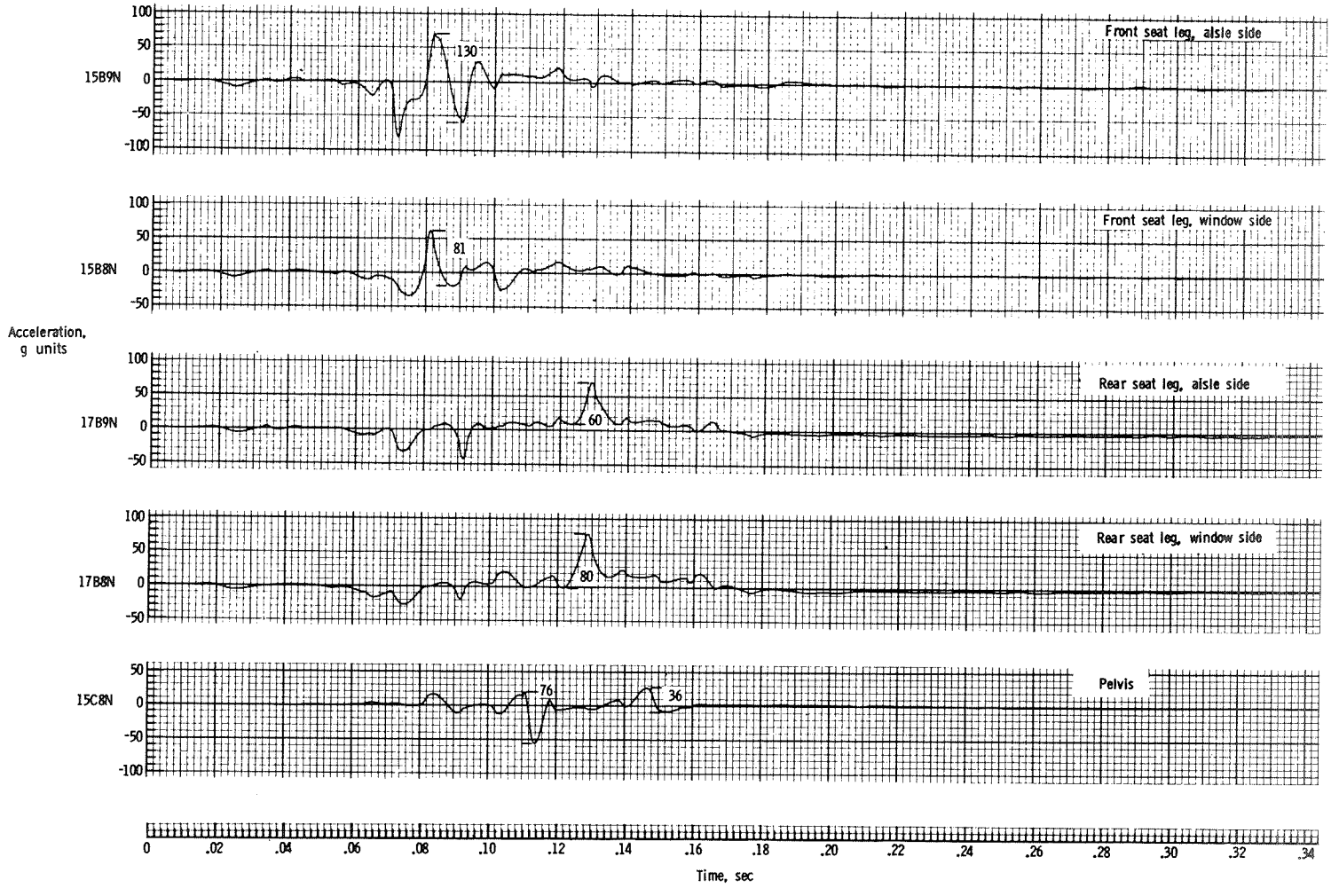

(a) 0° test.

Figure 23.- Normal accelerations on floor and on dummy pelvis at first-passenger location.

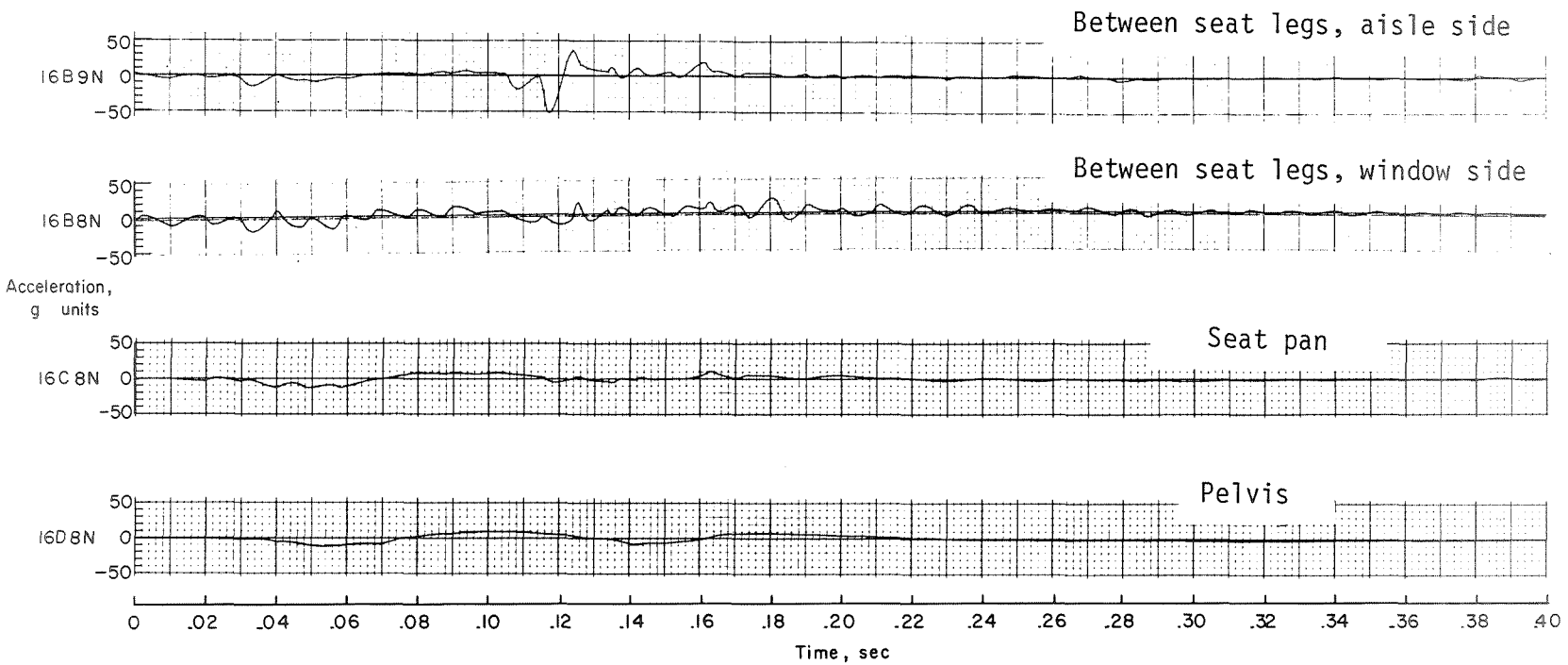

(b) -15^{o} test.

Figure 23.- Continued.

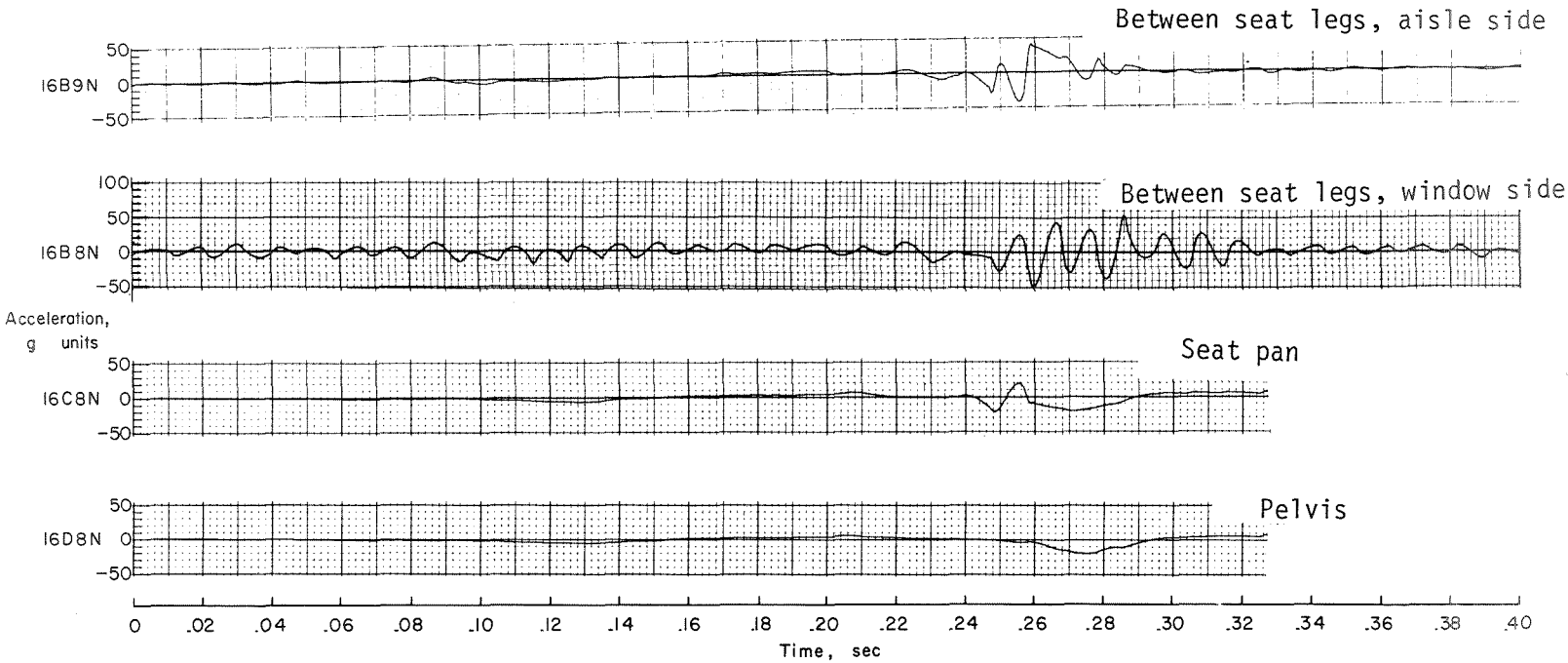

(c) -30^{o} test.

Figure 23.- Concluded.

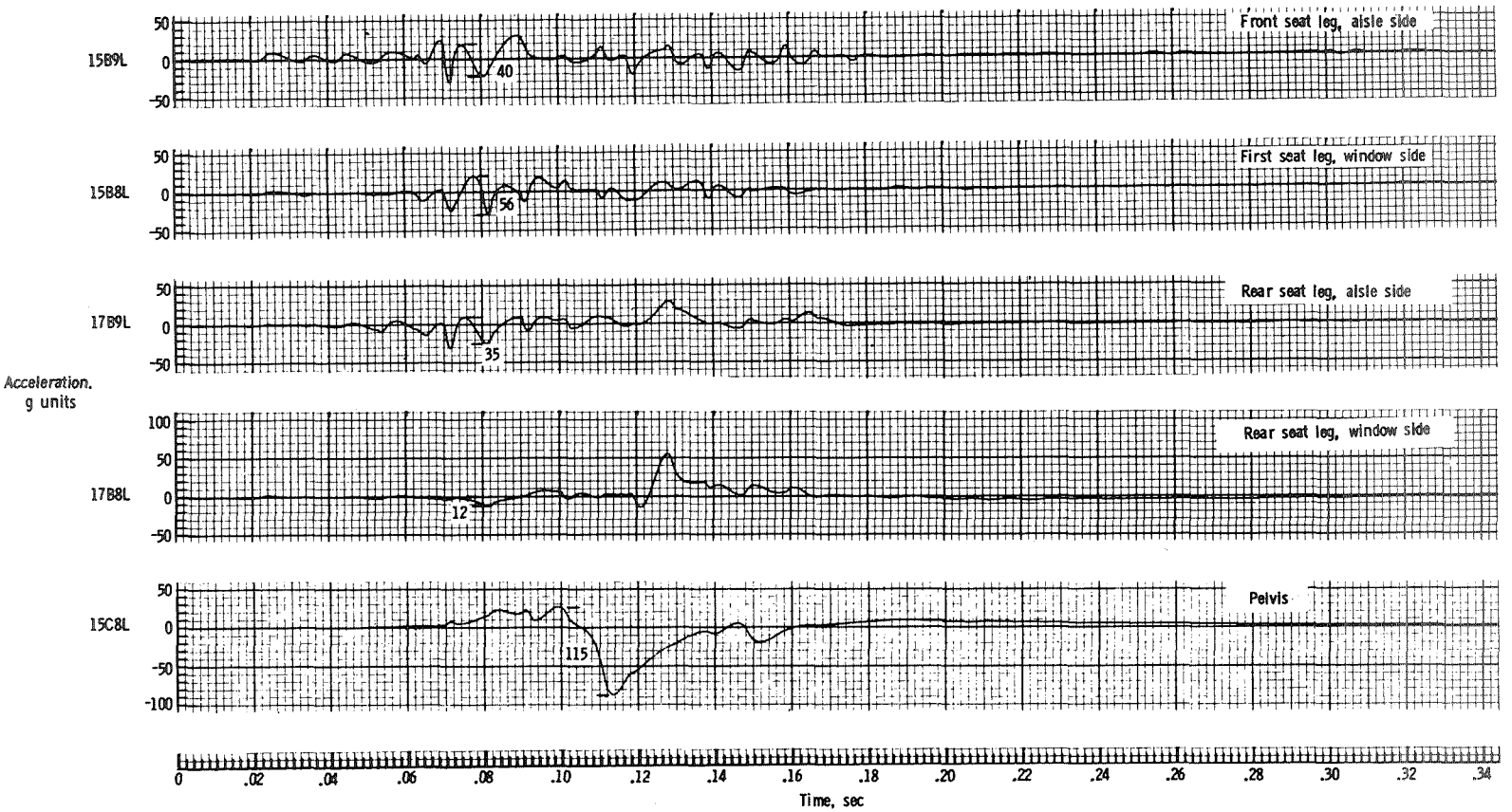

(a) 0° test.

Figure 24.- Longitudinal accelerations on floor and on dummy pelvis at first-passenger location.

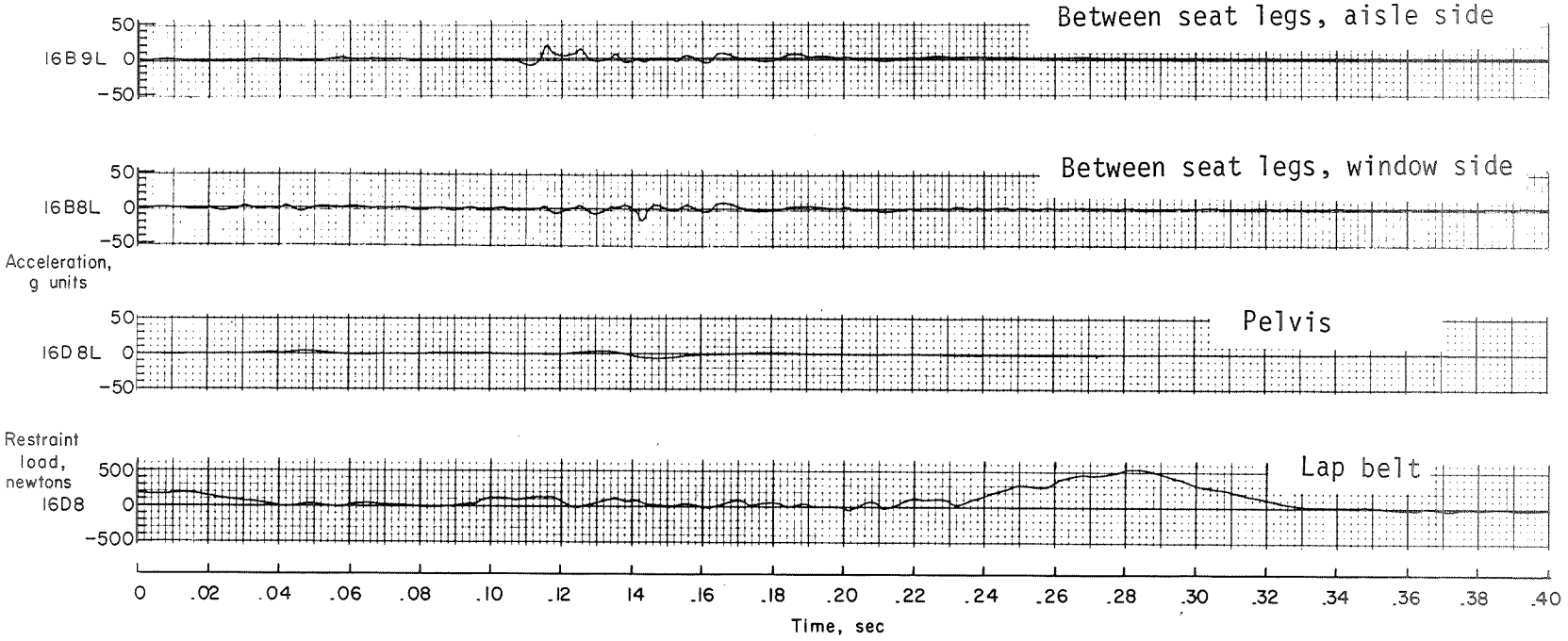

(b) -15° test.

Figure 24.- Continued.

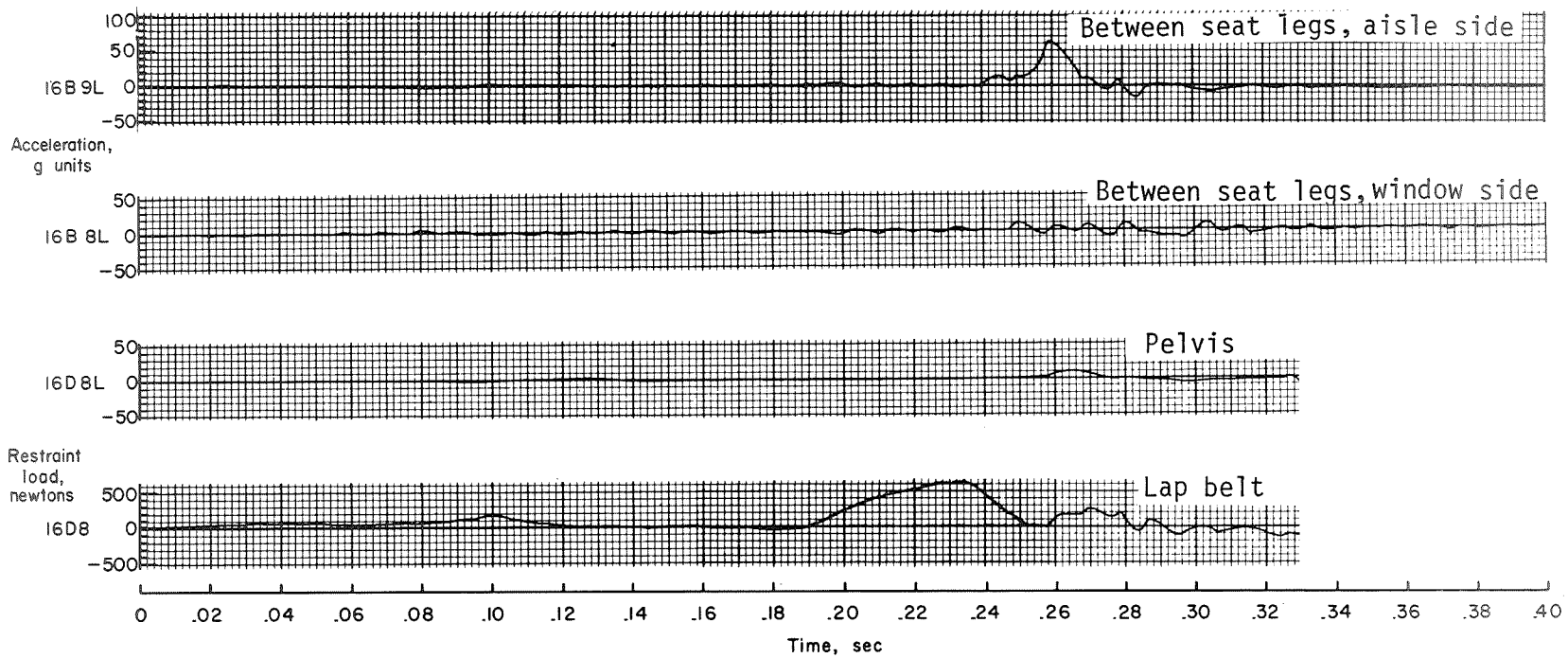

(c) -30^{o} test.

Figure 24.- Concluded.

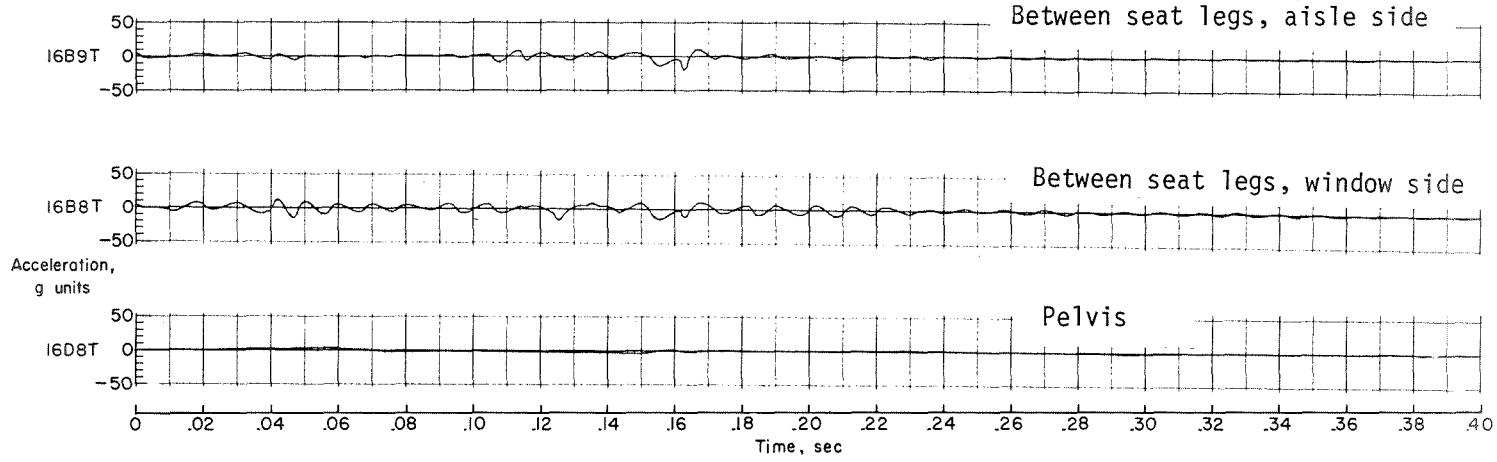

(a) -15^{o} test.

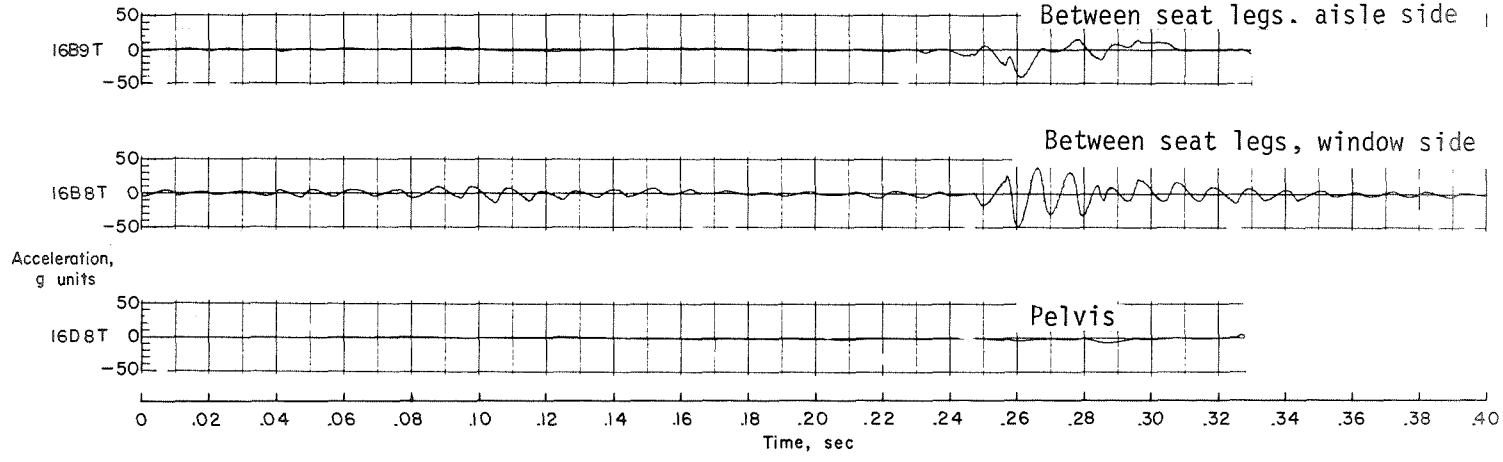

(b) -30^{o} test.

Figure 25.- Transverse accelerations on floor and on dummy pelvis at first-passenger location.

APPENDIX

ACCELEROMETER DATA

Included in this appendix is the complete set of acceleration time histories for the three crash tests and a schematic to help determine the accelerometer locations corresponding to the time histories. (See figs. A1 to A4.)

The data have been passed through a 4- to 3300-Hz band-pass filter during recording and then digitized at 4000 samples per second. The digitized data were smoothed by a least-squares fit through every 50 points on a third-order polynomial and a 10-point overlap for continuity.

The data are grouped according to the accelerometer location and orientation. The accelerometer location is represented in the schematic by an X,Y,Z coordinate system. The accelerometer normal, longitudinal, and transverse orientations are indicated on the traces by N, L, and T, respectively. Thus, the first accelerometer adjacent to the floor beam in the normal direction is represented by 2B9N. Each station block along the X-, Z-, and Y-axes is 25.4 cm in length.

On the data plots, the abscissa represents elapsed time in seconds. Zero time is the time at initial contact, that is, the time at which the fuselage first contacted the impact surface. For the -15° roll test, the initial wing ground contact ocurred at -0.070 sec and for the -30° roll test, the initial wing ground contact occurred at -0.066 sec. The accelerations in the ordinate are expressed in g units and each trace is identified by the location and and orientation of the recording accelerometer.

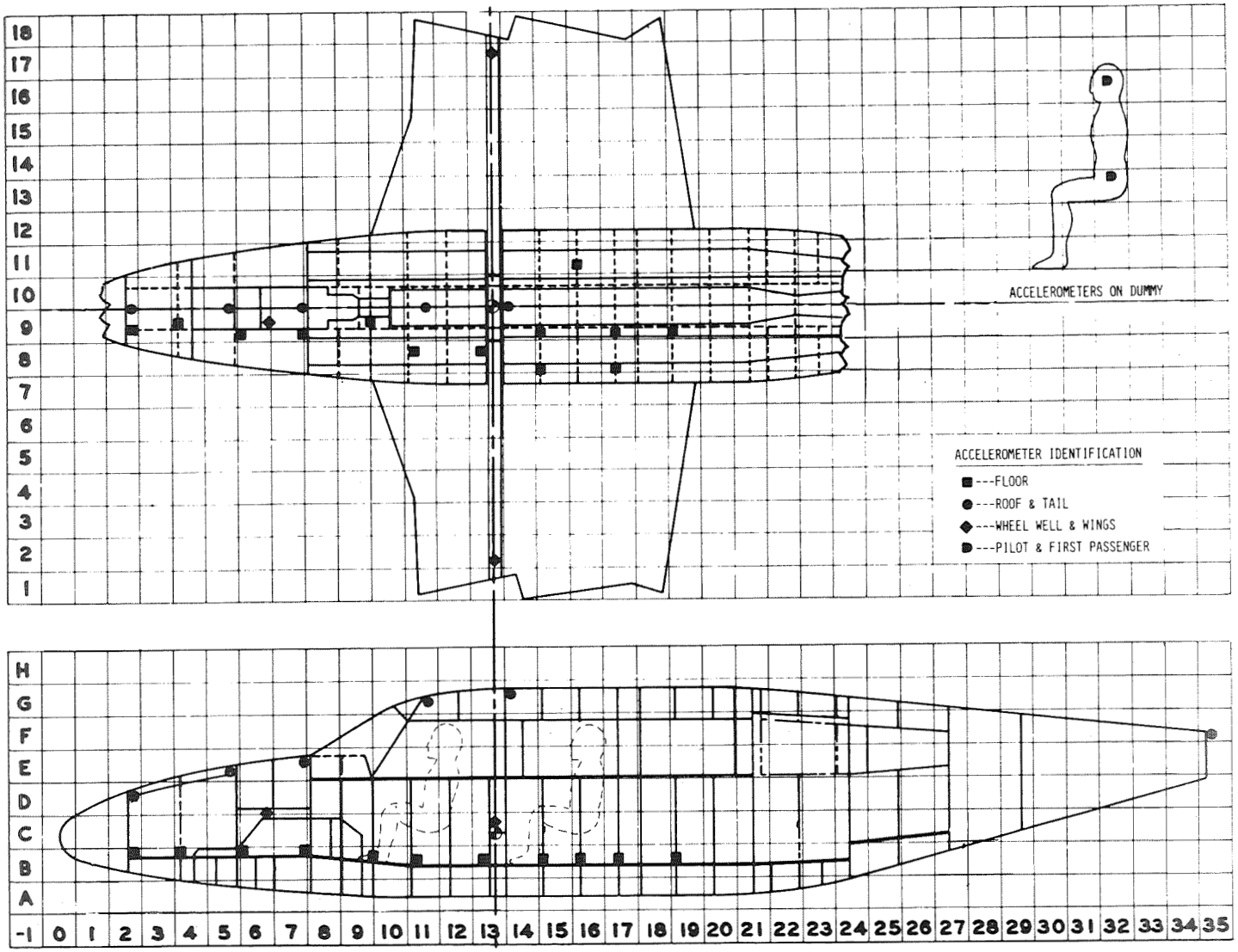

Figure A1.- Accelerometer locations (typical).

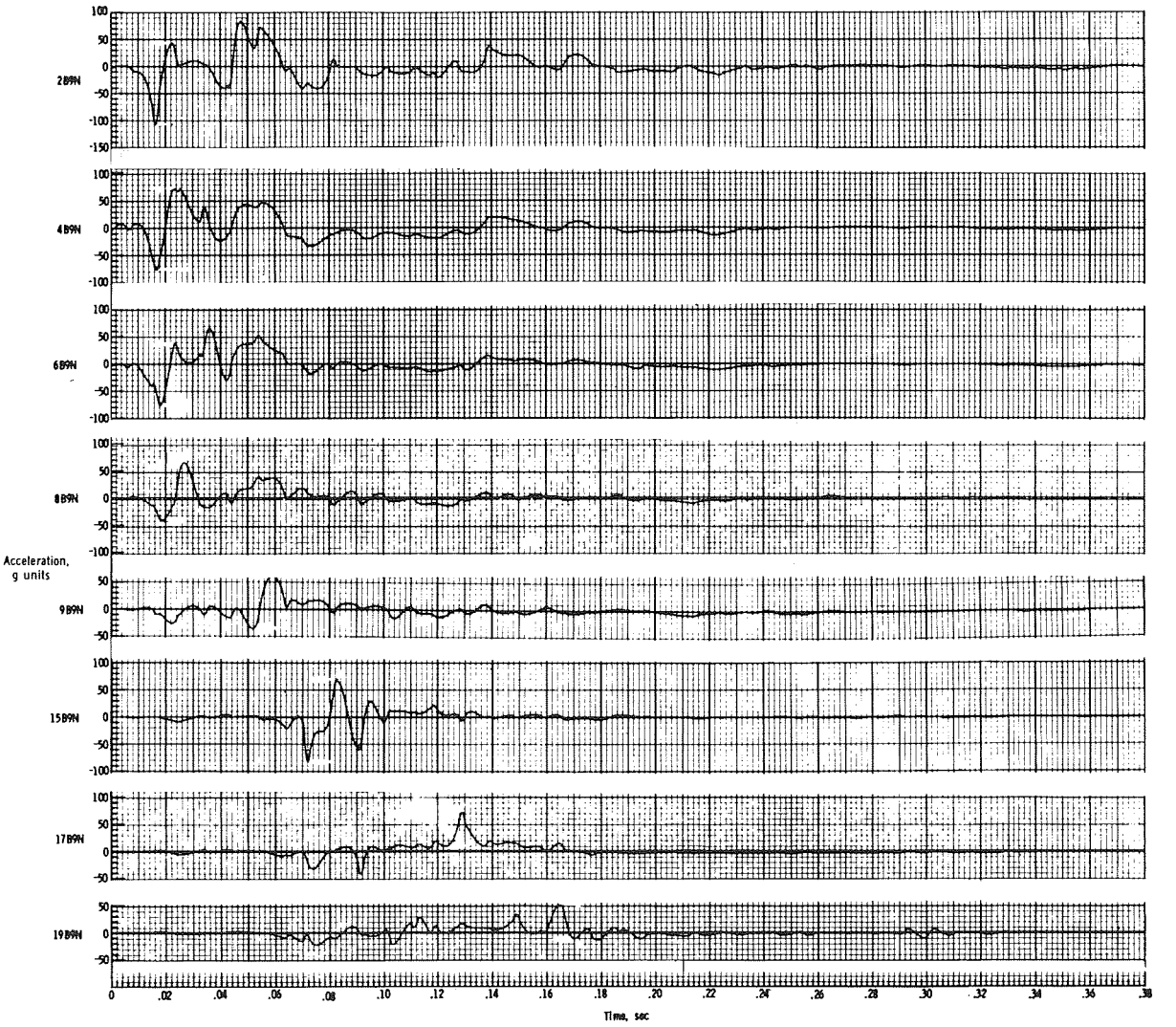

(a) Normal accelerations adjacent to floor beam.

Figure A2.- Acceleration time histories for 0° test.

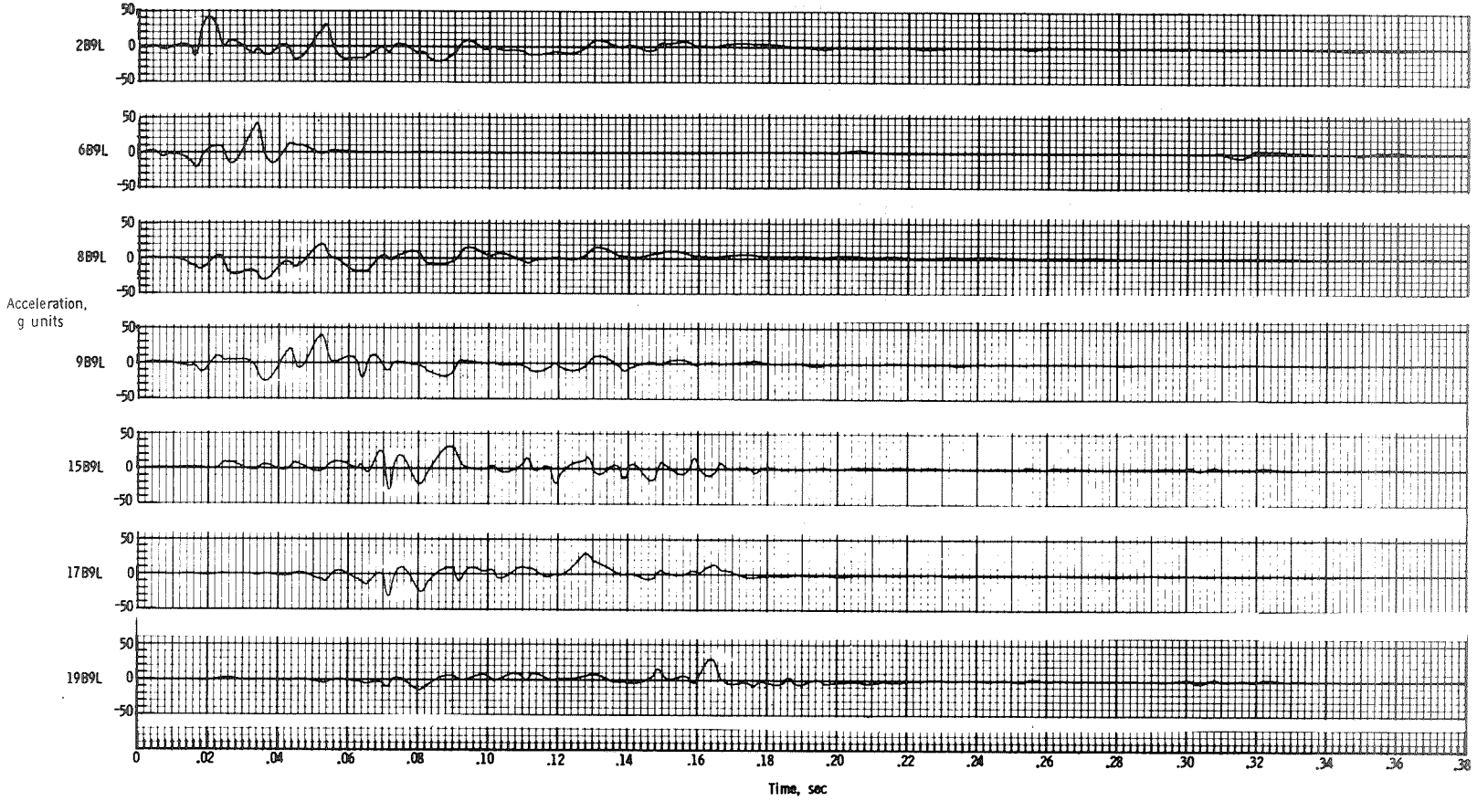

(b) Longitudinal accelerations adjacent to floor beam.

Figure A2.- Continued.

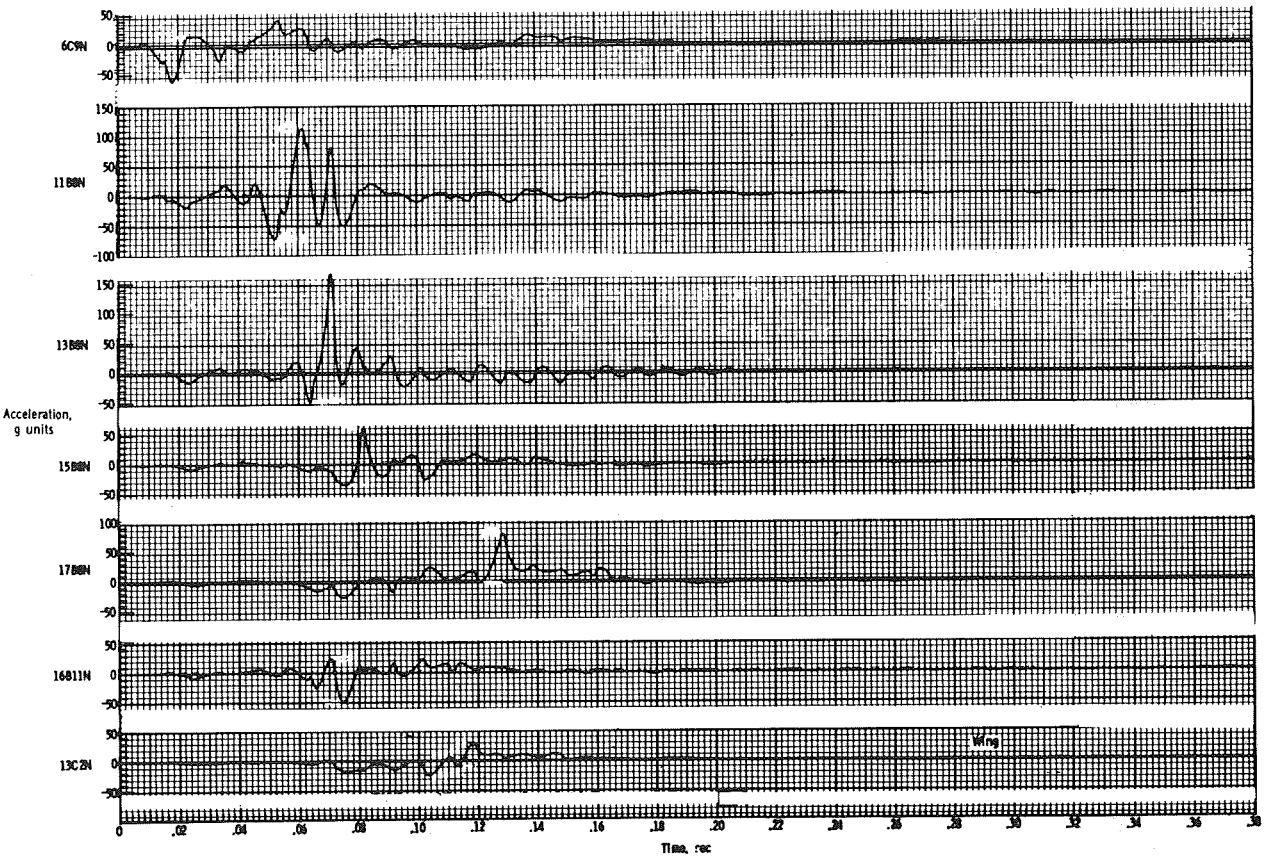

(c) Normal accelerations on cabin floor and wing.

Figure A2.- Continued.

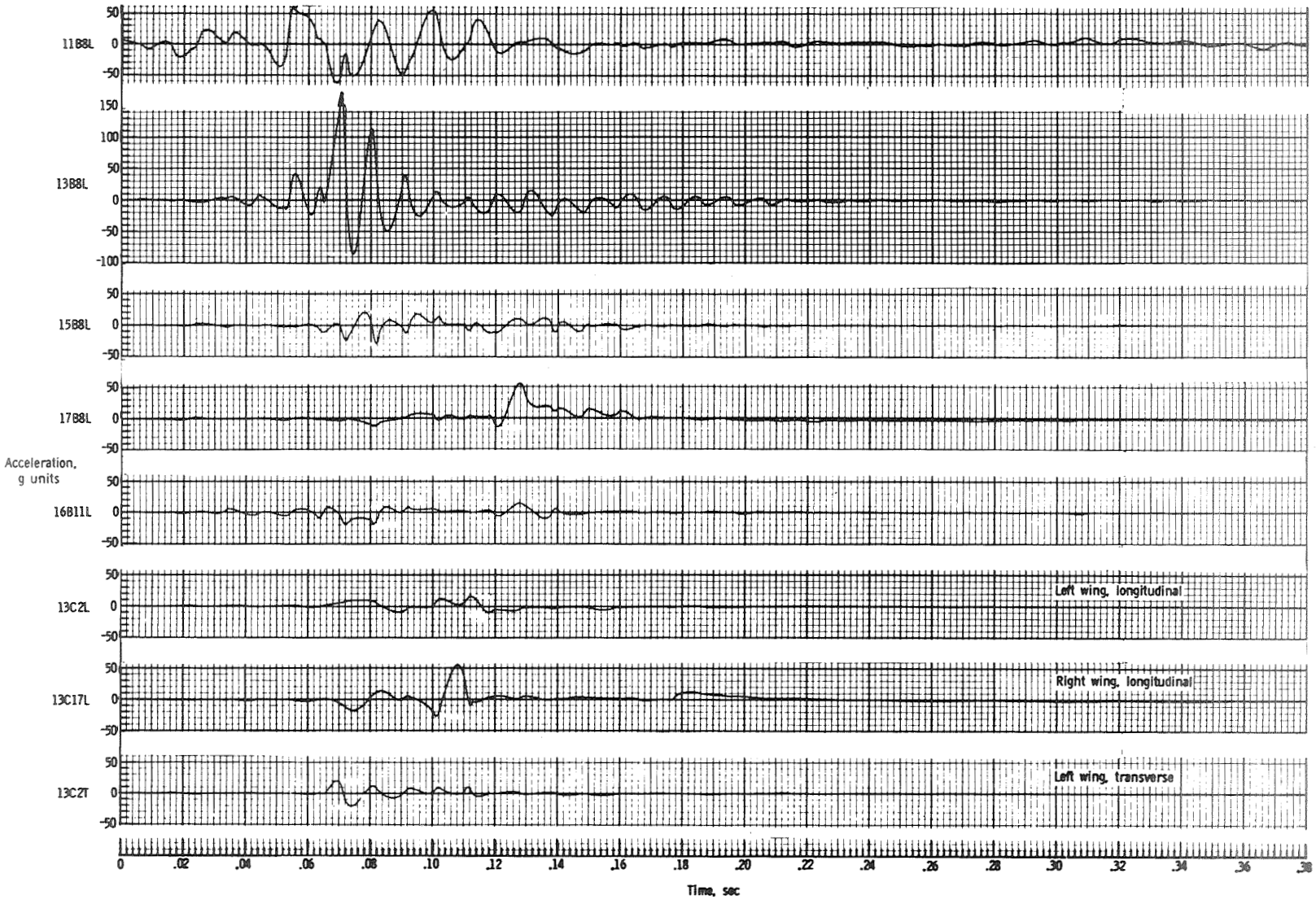

(d) Longitudinal accelerations on cabin floor and other accelerations.

Figure A2.- Continued.

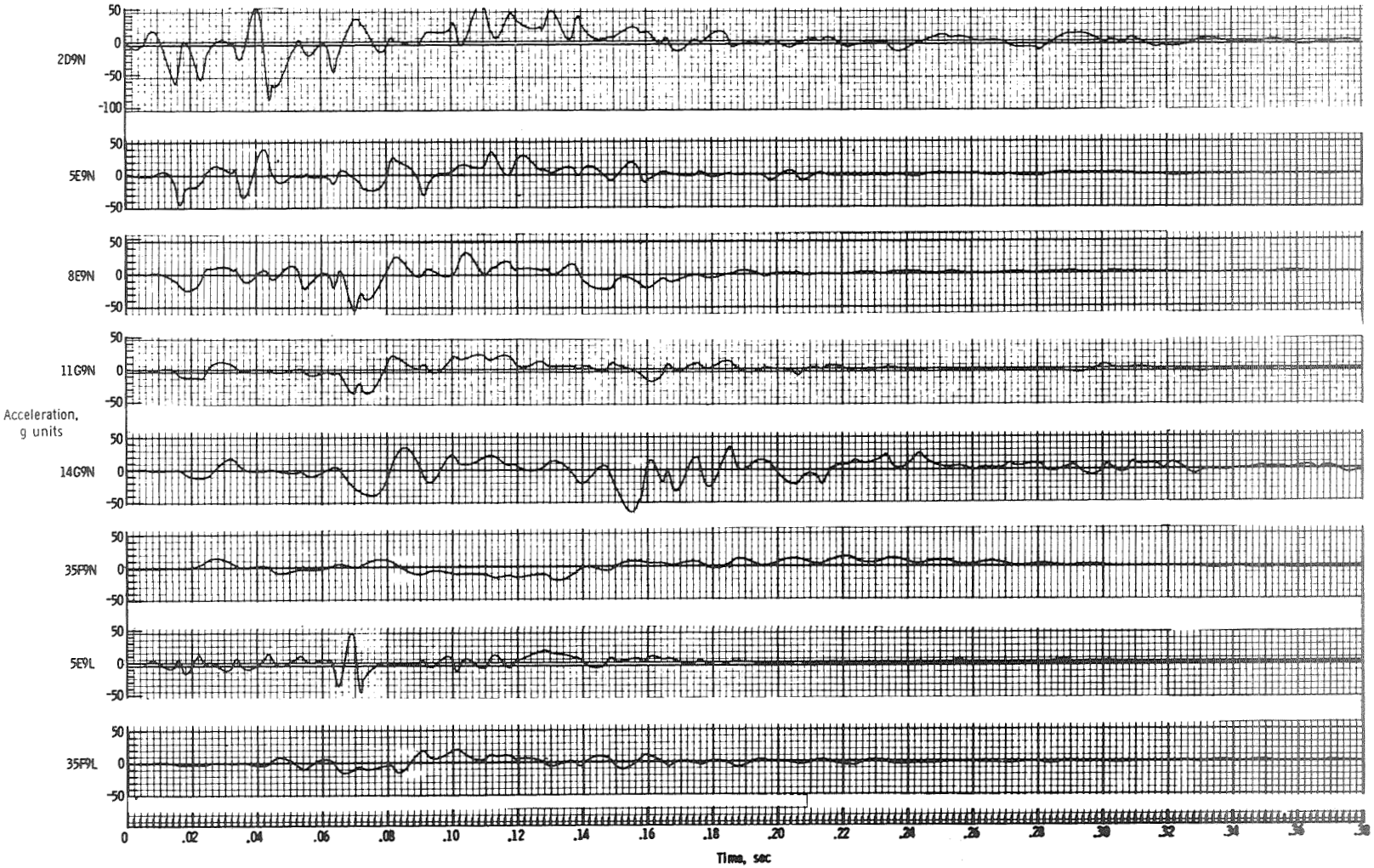

(e) Normal and longitudinal accelerations on roof.

Figure A2.- Continued.

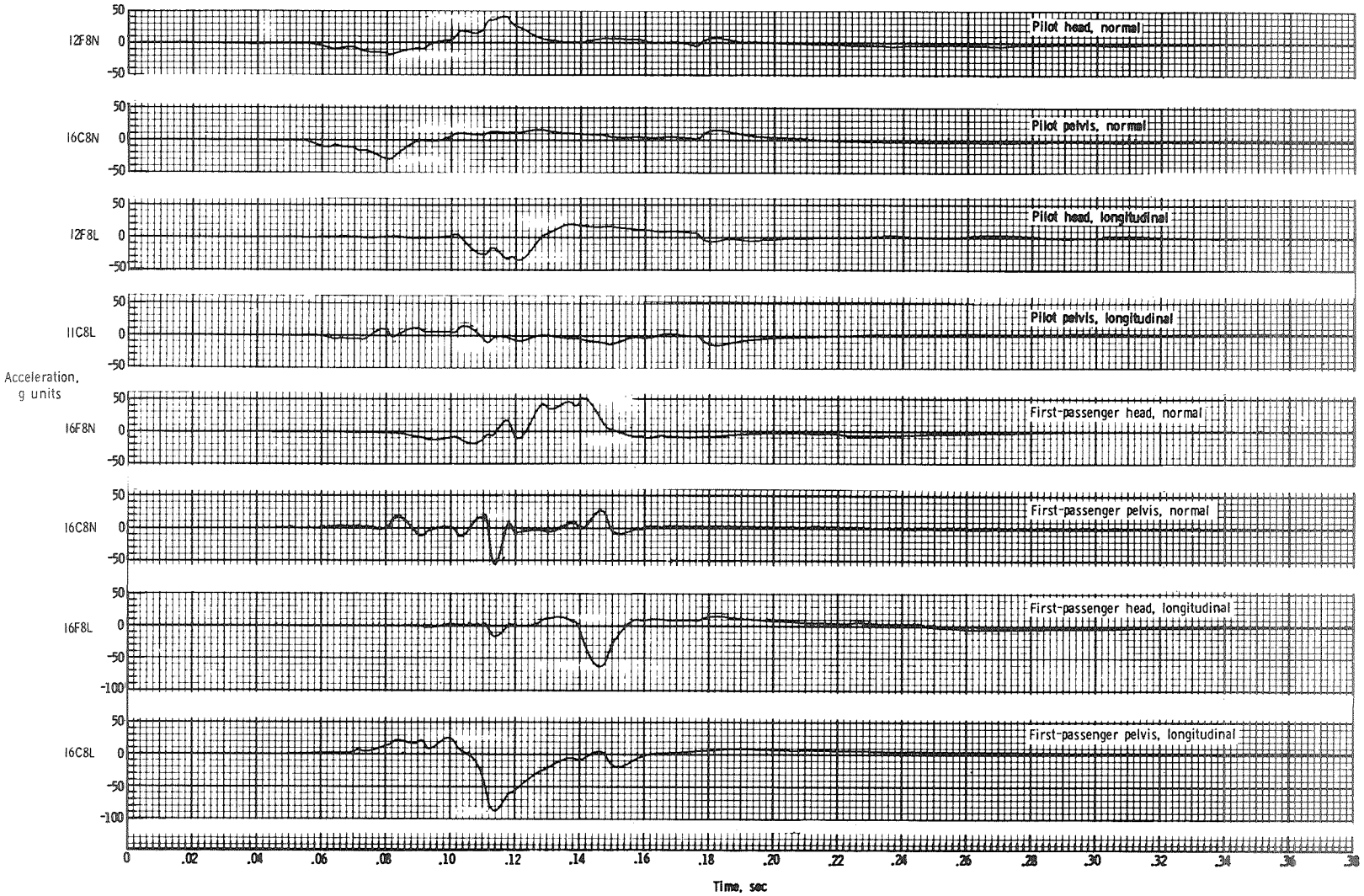

(f) Accelerations on pilot and first passenger.

Figure A2.- Concluded.

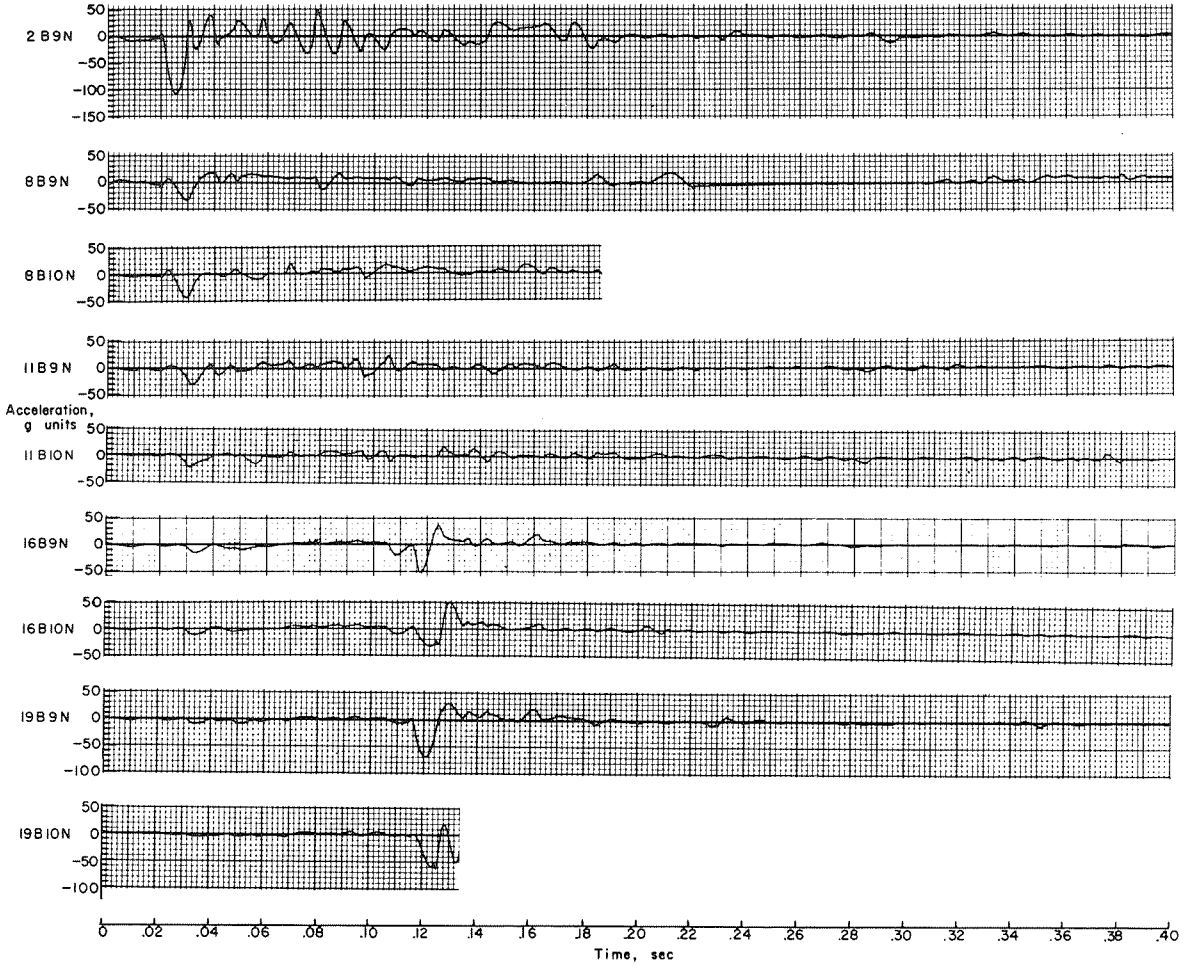

(a) Normal accelerations adjacent to floor beam.

Figure A3.- Acceleration time histories for -15° test.

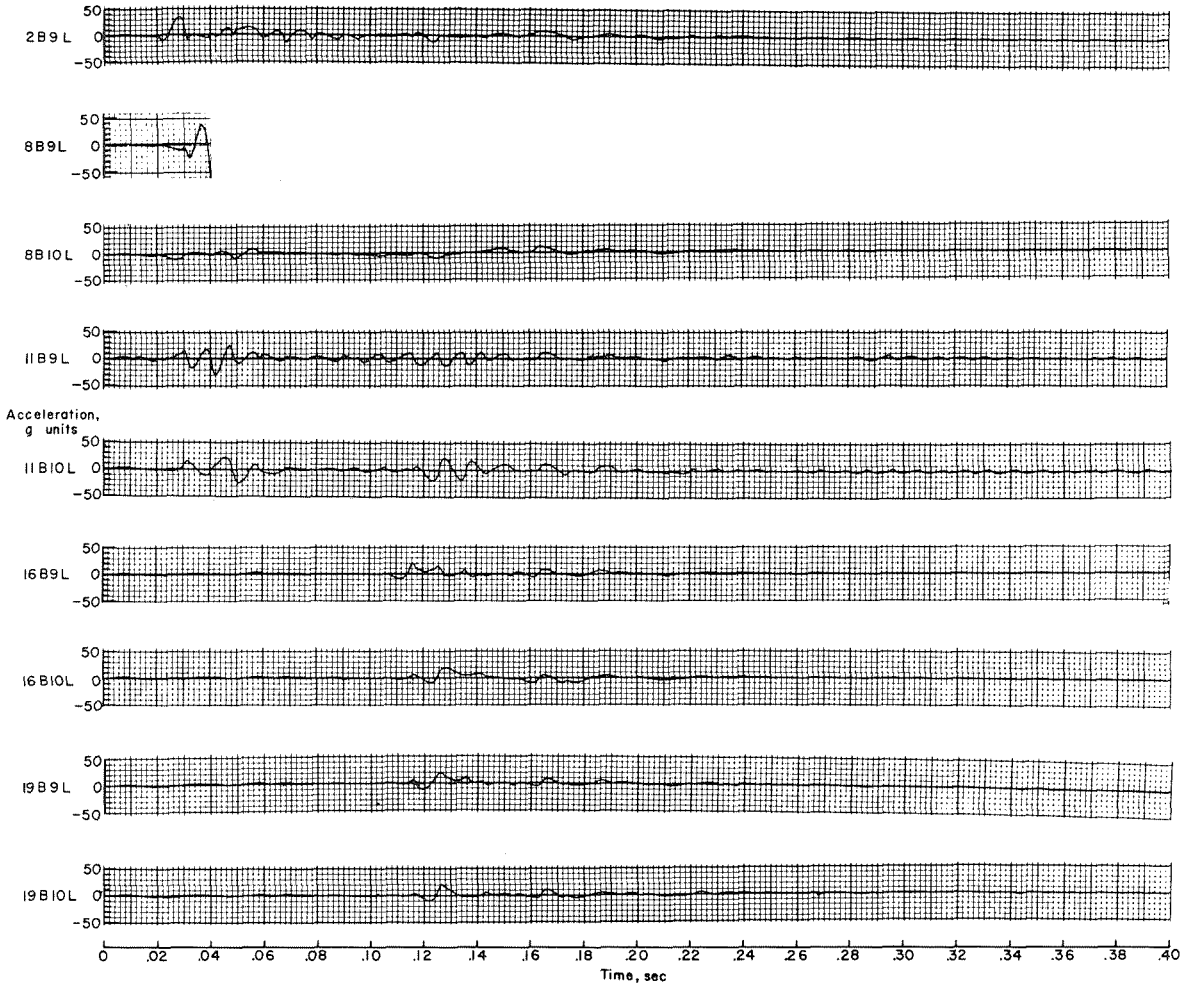

(b) Longitudinal accelerations adjacent to floor beam.

Figure A3.- Continued.

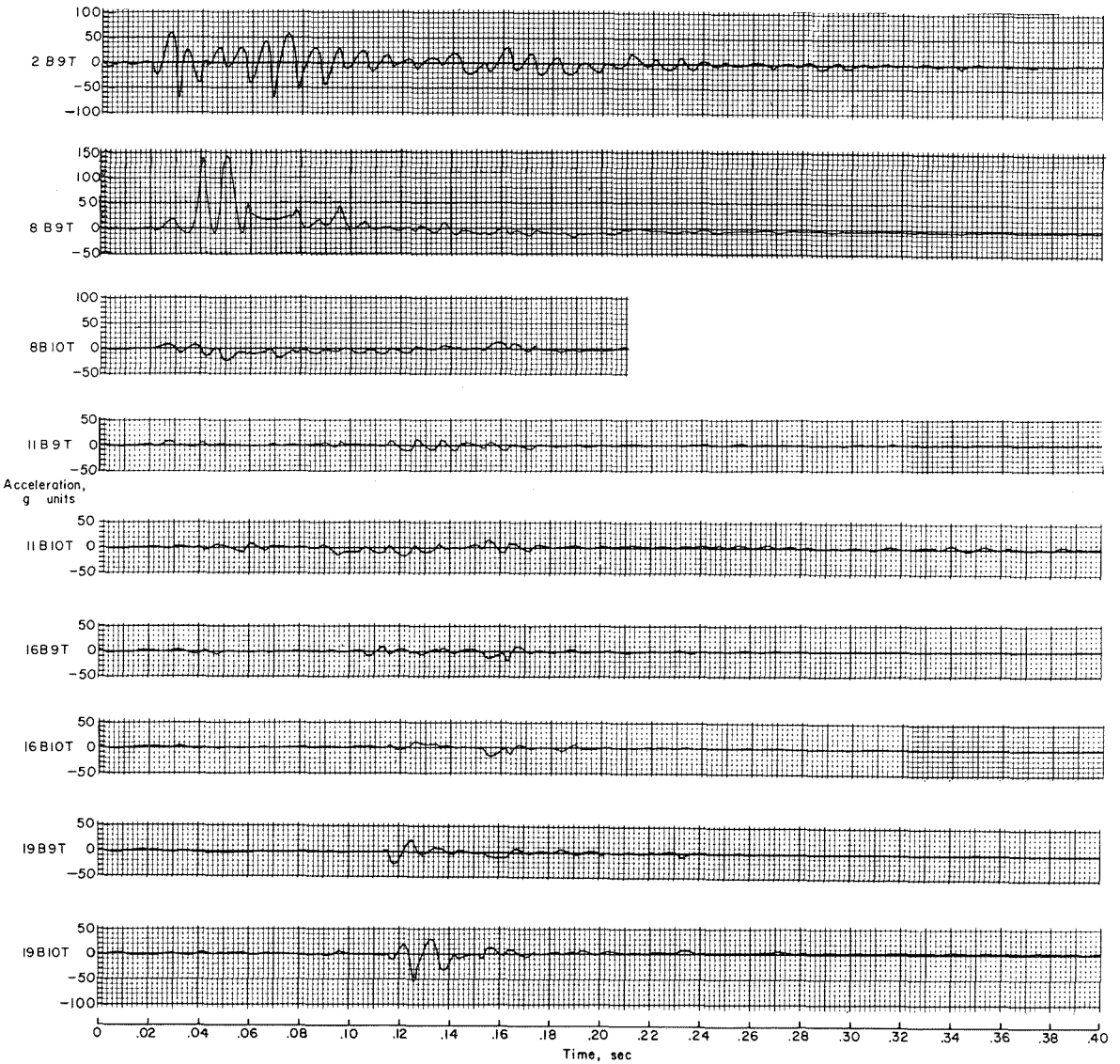

(c) Transverse accelerations adjacent to floor beam.

Figure A3.- Continued.

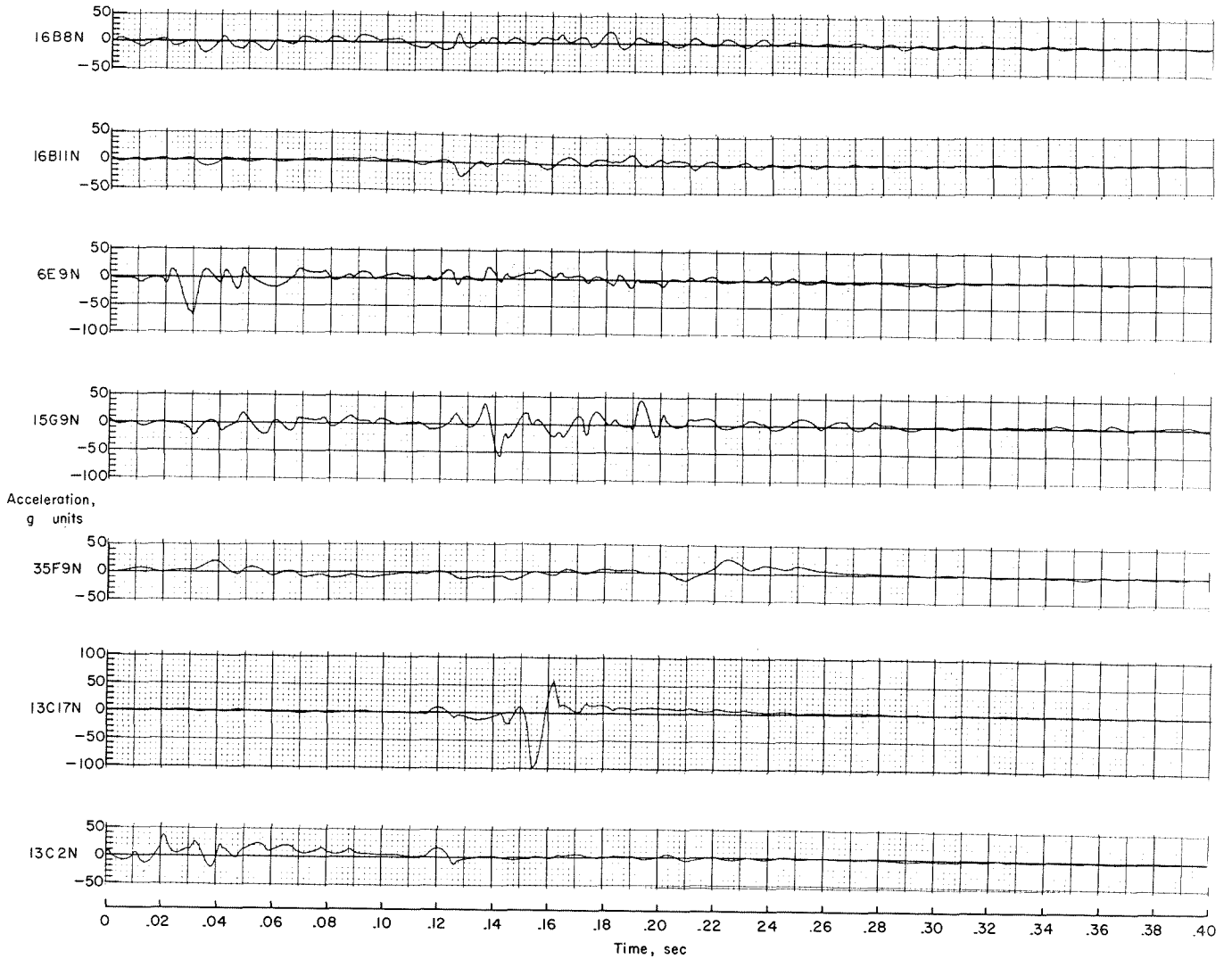

(d) Remaining normal structural acceleration.

Figure A3.- Continued.

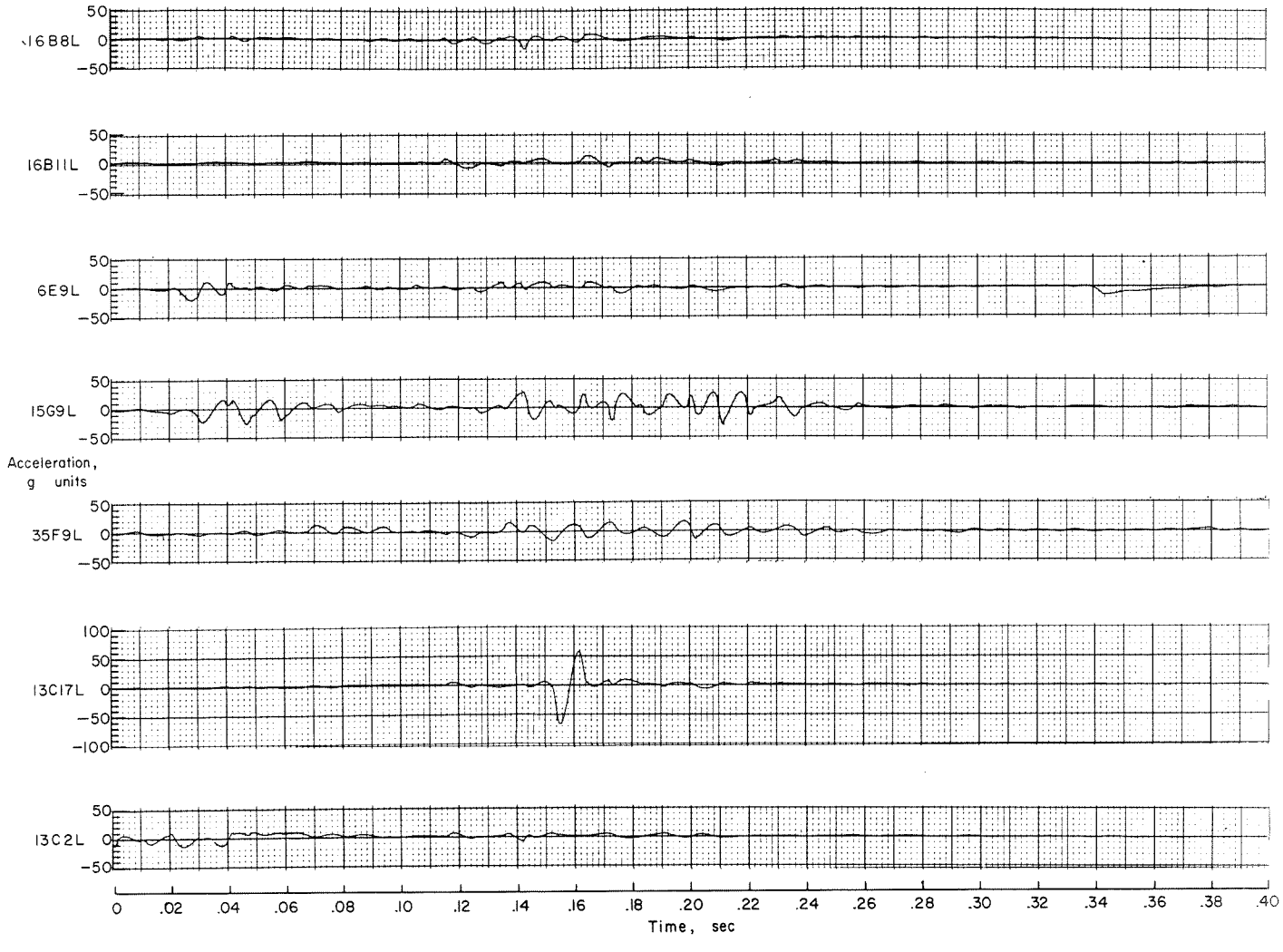

(e) Remaining longitudinal structural accelerations.

Figure A3.- Continued.

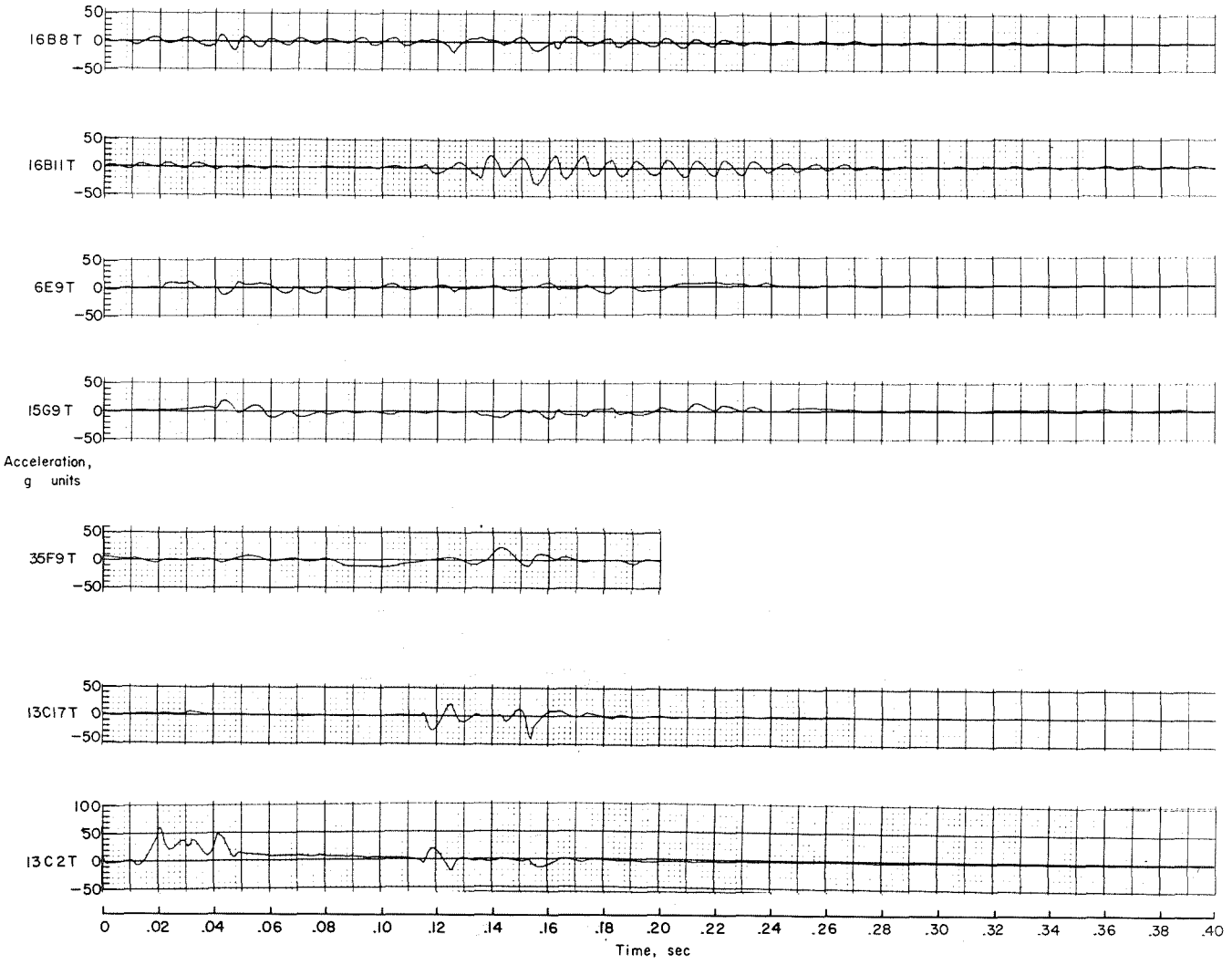

(f) Remaining transverse structural accelerations.

Figure A3.- Continued.

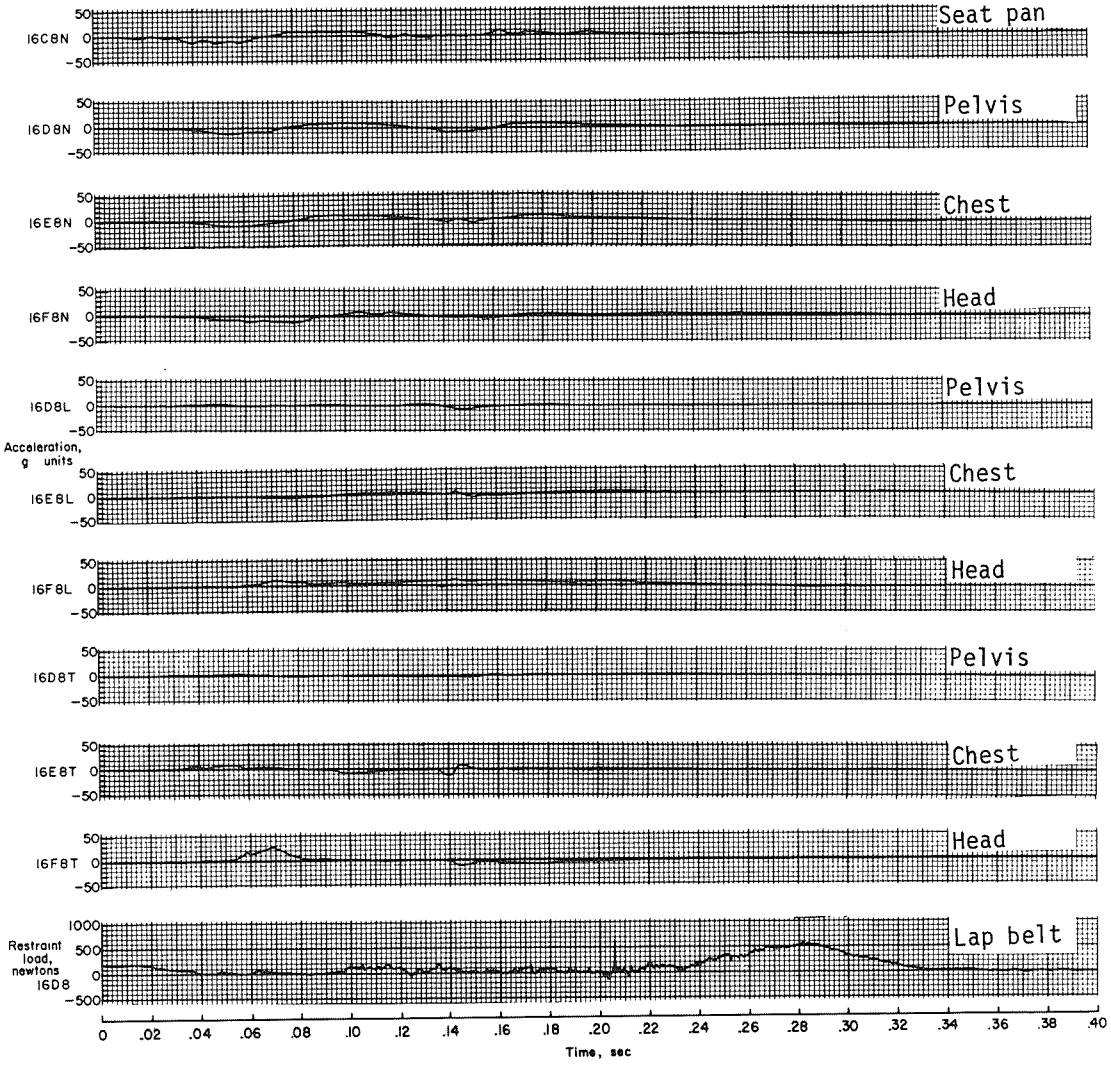

(g) Acceleration time histories in first-passenger dummy.

Figure A3.- Continued.

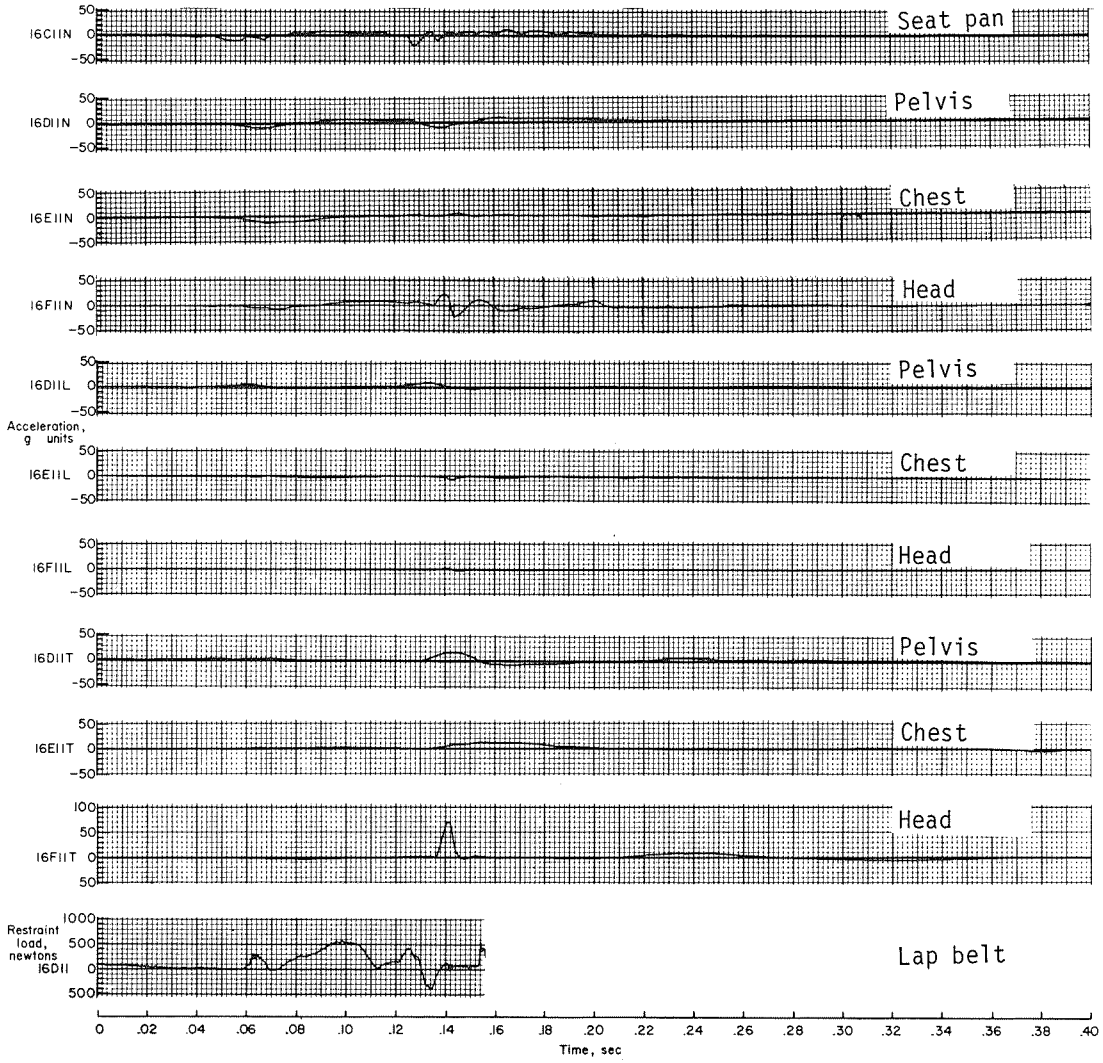

(h) Acceleration time histories in second-passenger dummy.

Figure A3.- Concluded.

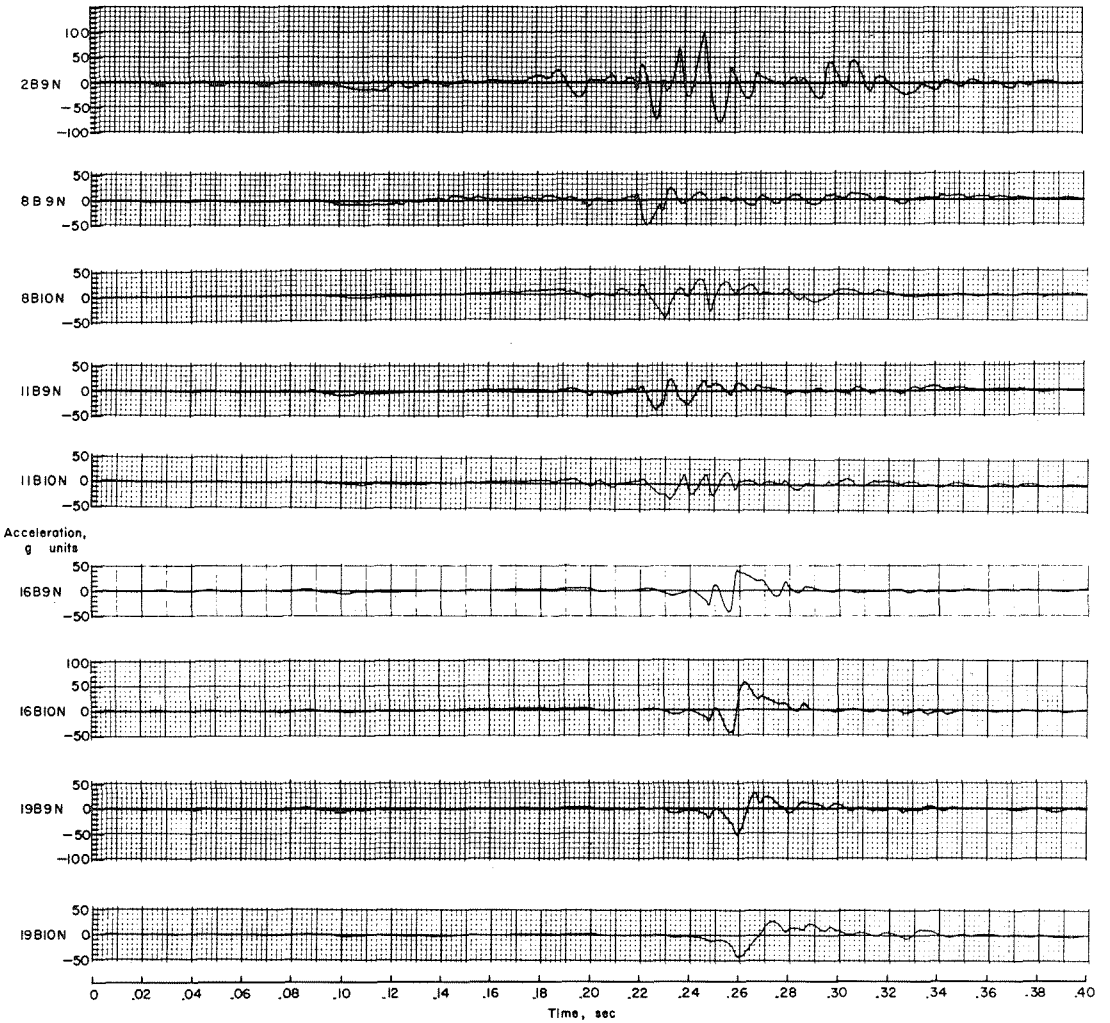

(a) Normal accelerations adjacent to floor beam.

Figure A4.- Acceleration time histories for -30° test.

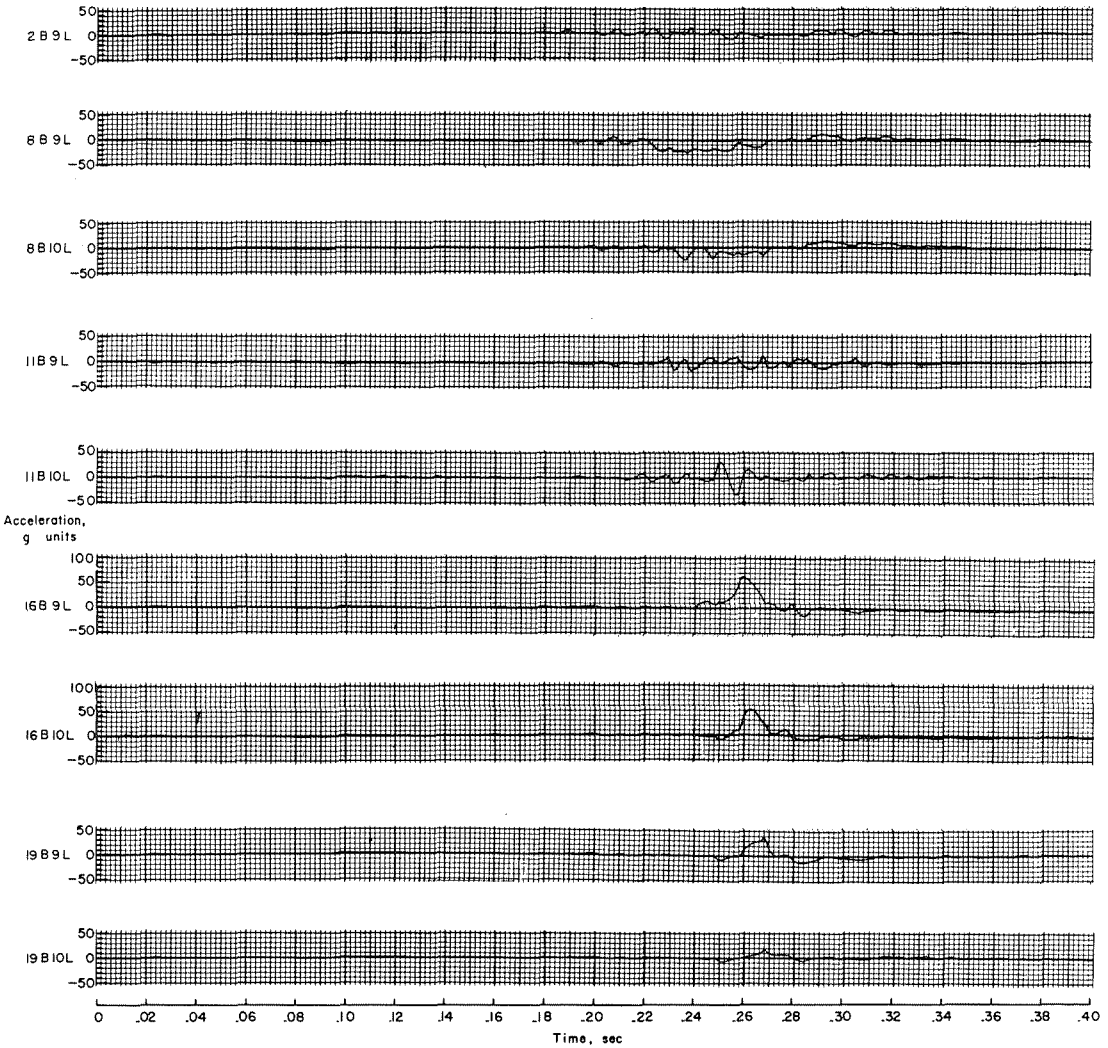

(b) Longitudinal accelerations adjacent to floor beam.

Figure A4.- Continued.

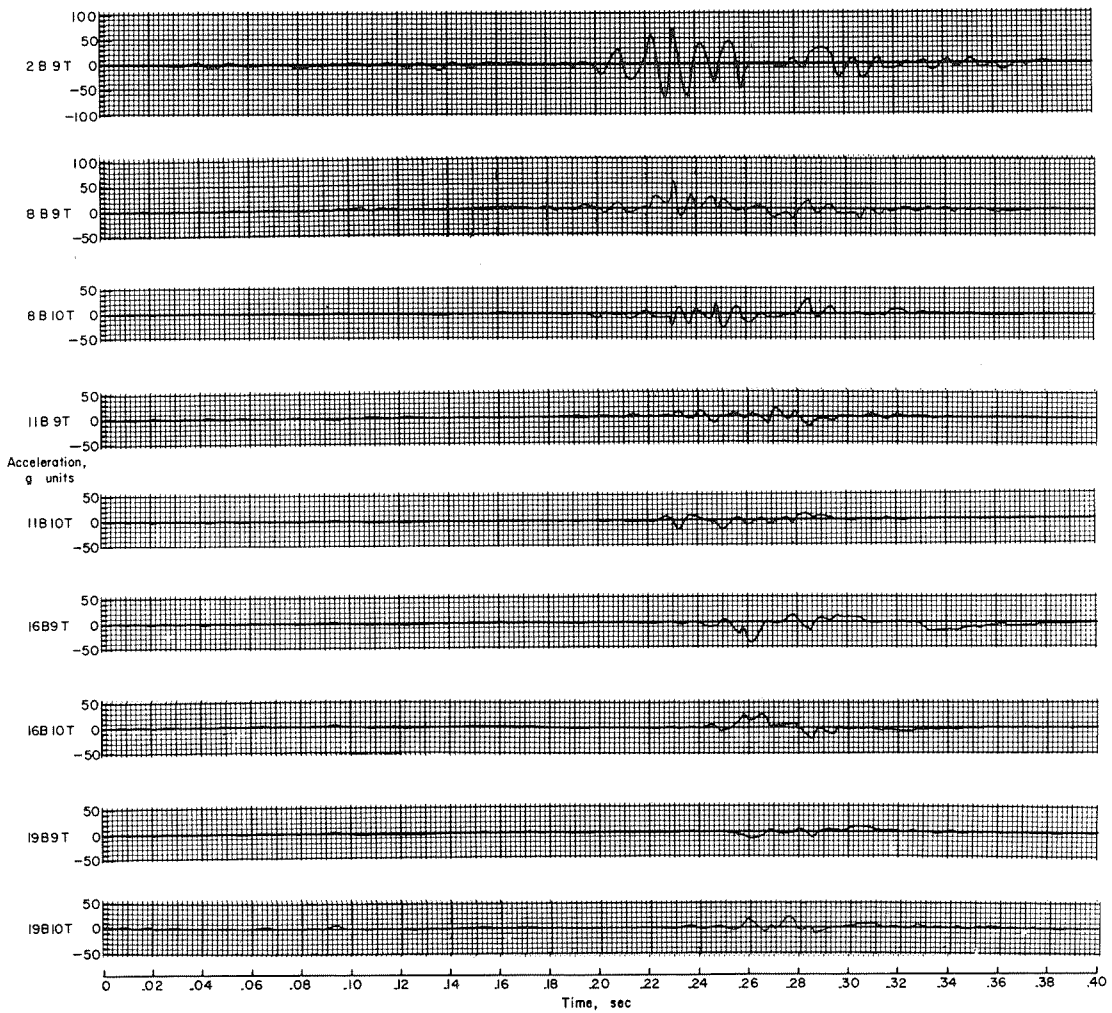

(c) Transverse accelerations adjacent to floor beam.

Figure A4.- Continued.

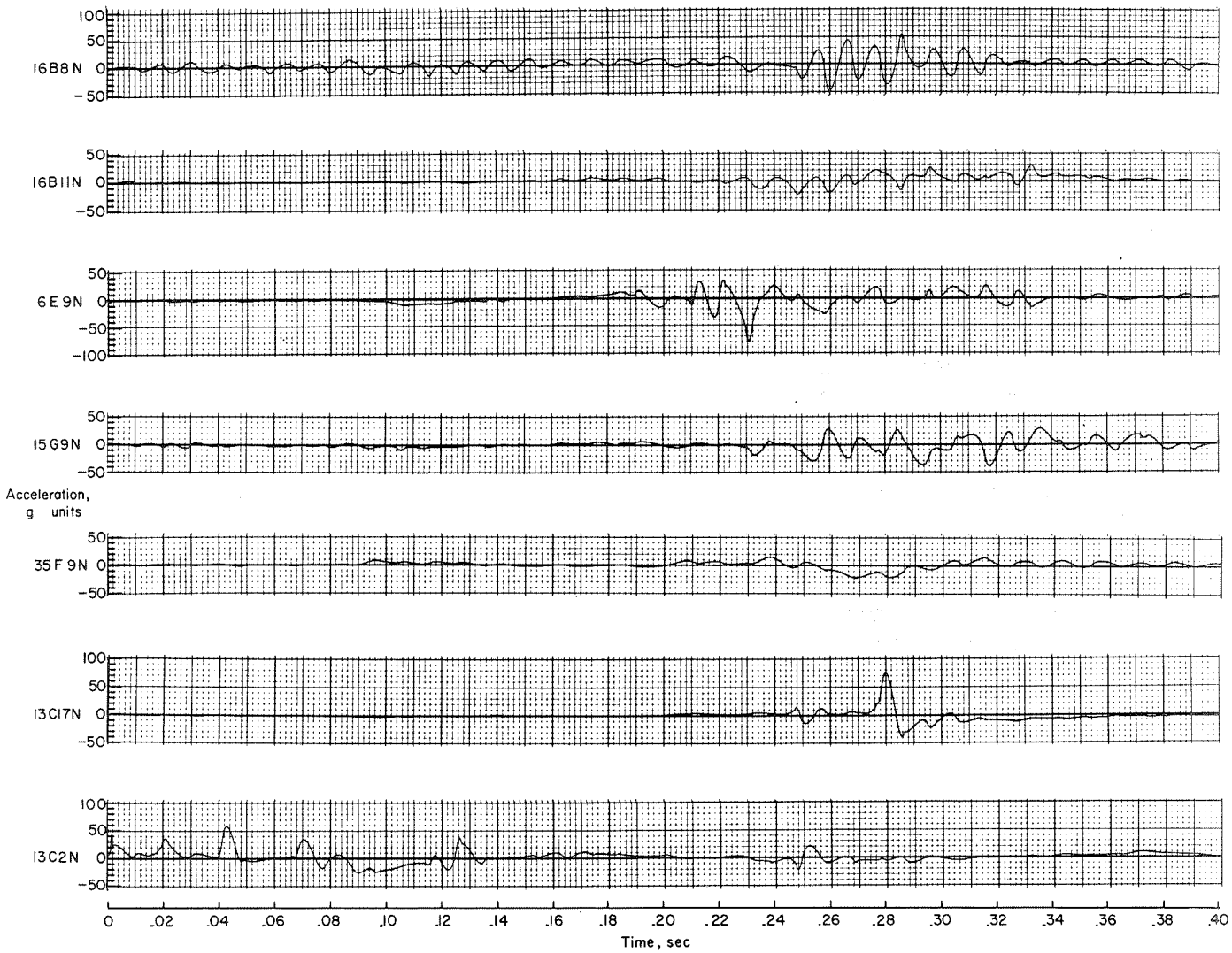

(d) Remaining normal structural accelerations.

Figure A4.- Continued.

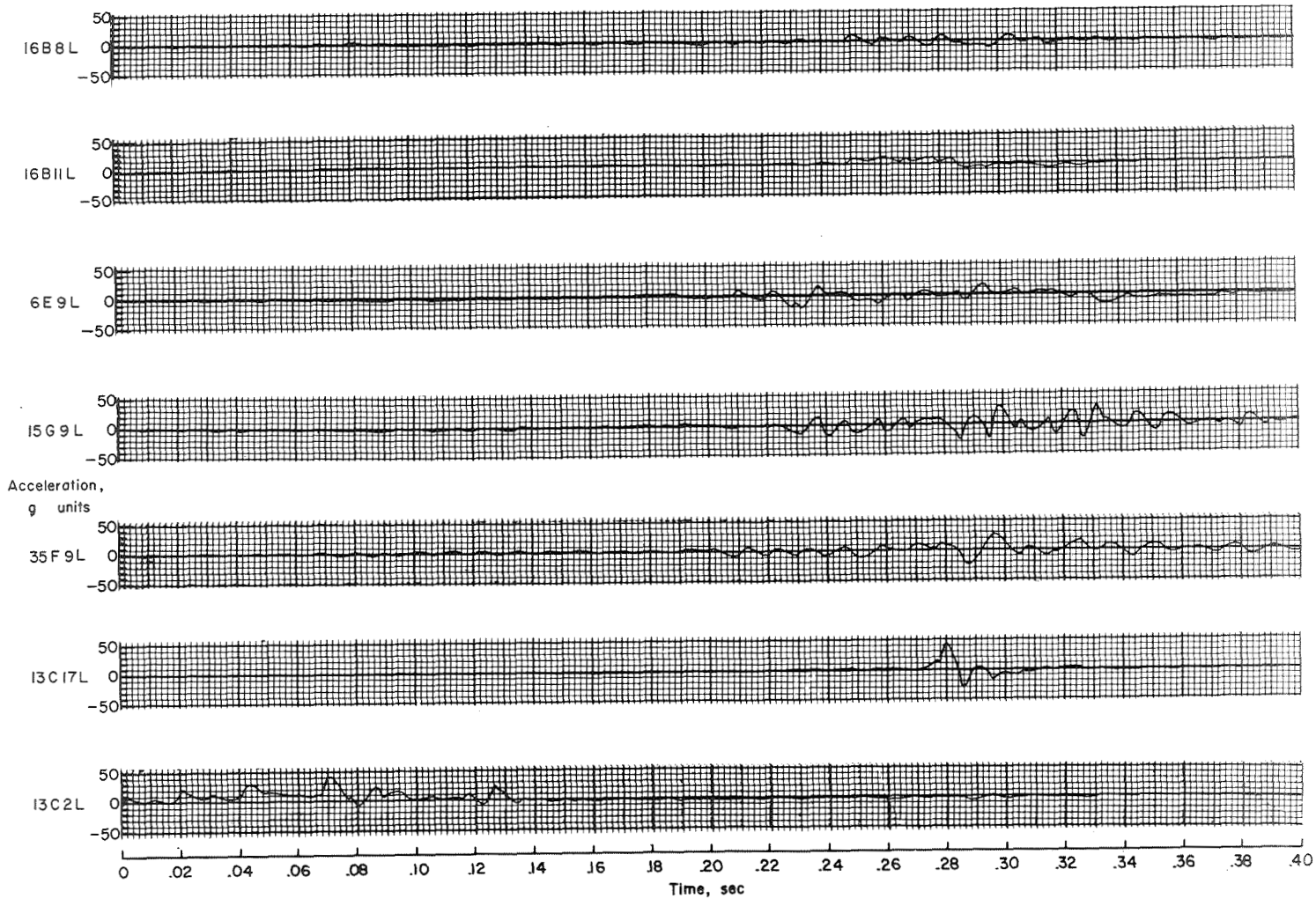

(e) Remaining longitudinal structural accelerations.

Figure A4.- Continued.

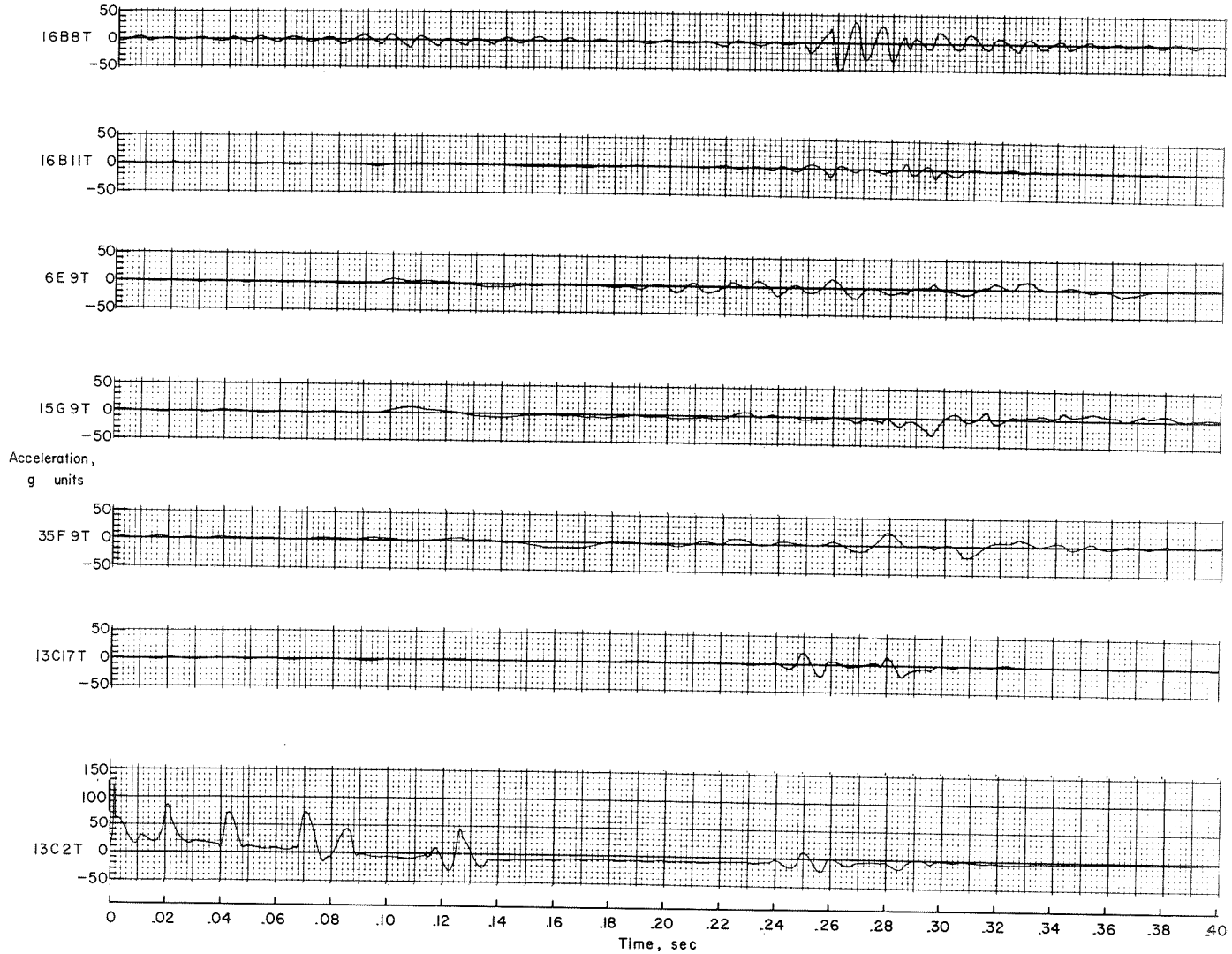

(f) Remaining transverse structural accelerations.

Figure A4.- Continued.

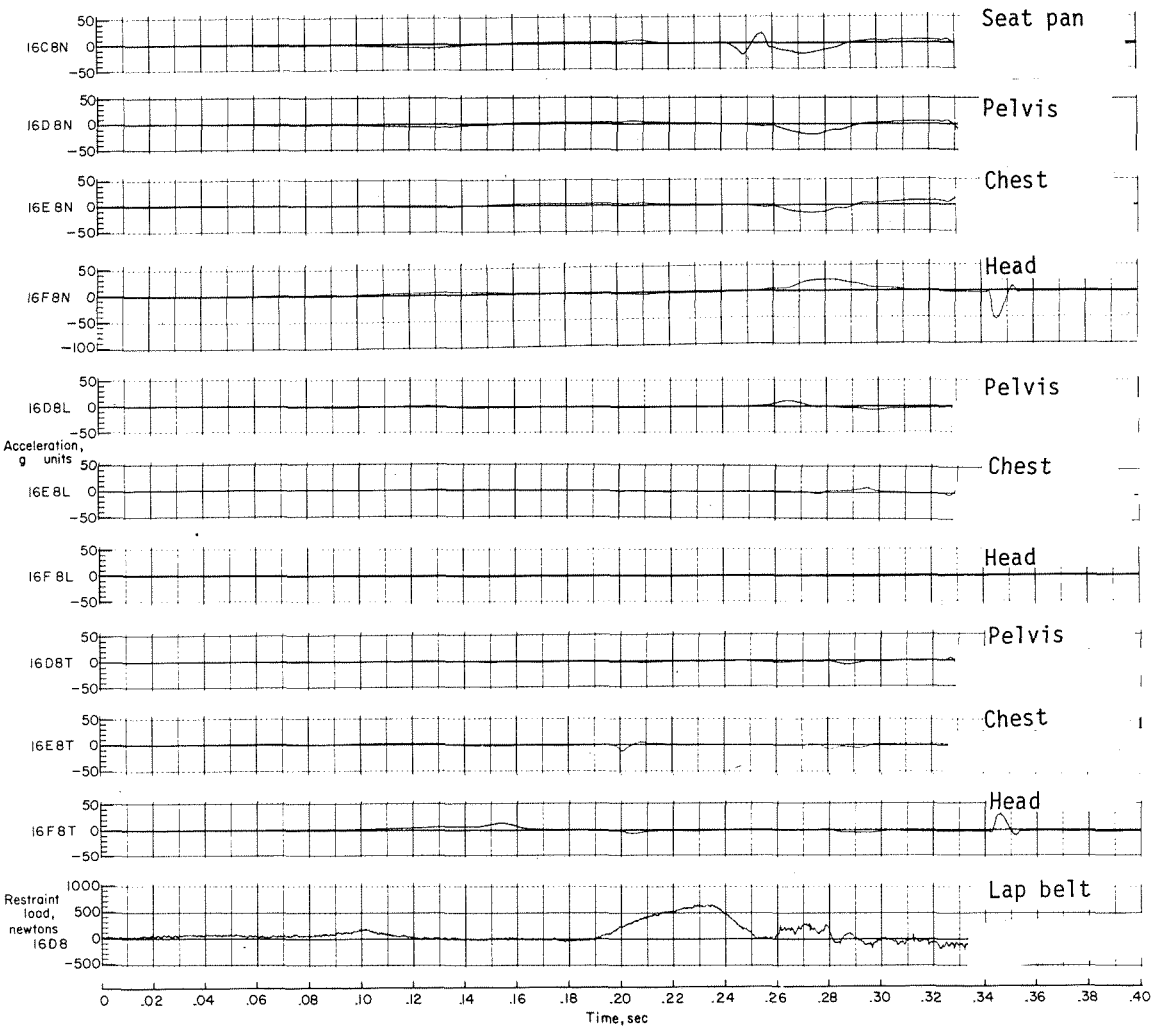

(g) Acceleration time histories in first-passenger dummy.

Figure A4.- Continued.

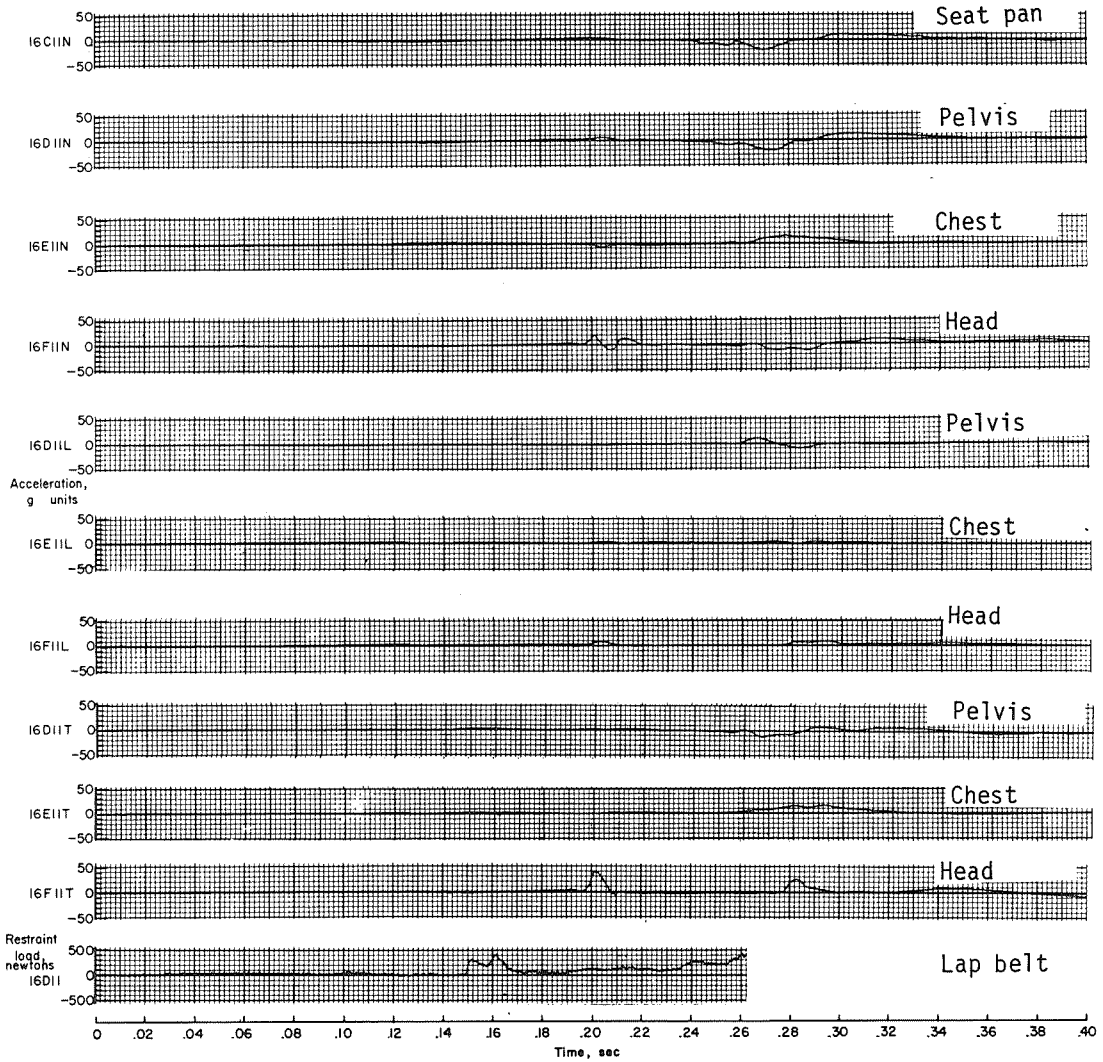

(h) Acceleration time histories in second-passenger dummy.

Figure A4.- Concluded.

1. Report No.	2. Government Accession No.	3. Recipient's Catalog No.
NASA TP-1477		

4. Title and Subtitle	5. Report Date
LIGHT AIRPLANE CRASH TESTS AT THREE ROLL ANGLES	October 1979
	6. Performing Organization Code

7. Author(s)	8. Performing Organization Report No.
Claude B. Castle and Emilio Alfaro-Bou	L-12778
	10. Work Unit No. 505-02-33-02

9. Performing Organization Name and Address	11. Contract or Grant No.
NASA Langley Research Center Hampton, VA 23665	
	13. Type of Report and Period Covered Technical Paper

12. Sponsoring Agency Name and Address	14. Sponsoring Agency Code
National Aeronautics and Space Administration Washington, DC 20546	

15. Supplementary Notes

Technical Film Supplement L-1256 available on request.

16. Abstract

Three similar twin-engine general-aviation airplanes were crash tested at the Langley impact dynamics research facility at 27 m/sec and at nominal roll angles of 0°, -15°, and -30°. Other flight parameters were held constant. The test facility, instrumentation, test specimens, and test method are briefly described. Structural damage and accelerometer data for each of the three impact conditions are presented and discussed.

17. Key Words (Suggested by Author(s))	18. Distribution Statement
Crash worthiness Airplane crash tests Crash dynamics General aviation Impact tests	Unclassified - Unlimited Subject Category 39

19. Security Classif. (of this report)	20. Security Classif. (of this page)	21. No. of Pages	22. Price*
Unclassified	Unclassified	75	$5.25

* For sale by the National Technical Information Service, Springfield, Virginia 22161

NASA-Langley, 1979

A motion-picture film supplement L-1256 is available on loan. Requests will be filled in the order received. You will be notified of the approximate date scheduled.

The film (16 mm, 9-1/2 min, color, silent) shows various views of three general-aviation airplane specimens at 24 and 400 pps for three roll angles during the impact sequence.

Requests for the film should be addressed to:

NASA Langley Research Center
Att: Photographic Branch, Mail Stop 425
Hampton, VA 23665

CUT

Date_____

Please send, on loan, copy of film supplement L-1256 to NASA TP-1477.

_____
Name of organization

_____
Street number

_____
City and State Zip code

Attention: Mr._____

Title_____

CUT

Place
Stamp
Here

NASA Langley Research Center
Att: Photographic Branch, Mail Stop 425
Hampton, VA 23665

National Aeronautics and
Space Administration

Washington, D.C.
20546

Official Business
Penalty for Private Use, $300

SPECIAL FOURTH CLASS MAIL
BOOK

Postage and Fees Paid
National Aeronautics and
Space Administration
NASA-451

NASA

POSTMASTER: If Undeliverable (Section 158 Postal Manual) Do Not Return